INVESTIGATIONS OF THE T-BURNER AND ITS ROLE IN COMBUSTION INSTABILITY STUDIES

Thesis by

Edward Harris Perry

In Partial Fulfillment of the Requirements

For the Degree of

Doctor of Philosophy

California Institute of Technology

Pasadena, California

1970

(Submitted May 26, 1970)

To My Wife,

CINDY

ACKNOWLEDGMENTS

To the many people who have contributed to these investigations, I am sincerely grateful. In particular, I wish to thank Professor Fred Culick for suggesting these studies and for maintaining a constant interest in their progress. The support, both financial and otherwise, provided by the Jet Propulsion Laboratory for the investigations is gratefully acknowledged. In addition, Mr. Warren Dowler and Mr. Winston Gin of the Solid Propellant Section of the Laboratory deserve a special word of thanks for their continual interest in the experiments.

The expert assistance of Mr. John Born and Mr. Walt Trapp in conducting the tests is likewise gratefully acknowledged, as are the many suggestions given by Mr. H. B. Mathes of the Naval Weapons Center at China Lake, California.

I am indebted to Mrs. Roberta Duffy for her excellent job of typing the manuscript, and to Mr. Frank T. Linton for his splendid job of preparing the many figures.

I am sincerely thankful for the personal financial support provided by the California Institute of Technology, the Ford Foundation, the Daniel and Florence Guggenheim Foundation, the National Science Foundation, and the California State Scholarship and Loan Commission.

For their encouragement, given at every step, I will be forever grateful to my parents.

Finally, my greatest debt of appreciation is owed my wife, Cindy, whose perseverance gave me encouragement and whose encouragement gave me perseverance.

ABSTRACT

Of several devices introduced to study combustion instability in solid rocket propellants, one, known as the "T-burner," has become the most widely used. With this device the response of a burning propellant to a small pressure disturbance can be measured. Such information is vital both to the understanding of unsteady combustion processes as well as to the assessment of the stability characteristics of solid rocket motors.

Although the T-burner has been used for several years, several questions concerning the device have arisen and, for the most part, have remained unanswered. Moreover, little effort has been given toward showing the relevance of T-burner data to predictions of instability in rocket motors.

The present investigations, comprising over 400 test firings in T-burners of various lengths and diameters, were undertaken with the major objective of gaining a better understanding of the T-burner itself in order to answer some of these unresolved questions. Another objective was to compare T-burner predictions of rocket motor instability with actual observations made in a previous study.

Among the investigations was a comparison of several ignition procedures which showed clearly that a poor, uneven ignition can seriously affect the test results. Included among the ignition studies were tests conducted in transparent chambers to permit high-speed

motion photography of the firings. These tests confirmed the common assumption that the T-burner is basically a one-dimensional device.

Tests using burners of different diameters showed that although the acoustic losses of the T-burner are nearly independent of diameter, the limiting amplitude of the oscillations is strongly dependent on the latter. The dilemma raised by these observations was resolved by measurements which indicate that the heat transfer from the combustion gases to the burner wall is strongly dependent on the amplitude of the waves. From these measurements emerged a non-linear description of the damping in the T-burner which accounts for both the behavior of the losses as well as that of the limiting amplitude.

When two independent T-burner methods were compared, the results obtained were initially in very poor agreement. However, when the T-burner losses were assumed to be non-linear as mentioned earlier, excellent agreement was observed.

Finally, the T-burner predictions of instability in rocket motors were in rather poor agreement with direct observations made in a previous study. Although this lack of agreement is not understood, it is doubtful in the light of the present investigations that the major error lies in the T-burner measurements, for these should be relatively accurate. Moreover, these results indicate the need for

more comparisons of this type in order to determine the usefulness of the T-burner in predicting combustion instability in solid propellant rockets.

TABLE OF CONTENTS

I. INTRODUCTION

For a number of years, combustion instability has been recognized as one of the most serious problems encountered in the development of solid propellant rockets. Because of the coupling between the combustion of the propellant and the conditions within the rocket motor, small pressure disturbances are often driven to large amplitude oscillations which frequently produce dramatic, and even catastrophic, changes in the motor's performance.

For this reason, considerable attention has been given in recent years to gaining a better understanding of this problem. Presumably, a thorough understanding would eliminate combustion instability in motor development programs through careful motor design and propellant selection. Because of the many complexities involved, however, such a complete understanding is still lacking, and the rocket engineer must content himself with trying to eliminate the problem if it arises in his particular program. Acoustic baffles and resonators placed at strategic locations inside the motor are often used for this purpose along with changes in the propellant composition. By increasing the acoustic damping of the chamber, all of these tend to stabilize the motor. While usually successful, such methods are also costly in time and resources.

The considerable progress made in the past few years toward understanding and eliminating combustion instability is certainly due

in part to the recognition of the similarity between the unstable pressure oscillations and the classical acoustic modes of the rocket chamber. The problem of determining the stability characteristics of solid rocket motors reduces to an elaborate acoustics problem in which account is taken of the mean flow and the fact that the chamber walls are not rigid and are therefore capable of exchanging energy with the acoustic field. The burning propellant surface, which forms the major part of the chamber walls in an internal-burning motor, is characterized by an acoustic admittance and therefore enters the problem as a specified boundary condition. The rate of energy transfer to the acoustic field from the burning propellant is related to the real part of this complex acoustic admittance. Because of this, the admittance, and particularly its real part, can be regarded as a measure of the propellant's ability to drive pressure oscillations.

Treating the problem in this way, Bird, McClure, and Hart[1] and somewhat later, Culick[2], examined the stability of acoustic oscillations in solid rocket motors. From the latter analysis came an expression for the growth rate of the oscillations in terms of properties of the mean flow and the real part of the propellant admittance. An equation for the stability boundary resulted from setting this growth rate equal to zero. If the nature of the flow field is known, then this equation permits calculations of the motor's stability characteristics from knowledge of the admittance alone.

Somewhat earlier[3,4] a device had been introduced as a means of studying combustion instability on a laboratory scale. This device, which later became known as the "T-burner" because of its appearance, consists of a tubular acoustic cavity in which solid propellant is burned. During the firing, oscillations spontaneously appear in the burner and are driven to appreciable amplitudes by the burning propellant. By measuring the growth rate of these oscillations, one can infer the real part of the admittance. In principle, these values coupled with an analysis of the rocket motor such as that mentioned above should enable one to make predictions of the stability characteristics of a given motor design. In practice, however, this has not become the case for several reasons.

First is the fact that little attempt has been made to establish firmly the relevance of T-burner measurements to such predictions. Naturally, until such attempts are made, the skepticism which accompanies most new methods will remain with the T-burner. Equally important is the fact that, although the T-burner has been involved in many studies, ranging from efforts to detect "entropy waves" leaving the burning surface[5] to investigations of the effects of compositional variables on the propellant response[6], several questions concerning the T-burner itself have arisen and have remained unanswered for the most part. Thus, the aforementioned skepticism is somewhat justified.

One notable attempt to resolve some of the conflicting opinions concerning the T-burner became known as the "Round Robin" studies and is discussed in detail in reference 7. Those studies, which included some of the present investigations, compared results obtained in T-burners of various configurations by different laboratories using the same propellant but different techniques. Although the Round Robin series did little to answer some of the questions concerning the burner, it did bring into focus the need for further investigations in several areas. First, the effects of chamber size needed to be examined along with those associated with different ignition techniques. Since there are two common methods of conducting T-burner tests, a side by side comparison of these was needed. In addition, it was obvious that a good understanding of the acoustic losses in the T-burner was lacking.

The present investigations, therefore, were undertaken with the objective of gaining a better description of the T-burner itself in order to answer these and other questions about the burner. A second goal of the studies was to show the relevance of T-burner data to predictions of instability in rocket motors.

In all, over 400 test firings were conducted in a variety of T-burners under a variety of conditions. In some of the early tests it was recognized that ignition procedures can have a significant effect on test results. The reasons for such effects were made clear by

tests conducted later in transparent chambers to permit high-speed motion photography of the firings. By examining the photographic records obtained from these tests, it became obvious why one of the four ignition procedures compared consistently provided better test results. In addition, the transparent burner firings showed very clearly that the T-burner is a one-dimensional device for the most part. Since this is one of the basic assumptions of the analysis describing the behavior of the burner, it was encouraging to have it confirmed so vividly.

The aspect that received the greatest amount of attention in the studies was the nature of the acoustic losses in the T-burner. Since the validity of the entire T-burner technique rests on assumptions made regarding these losses, it is imperative that they be understood as fully as possible. Tests conducted in burners of different diameters showed that the losses are nearly independent of chamber diameter. Since it had been expected that the losses would vary inversely with diameter, this presented a dilemma which remained unresolved during most of the investigations. However, later measurements showed that the heat transfer from the combustion gases to the chamber wall is dependent on the amplitude of the oscillations. From these measurements emerged a non-linear description of the T-burner losses which is supported by several independent sets of observations. Not only does this description account for the observed losses, but it

also offers an explanation for the nature of the limiting amplitude of the oscillations. When two independent T-burner methods were compared, the test results initially agreed very poorly. However, when the T-burner losses were taken to be non-linear in the way proposed, excellent agreement was found. Thus, the losses inferred during these studies appear to account for a number of heretofore unexplained features of the T-burner.

Finally, T-burner predictions of instability in rocket motors were found to be in poor agreement with direct observations made in a previous study. This lack of agreement is not understood, but it is doubtful if it is due to large inaccuracies in the T-burner method. In any case, it underscores the need for more comparisons of this type in order that the T-burner's role in such studies can be defined more clearly.

II. DESCRIPTION OF THE T-BURNER AND ITS PRIMARY ROLE

The T-burner, shown in cross section in Figure 1, is basically a centrally-vented cylindrical chamber with disks of solid rocket propellant bonded in the ends. Shortly after ignition of the propellant, pressure oscillations appear in the burner and grow until a limiting amplitude is reached. Remaining at this amplitude until burn-out occurs, they then decay because of losses present in the chamber. The frequency of the oscillations, corresponding closely to the lowest acoustic frequency of the chamber given by

$$f = \bar{a}/2L \qquad (2.1)$$

where $\bar{a}$ is the mean speed of sound, is varied by changing the chamber length, L, from test to test.

Later it will be shown how the real part of the propellant admittance can be inferred from measurements of the rate at which the oscillations grow. As mentioned earlier, the admittance is a measure of the propellant's ability to drive the pressure oscillations. It is defined as the complex ratio of the perturbation in the gas velocity normal to and at the burning surface to the pressure fluctuation there. Normalized with respect to the mean chamber pressure and speed of sound at the burning surface, the admittance is

$$A_b = \frac{\gamma P}{a_b} \frac{u'}{p'} \quad . \qquad (2.2)$$

From this it is apparent that a component of the velocity fluctu-

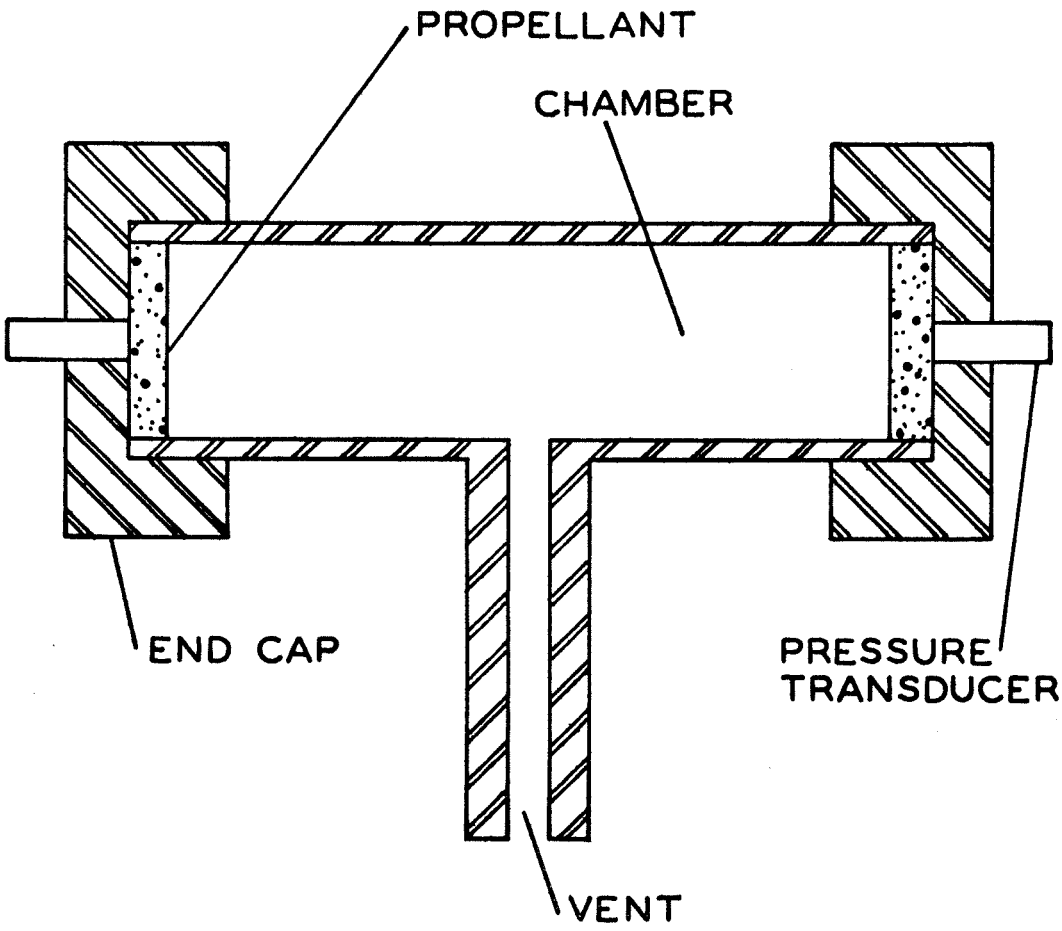

Figure 1. Typical T-burner Configuration.

ation is in phase with the pressure fluctuation. If phases are measured with respect to the pressure, then the in-phase portion of the velocity is proportional to A_b^r, the real part of the admittance. The rate at which mechanical "p-v" work is done at the burning surface is equal to the time average of the product of the in-phase velocity and pressure there, and is therefore proportional to the real part of the admittance also. In fact, it is easy to show[8] that this mechanical work rate per unit area of burning propellant surface is given by

$$\dot{W}_{mech} = \frac{\frac{1}{2}\gamma P}{a_b} A_b^r p'^2 \quad . \tag{2.3}$$

By the same token, the mean flow can perform work on the waves, and the total rate of energy addition to the acoustic field is the sum of the two effects. At the same time, however, losses such as viscous and thermal dissipation near the chamber walls remove energy from the waves. Naturally, in order for the oscillations to grow, the gains must exceed the losses. In the T-burner this is often the case, since the losses are relatively small.

Besides the admittance, another quantity of interest in combustion instability studies is the response function of the propellant. Defined as the ratio of the change in the propellant burning rate to a fluctuation in pressure, the response function in normalized form is

$$R_b = \frac{P}{\bar{r}} \frac{r'}{p'} \quad . \tag{2.4}$$

Since the mass flux at the burning surface is related to the burning rate by

$$m = \rho_s r \tag{2.5}$$

where ρ_s is the density of the propellant, the response function can also be written as

$$R_b = \frac{P}{\bar{m}} \frac{m'}{p'} \quad . \tag{2.6}$$

Like the admittance, the response function is also complex since the fluctuations are generally not in phase.

The response function, rather than the admittance, is of particular importance to theoretical models of the combustion zone, since these are concerned with the unsteady burning rate as a function pressure at the propellant surface.

The steady burning rate of many solid propellants is given quite well by the familiar "burning rate law,"

$$r = a_1 p^n \tag{2.7}$$

where a_1 and n, both empirical constants for a particular propellant, are the burning rate coefficient and burning rate exponent, respectively. From this it is easy to show that

$$\frac{r'}{\bar{r}} = n \frac{p'}{P} \quad . \tag{2.8}$$

Combining this with equation (2.4) reveals that in the limit of zero frequency, the response function is

$$(R_b)_{f=0} = n \quad . \tag{2.9}$$

This relation is often used to eliminate one of the arbitrary constants appearing in the combustion models. As a result, most theoretical descriptions of the combustion zone include the steady burning rate exponent as a parameter[8]. In fact, usually the response function predicted by these models is proportional to the burning rate exponent, with the constant of proportionality depending on such factors as the temperature of the burning surface. Thus, the steady state behavior is woven rather intimately into the descriptions of the unsteady burning.

The response function becomes of interest in T-burner studies when its relationship to the admittance is realized. The mass flux at the burning surface is given by

$$m = \rho u \quad , \tag{2.10}$$

where ρ and u are the density and velocity of the combustion gases. From this it follows that

$$\frac{m'}{\bar{m}} = \frac{\rho'}{\bar{\rho}} + \frac{u'}{\bar{u}} \quad . \tag{2.11}$$

Combining this with the definitions of the response function and admittance results in the following:

$$R_b = \frac{A_b}{\gamma M_b} + \frac{\rho'/\bar{\rho}}{p'/P} \quad , \tag{2.12}$$

where M_b is the Mach number of the mean flow at the burning surface.

If the oscillations are isentropic, then

$$\frac{\rho'}{\bar{\rho}} = \frac{1}{\gamma} \frac{p'}{P} \quad , \tag{2.13}$$

and the former expression reduces to

$$R_b = \frac{1}{\gamma M_b} (A_b + M_b) \quad . \tag{2.14}$$

In general, however, the oscillations are not isentropic. In fact, considerable effort has been spent in proving the existence of "entropy waves" leaving the burning surface[5]. Nevertheless, for the present purposes, it will suffice to assume that isentropic conditions prevail and that equation (2.14) is valid. In that case, T-burner measurements of the admittance may be interpreted as measurements of the response function, thus broadening the T-burner's role.

Since several analyses of the linear behavior of the T-burner have been given elsewhere[7, 9], only the general approach and final results will be discussed here. More details are given in Appendix B.

One of the basic assumptions of these analyses is that the gasdynamics within the burner can be adequately described by the linearized equations of motion. Of course, this is valid only for sufficiently small amplitudes of oscillation. Within this range of validity, the equations of motion are the usual equations of linear acoustics with "source" terms present to allow for the mean flow. Equation (2.2), defining the propellant admittance, is used to relate the acoustic ve-

locity and pressure at the burning surface.

Upon carrying out such an analysis, one finds that ideally the amplitude of the oscillations should grow exponentially in time as

$$p' \sim e^{\alpha t} \tag{2.15}$$

where the "growth constant," α, is related to the admittance by

$$\alpha = \frac{2a_b}{L} \frac{S_b}{S_c} (A_b^r + M_b) \tag{2.16}$$

in which a_b is the speed of sound at the burning surface and S_b/S_c is the ratio of the burning surface area at each end to the chamber cross-sectional area. Normally, this ratio is unity, but in one modification of the basic T-burner method it is varied from test to test.

Opposing the growth of the oscillations, however, are the acoustic losses of the chamber which, when the driving by the propellant ceases, cause the oscillations to decay in time as

$$p' \sim e^{-\alpha_d t}, \tag{2.17}$$

where α_d, defined here as a positive number, is the chamber "decay constant."

The observed growth constant, α_g, is presumably the net result of the two opposing effects:

$$\alpha_g = \frac{2a_b}{L} \frac{S_b}{S_c} (A_b^r + M_b) - \alpha_d \quad . \tag{2.18}$$

Rearrangement of this equation shows how the real part of the admittance is inferred from measurements of the observed growth

and decay rates and knowledge of the mean flow Mach number:

$$A_b^r = \frac{L}{2a_b}\frac{S_c}{S_b}(\alpha_g + \alpha_d) - M_b \quad . \tag{2.19}$$

The mean flow Mach number can be related easily to known propellant properties. By definition,

$$M_b \equiv \frac{\bar{u}_b}{a_b} \quad ; \tag{2.20}$$

but, by continuity,

$$\rho_b \bar{u}_b = \rho_s \bar{r} \quad , \tag{2.21}$$

and for a perfect gas,

$$\rho_b = \frac{\gamma P}{a_b^2} \quad . \tag{2.22}$$

Thus,

$$M_b = \frac{\rho_s \bar{r} a_b}{\gamma P} \quad . \tag{2.23}$$

Because of heat losses at the chamber walls, the mean speed of sound in the chamber, $\bar{a}$, is lower than that at the burning surface. Generally, values for a_b based on theoretical flame temperatures are sufficiently accurate for use in reducing T-burner data. Thus, the real part of the admittance is completely determined once the T-burner data are obtained.

In addition, if the oscillations are assumed isentropic, the above relations combined with equation (2.14) provide the following expression for the response function:

$$R_b^r = \frac{P}{4\rho_s \bar{r} a_b} \frac{2L}{a_b} (\alpha_g + \alpha_d) \frac{S_c}{S_b} \quad . \tag{2.24}$$

Were there no heat losses to the wall, the speed of sound would be constant throughout the chamber, and by equation (2.1) could be related to the frequency. In that case, the above would reduce to a form presented quite often in the literature as the basic T-burner equation:

$$R_b^r = \frac{P}{4\rho_s \bar{\bar{r}} \bar{a}} \frac{\alpha_g + \alpha_d}{f} \frac{S_c}{S_b} \quad . \tag{2.25}$$

From the preceding discussion, however, it should be apparent that this equation is valid only under very special circumstances. Equation (2.19), on the other hand, is quite generally valid, which emphasizes the fact that the primary role of the T-burner is to measure the real part of the admittance and not the response function.

III. DESCRIPTION OF EXPERIMENTAL EQUIPMENT AND PROPELLANTS

Hardware

From the standpoint of hardware the T-burner is a very simple device, consisting of little more than a chamber with caps on the ends and a vent in the center. Although simple enough in concept, the T-burner hardware has nonetheless been approached in perhaps as many ways as there are laboratories using the device. Some of these approaches are described in reference 7, which presents T-burner results and suggestions obtained from a number of studies, including some of the present investigations. Among these various approaches are different end cap arrangements. Some investigators have bonded the propellant into the cap itself rather than into the chamber, as was done in the present studies. Also, to reduce possible asymmetric effects near the vent, multiple vents have been used. In the present case, however, only a single vent located at the center of the chamber was employed. The vent diameter was 0.4 inches in the great majority of the tests, but, to see if this had any effect on the data, a few tests were conducted using 0.25-inch diameter vents. The fact that no differences in the data were observed supports the generally held belief that the vent , located at the pressure node of the oscillation, plays little, if any, role in the T-burner tests.

Because the frequency is determined essentially by the chamber length, burners of varying lengths must be used to cover the frequency range of interest. To increase the number of lengths available from a given set of hardware, several short chambers can be coupled together to form longer burners. The present tests used T-burners varying in length from 3.25 to 43.5 inches, covering a frequency range of from 0.3 to 6.4 kHz. The burners longer than 10 inches consisted of at least two, and as many as four, short sections. In Figure 2 one of these longer burners is shown disassembled.

For these low-frequency burners, the threaded end cap shown in the figure was used. However, since this required a 2.5-inch threaded section on each end of the chamber, it was unsatisfactory for burners shorter than 7.0 inches. In Figure 3 one of the short, high-frequency burners is shown, along with the bolt-together end caps used with these chambers. The bolts, extending the length of the burner, were used to pull the caps toward one another until these were tightly seated on the chamber.

The majority of the tests were done with chambers having an inner diameter of 1.5 inch. However, to examine the effects of chamber size, a number of tests used burners with diameters of 1.0 inch and 2.5 inches. Most of the T-burners in use today at various laboratories fall within this range, with notable exceptions in the 5.5-inch and 8.5-inch diameter burners used at the Naval Weapons Center[10]

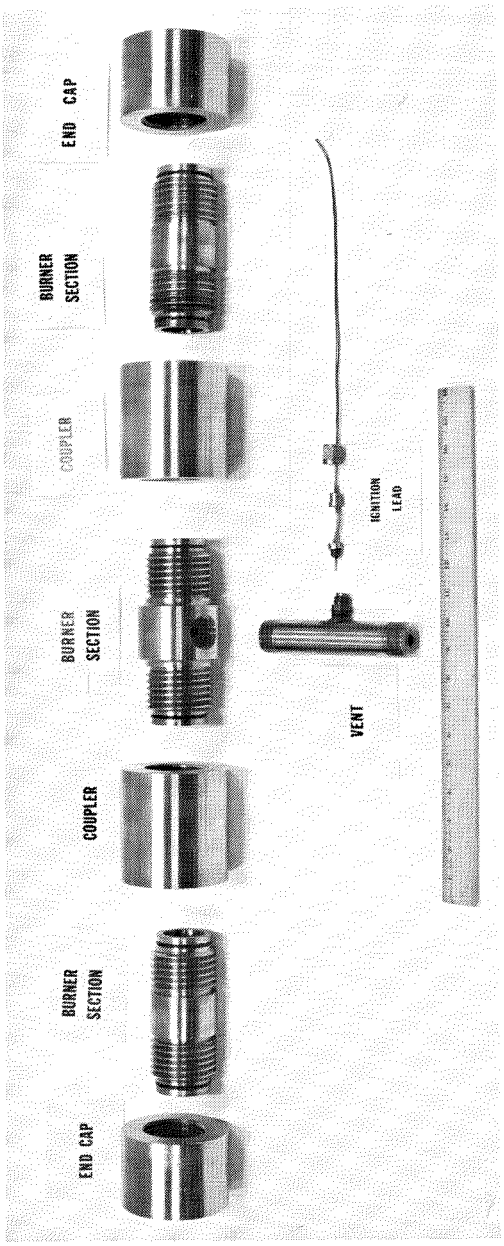

Figure 2. A Low-Frequency T-Burner Disassembled to Show the Various Components.

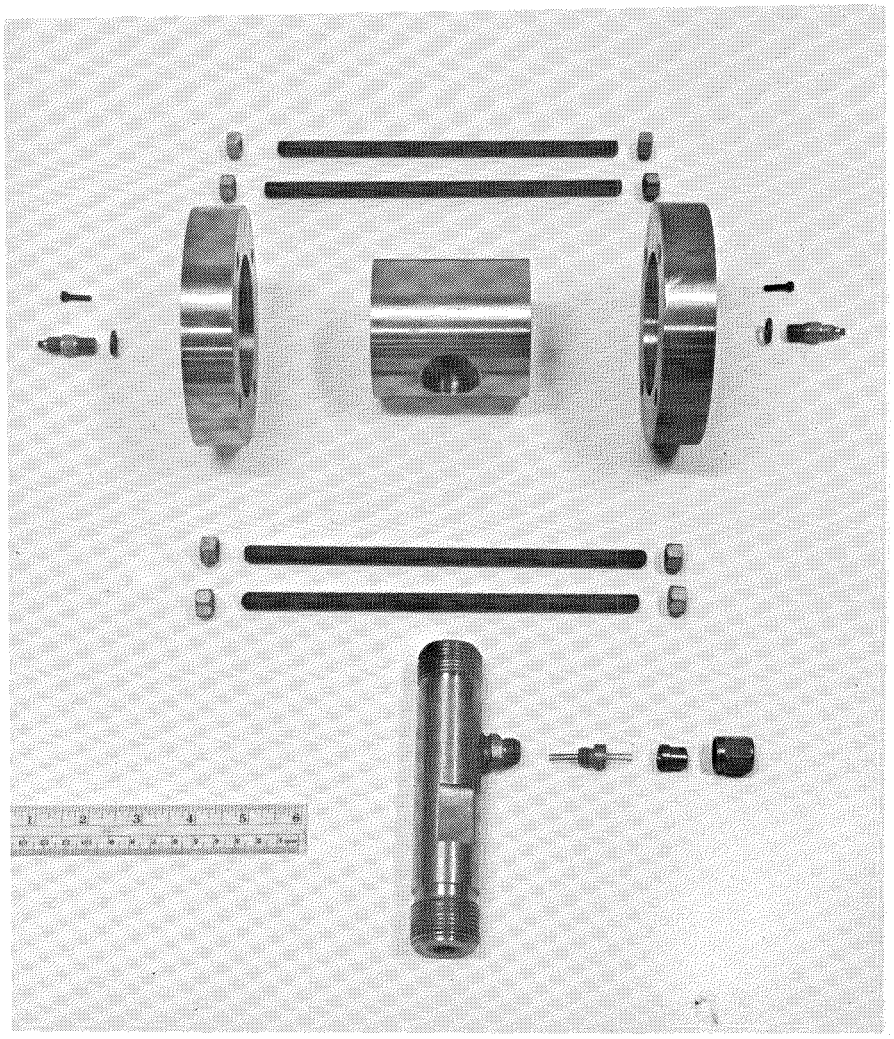

Figure 3. A Disassembled High-Frequency T-Burner Using Bolt-Together End Caps. The Pressure Transducers Used Are Shown Alongside the End Caps.

and Allegheny Ballistic Laboratory[11], respectively.

Depending on the end cap arrangement and the chamber diameter, the wall thickness varied from 0.5 to 1.0 inch. Although practically any material can be used in fabricating T-burner hardware, the type 304 stainless steel employed for the present burners proved very satisfactory in withstanding repeated firings.

Besides frequency, the other main independent test variable is chamber pressure, which should be constant during the firing. Of two popular ways of controlling this variable, the first is to attach a sonic nozzle to the vent, allowing the burning propellant to establish the pressure as it does in a rocket motor. The principal objection to this approach is that vital information may be lost because of the pressure transients at the beginning and end of the test.

The second method, and the one adopted here, uses a large surge tank attached to the vent. Before each firing, this tank, and hence the chamber, is pressurized with nitrogen gas. The mass of nitrogen in the tank being much greater than that of the combustion gases evolved, the pressure rises only slightly during the firing. An estimate of the pressure rise can be given by assuming the combustion gases, at temperature T_c, mix completely and adiabatically with the nitrogen at the initial ambient temperature, T_i. Letting M_i and m_p denote the masses of the nitrogen and propellant, respectively, and T_f the temperature of the final mixture, a simple energy balance

shows

$$C_{vi} M_i T_i + C_{vc} m_p T_c = (M_i + m_p) C_{vi} T_f \quad , \tag{3.1}$$

where it has been assumed that the specific heats of the mixture are equal to that of nitrogen. For a large tank, M_i will be much greater than m_p, and this equation, after rearrangement, becomes approximately

$$\frac{T_f}{T_i} \cong 1 + \frac{C_{vc}}{C_{vi}} \frac{m_p}{M_i} \frac{T_c}{T_i} \quad . \tag{3.2}$$

Since the process occurs at constant volume, the perfect gas equation shows the ratio of final to initial pressure is

$$\frac{P_f}{P_i} = \frac{M_i + m_p}{M_i} \frac{T_f}{T_i} \tag{3.3}$$

or

$$\frac{P_f}{P_i} = \left(1 + \frac{m_p}{M_i} \right) \frac{T_f}{T_i} \quad . \tag{3.4}$$

With equation (3.2), this becomes approximately

$$\frac{P_f}{P_i} \cong 1 + \frac{m_p}{M_i} \left(1 + \frac{C_{vc}}{C_{vi}} \frac{T_c}{T_i} \right) \quad . \tag{3.5}$$

Of course, for a perfect gas,

$$C_v = \frac{R}{\gamma - 1} \tag{3.6}$$

where R is the universal gas constant divided by the molecular weight of the particular gas. Since the average molecular weight of typical combustion gas mixtures is close to that of nitrogen, we find

$$\frac{C_{vc}}{C_{vi}} = \frac{\gamma_i - 1}{\gamma_c - 1} \tag{3.7}$$

where γ_i and γ_c are the specific heat ratios of nitrogen and the combustion gases. Thus, the pressure rise is approximately

$$P_f - P_i \cong \frac{m_p P_i}{M_i T_i} \left[T_i + \frac{\gamma_i - 1}{\gamma_c - 1} T_c \right] . \tag{3.8}$$

But, by the perfect gas law, if the chamber volume is neglected in comparison to the tank volume V,

$$P_i V = M_i R_g T_i , \tag{3.9}$$

where R_g is the gas constant for the pressurizing gas, in this case nitrogen. Combining the last two equations gives the following approximate expression for the pressure rise:

$$P_f - P_i \cong \frac{m_p R_g}{V} \left(T_i + \frac{\gamma_i - 1}{\gamma_c - 1} T_c \right) . \tag{3.10}$$

Thus, the rise depends on the amount of propellant burned as well as the volume of the tank and is essentially independent of mean pressure. Because of this latter fact, the relative pressure rise, which is usually the factor of concern, is obviously inversely proportional to the initial pressure. Thus, a given tank may be suitable for high mean pressures but almost useless for low pressure work, since the relative pressure rise in the latter case would be intolerable.

In the present tests, the volume of the surge tank was seven cubic feet. For the majority of the firings, the mass of the two pro-

pellant disks totaled about 25 grams. If, for the combustion gases, a temperature of 2000°K and a specific heats ratio of 1.25 are assumed, then the above equation predicts a pressure rise of about 20 psi, which is surprisingly close to observed values. In some tests, however, the rise was somewhat less than this, probably because of heat losses to the chamber walls. Thus, with a seven cubic foot tank and a typical mean pressure of 300 psig, the pressure was constant to within about five percent during the entire test. In Figure 4 is shown an assembled T-burner atop the surge tank used.

Instrumentation

Like the hardware, the instrumentation system was simple in principle. Shown in schematic form in Figure 5, it consisted of piezoelectric pressure transducers mounted in the ends of the burner, appropriate amplifiers and filters, a tape recorder, recording oscillograph, and a storage oscilloscope. Although not represented in the figure, thermocouples and their associated electronics were also employed in a few tests.

The most essential components of the instrumentation system were the Kistler 603-A piezoelectric pressure transducers mounted behind, but in contact with, the propellant. By using two transducers, both the amplitude and relative phase of the oscillations at the two ends of the chamber could be compared. In general, the oscillations were

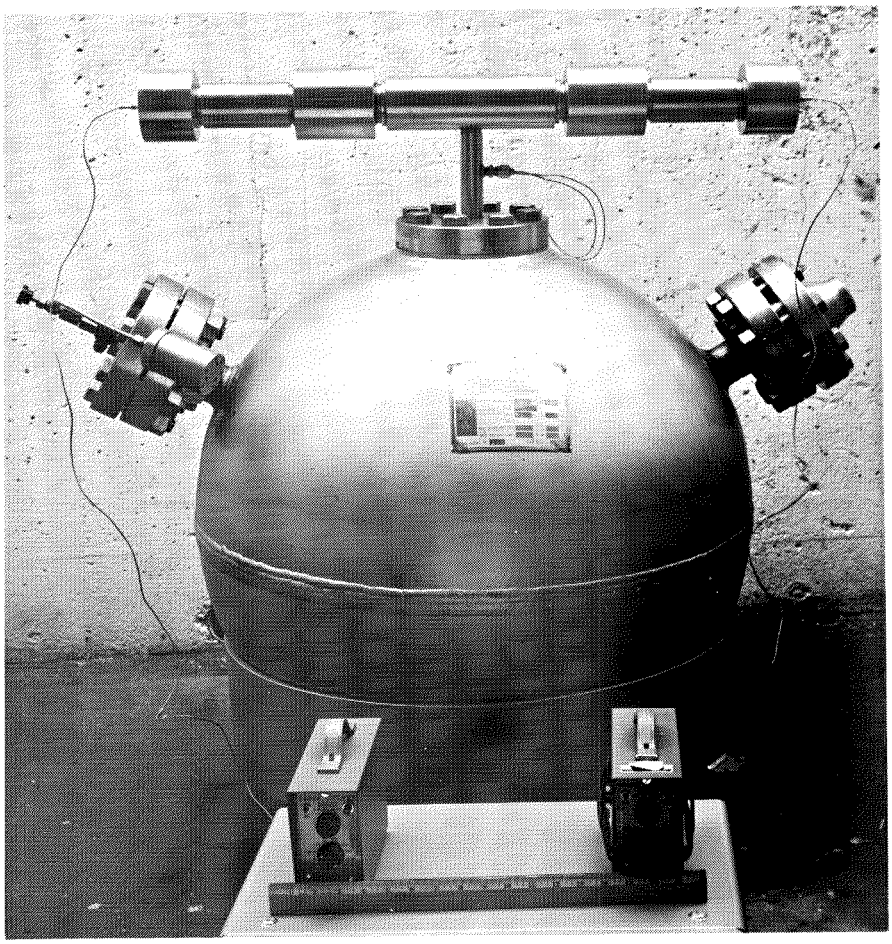

Figure 4. Assembled T-Burner Mounted on the Surge Tank.

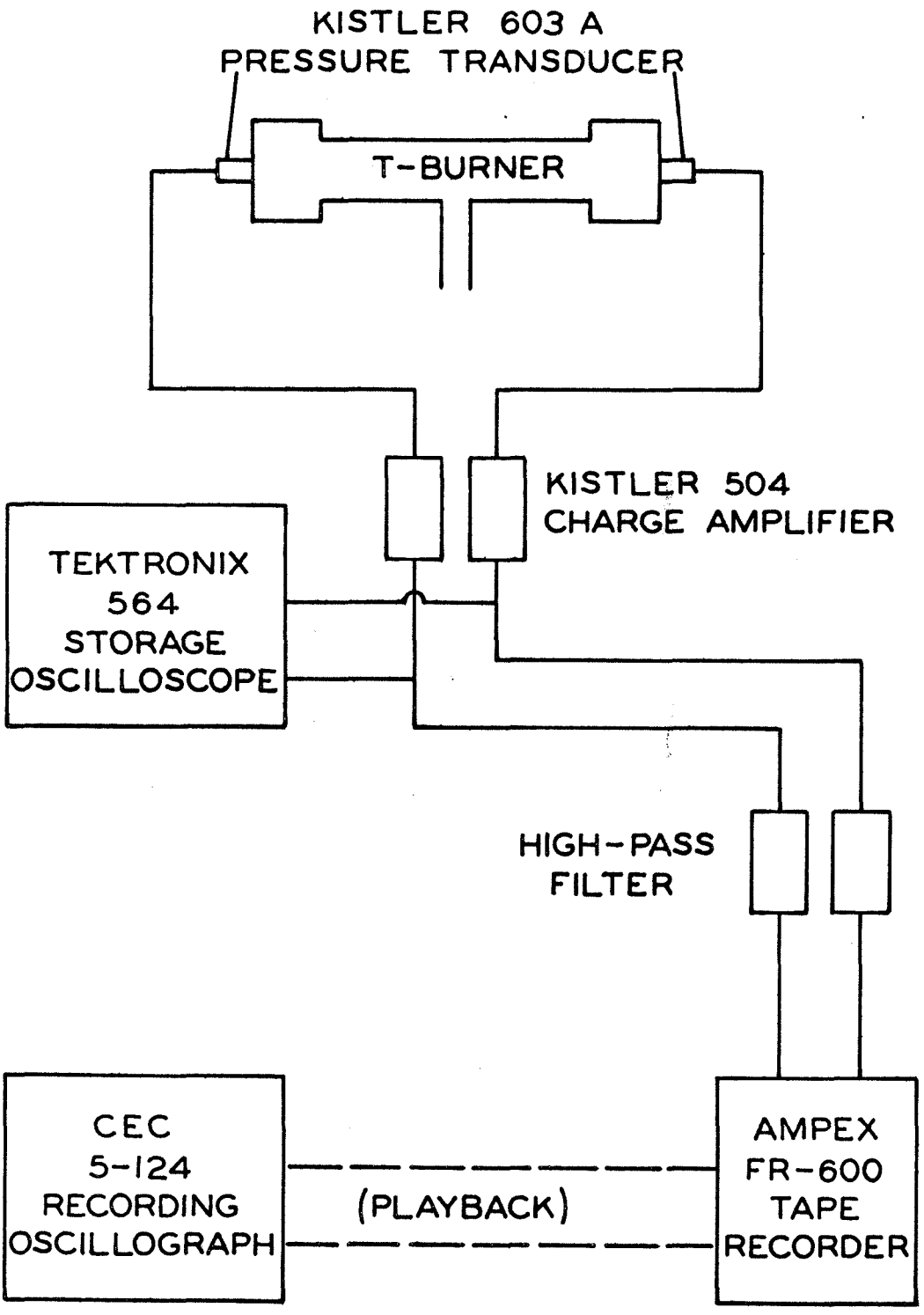

Figure 5. Block Diagram of Instrumentation System.

equal in amplitude at the two ends and approximately 180° out of phase, in agreement with the acoustic description of the oscillation mode.

Placement of the transducers behind the propellant, which is common practice in T-burner tests, afforded maximum protection for the transducers in addition to excellent observations of the oscillations. In order to be certain that the pressure signals were not being distorted or attenuated while passing through the quarter-inch thick propellant disks, some tests were conducted using a transducer mounted also in the chamber wall just ahead of the propellant. The data obtained at the two locations were in excellent agreement, confirming generally held opinions. This agreement came as little surprise, however, since tests conducted in the normal way had shown no transducer signal change as the propellant thickness grew smaller during the test.

A 0.020-inch thick layer of General Electric RTV-580 silicone rubber covering the transducer face provided considerable protection against the high temperatures. Nevertheless, a slight drift of the transducer signals, arising presumably from thermal effects, was observed during the early tests. This was later compensated by passing the signals through coupling transformers having a flat frequency response between 0.05 and 15.0 kHz.

To assure good contact between transducer face and the rear

of the propellant, Dow Corning DC-11 silicone grease was applied to the latter before the end cap, containing the transducer, was attached. Excess grease was removed through a small bleed port as the end cap was seated into place.

Although the principal data came from the tape playbacks onto the oscillograph, the storage oscilloscope records were particularly useful in observing qualitative trends. These, of course, were considerably less apparent in the rather lengthy oscillograph traces.

Propellants

To distinguish between those effects arising from individual propellant peculiarities and those inherent in the T-burner itself, four different composite propellants were used. A lengthy search for suitably unstable propellants was avoided by selecting only those which had exhibited combustion instability in prior studies. In Table A are found some of the pertinent properties of the propellants chosen. Although not mentioned in the table, none of the propellants contained metal powders. Since it has long been known that the presence of solid particles in a gas can lead to large attenuation effects, it was decided to use only non-metallized propellants in order to study the damping characteristics of the burner itself.

The first propellant listed in the table, A-13, was generously supplied by the Naval Weapons Center at China Lake, California.

TABLE A. Pertinent Properties of the Four Propellants Used.

Propellant	A-13	T-17	540-A	A-35
Binder/Oxidizer	PBAN[1]/AP[2]	PS[3]/AP	PPG[4]/AP	PU[5]/AP
Specific Heats Ratio, γ	1.28	1.25	1.22	1.25
Density (gm/cm^3)	1.56	1.58	1.63	1.58
Burning Rate at 300 psig (cm/s)	0.48	0.78	0.50	0.46
Burning Rate Exponent at 300 psig	0.42	0.38	0.15	0.0
Flame Temperature at 300 psig (^oK)	2100	2050	2900	2160

[1] Polybutylacrylonitrile acrylic acid

[2] Ammonium perchlorate

[3] Polysulfide

[4] Polypropylene glycol

[5] Polyurethane

Having been chosen for a number of prior T-burner studies, this propellant was an obvious choice. Among the propellants used, A-13 was the most unstable by almost any standard.

A decade ago, the second propellant, T-17, had been used in the most comprehensive study of combustion instability in actual rocket motors. By carrying out T-burner tests with this propellant it was intended to show the relevance of T-burner data to rocket motor stability predictions.

Previous instability studies at the Jet Propulsion Laboratory had included investigations of the third propellant selected, 540-A. During the present experiments it was realized that this propellant offered a particularly interesting feature, as far as instability considerations are concerned, since its burning rate is almost constant for pressures between 500 and 1250 psig. From equation (2.7) it is seen that this requires a very small burning rate exponent over that pressure range, which, according to most combustion models, implies that the propellant is stable. The fact that the present T-burner investigations found 540-A to be far from stable in this pressure region indicates again the lack of a thorough understanding of combustion instability in solid propellants.

Finally, the fourth propellant, A-35, was also supplied by the Naval Weapons Center, and, like the 540-A propellant, exhibited a near zero burning rate exponent over a moderate pressure range. In

comparison to the other three propellants, A-35 was only weakly unstable and was therefore used in only a few firings.

IV. DATA REDUCTION METHODS

During the Round Robin T-burner tests[7] mentioned earlier, it became clear that different interpretations of the same test record could account for significant variations in data reported by various investigators. In fact, one of the main results of the Round Robin series was a set of standards for interpreting T-burner tests in a uniform manner. For tests that produce near ideal records, such standards can be applied easily and minimize the amount of interpretation possible. Unfortunately, not all records are so ideal, and the problem of test interpretation reappears.

Since most of what follows is concerned with information obtained from test records, two such records will be discussed and the methods used for deriving and reducing the test data described. Obviously, these two cases cannot begin to cover the spectrum of features observed in the many firings, but they do illustrate the typical test characteristics as well as some of the less common features.

In Figure 6 is shown a condensed oscillograph record for a near ideal test. The oscillatory pressure is given as a function of time, which increases from left to right. Due to the extensive compression along the time axis required for presentation here, only the envelope of the waves is apparent. Naturally, in the full-length records, the individual oscillations were clearly discernable.

In this test, the oscillations begin very soon after ignition,

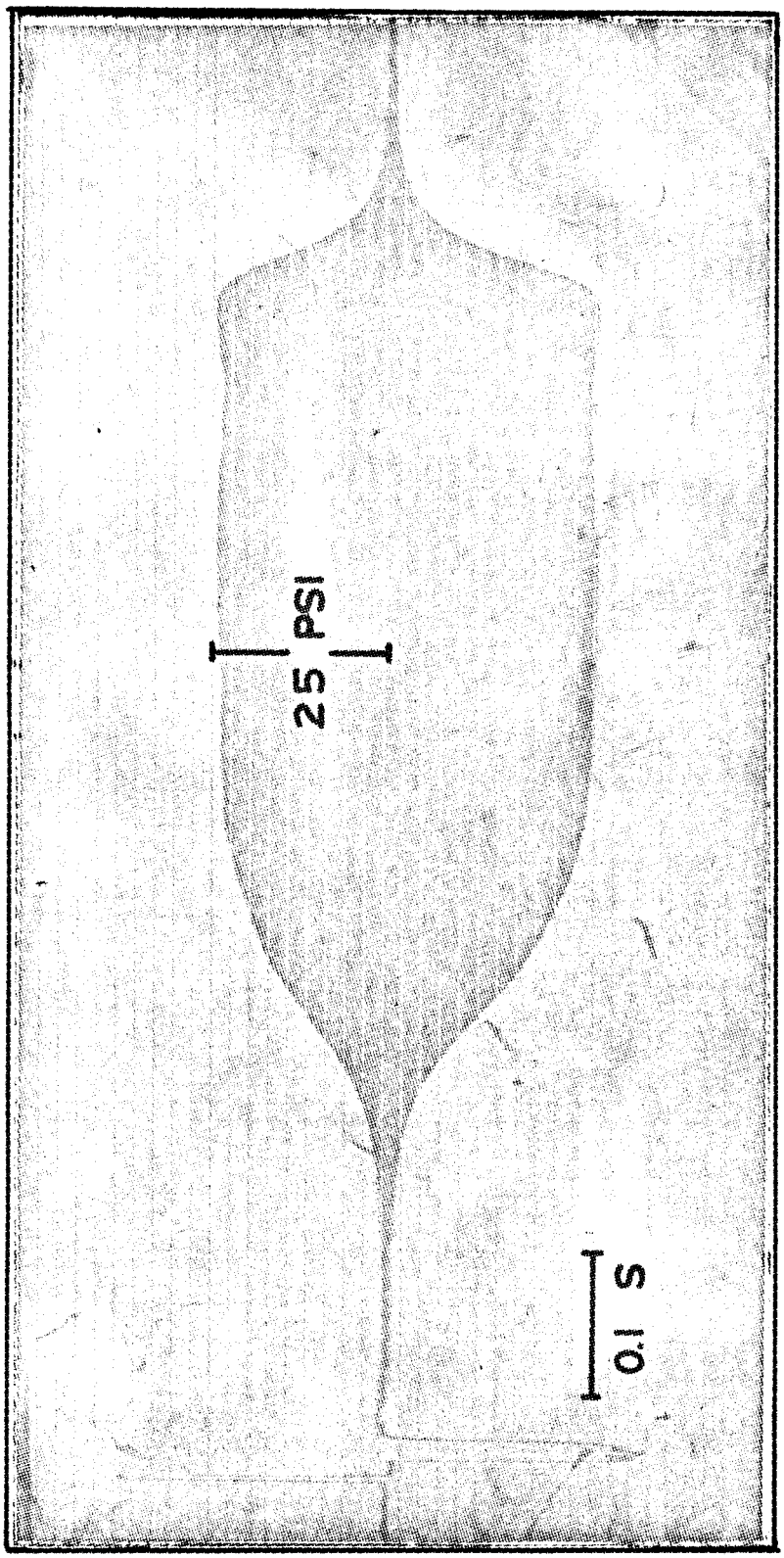

Figure 6. Oscillograph Record of a Near Ideal Test.

but almost 0.2 second elapses before the amplitude is large enough to be measured accurately. By statically calibrating the pressure transducers prior to each set of tests on a dead-weight tester, the amplitude could be determined to an accuracy of two to three percent. For this particular test, the waves grow until a limiting amplitude, $\bar{p}'$, of 25 psi is reached at about 0.45 second into the test. The amplitude remains essentially constant until burnout, which occurs at 0.82 second. Then, because of losses in the chamber, the oscillations decay and finally disappear during the next 0.1 second. Thus, less than a second is required for the entire firing.

For a variety of reasons, one is interested in measuring the mean burning rate of the propellant. Since the propellant thickness was known very accurately, the mean burning rate was determined with an accuracy of about three percent by dividing this thickness by the observed burn time.

Frequency measurements were obtained by counting the number of oscillations occurring in a short interval of time. By including a 1.0 kHz reference signal on the tape recordings, the accuracy of these measurements was very good.

The most important T-burner measurements are those of the growth and decay constants of the oscillations, since the admittance is determined from these. Unfortunately, they are also among the most difficult data to obtain accurately because they involve consider-

able test interpretation and data reduction.

As a rule, growth constant data show less scatter than do those obtained for decay constants. A probable reason for this is that chamber conditions are changing rapidly during the decay, and hence, the decay rate may vary with time. Considering this, it is surprising that the decay rates observed in most of the tests remained as constant as they did.

For a majority of the tests, the growth and decay constants were determined to an estimated accuracy of five percent. These measurements were made by plotting the amplitude during growth and decay semi-logarithmically against time. By fitting the best straight line to the plots and calculating its slope, the appropriate constant was determined. As an example, if p'_1 and p'_2 are the amplitudes at times t_1 and t_2 on the straight line portion of the semi-logarithmic growth plot, then the growth constant is

$$\alpha_g = \frac{\ell n(p'_2/p'_1)}{t_2 - t_1} \quad .$$

For the test of Figure 6, the amplitude versus time plots, along with the calculations for the growth and decay constants, are shown in Figure 7. In the upper plot, the time origin has been taken as that instant when oscillations first appeared. In the lower plot, burnout has been taken as the origin in time.

The growth and decay frequencies were defined as those values

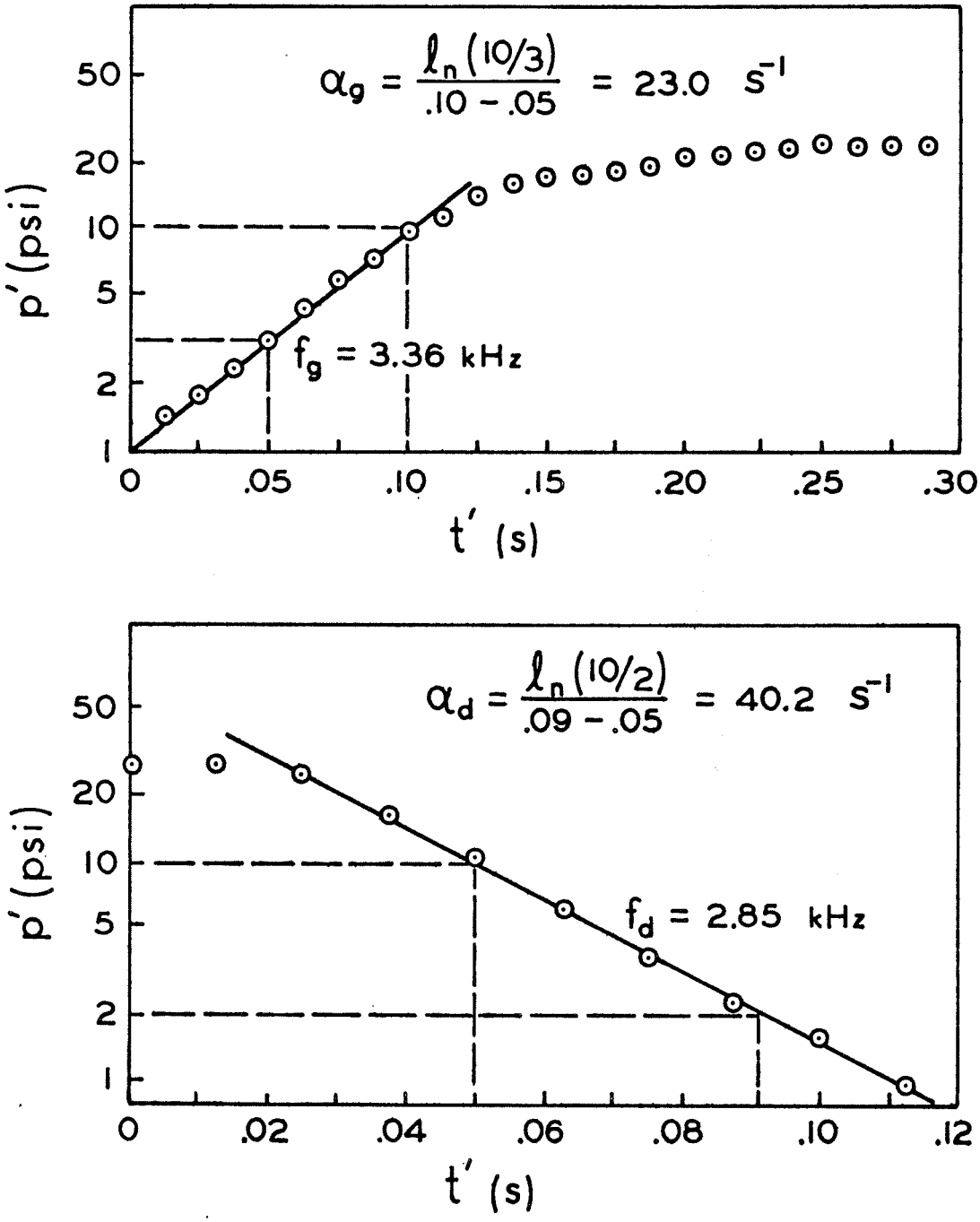

Figure 7. Plots Showing the Method Used to Calculate the Growth and Decay Constants.

falling approximately midway along the straight line portion of the plots. In Figure 7 these are indicated as 3.36 and 2.85 kHz, respectively. As a rule, the frequency did not vary greatly during growth, although a slight decrease was usually observed. During decay, however, decreases of up to 25 percent were often present, due to the rapid cooling of the gases.

Although a majority of the tests resulted in records similar to that shown in Figure 6, a number produced less satisfactory results for one reason or another. One such case is shown in Figure 8 where, among other things, it is apparent that the oscillations do not reach a well-defined limiting amplitude. Instead, upon reaching what appears to be a limiting value at about 0.4 seconds after ignition, the waves continue to grow slowly during the remainder of the test. In such cases, the limiting amplitude was taken as the average value observed. What is meant by "average value" will become more apparent in Section X, which discusses the nature of the limiting amplitude in greater detail.

A second feature of this test is that the oscillations appear almost immediately after ignition, then decay, and finally start to grow. This behavior was observed often in tests, such as this one, conducted at frequencies of less than 1 kHz. The response of the propellant is very high at low frequency, which means that any disturbance, such as the ignition pressure itself, is significantly amplified. However, be-

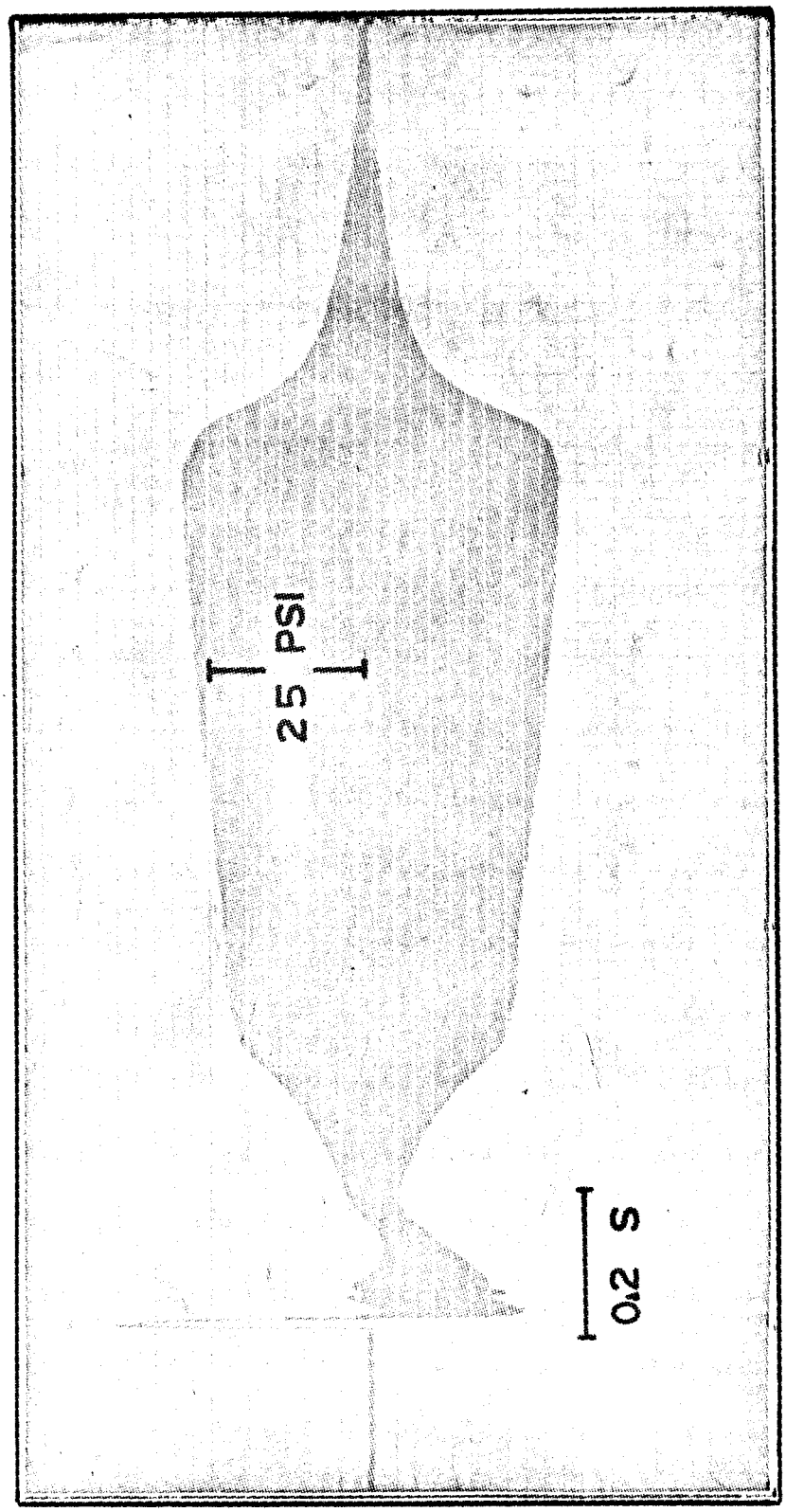

Figure 8. Oscillograph Record of a Less Ideal Test.

cause a short interval of time elapses before the propellant is burning over its entire surface, the chamber losses overcome the driving, and the waves decay. The ignition transient is soon over, and then the burning propellant does indeed begin to drive the waves.

Naturally, under circumstances such as these, the growth is not exponential at first. However, after a short transition period, the waves do grow exponentially, and the growth constant can be calculated as before.

The most curious feature about this particular test is the decay, which, as shown in Figure 9, occurs in two distinct stages. Immediately after burnout, the amplitude decreases with an initial decay constant, α_{di}, of 11 s^{-1} while the frequency drops from .68 kHz to .52 kHz. Then, a distinct change in the decay rate occurs, and the final decay constant, α_{df}, is only about half the initial value. Likewise, the rate of frequency decrease is much less during the second stage.

This behavior was observed often in low frequency tests, particularly in those using 540-A propellant, and was quite reproducible. It is decidedly different from that caused by poor ignition procedures, which will be described in Section VI. It presumably arises from the fact that chamber conditions change significantly during decay. In the longer chambers the gases, even during burning, are relatively cool over a large portion of the chamber because of heat transfer to the walls. In addition, because the losses are fairly small at low fre-

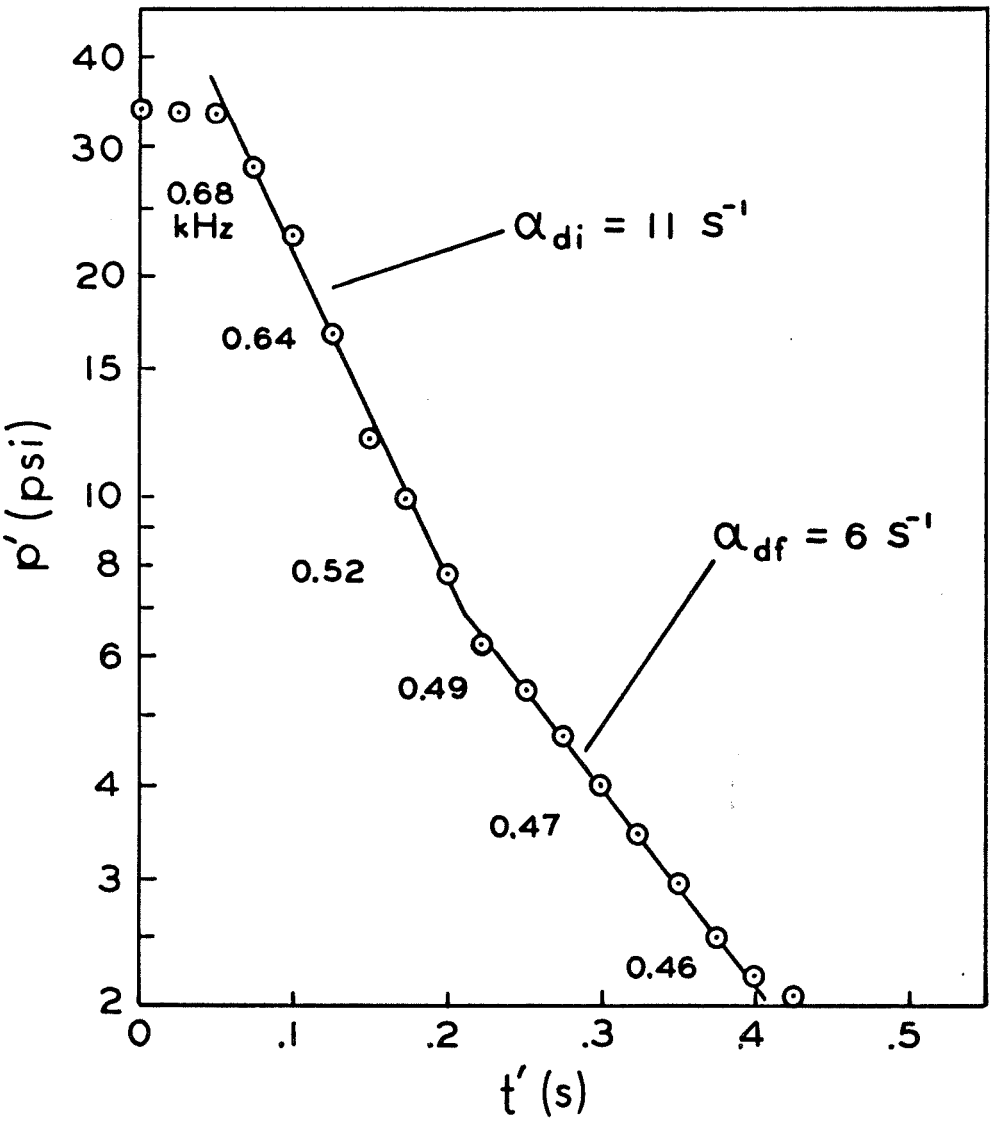

Figure 9. Decay Plot for Test Shown in Figure 8. Two Distinct Decay Rates Are Apparent.

quency, the decay period can be quite long. Thus, the gases become even cooler during the decay, and, conceivably, can begin to condense on the walls. As a result, the decay rate changes significantly.

Naturally, it is in firings such as this that test interpretation becomes very important. All of the various T-burner analyses[7,9], including that outlined in Appendix B, assume linearized behavior in the burner. Thus, to be valid, measurements of growth and decay should be made while the amplitude is very small. For the growth constant, this presents no particular problem. However, for the decay constant, the situation is more complex. There, because of rapidly changing chamber conditions, if one waits until the amplitude is small, he may measure chamber losses under conditions quite different from those present during growth. On the other hand, by taking measurements immediately after burnout, the assumptions of linear behavior may be violated. Obviously, compromise is the only way out of this predicament. As a result, decay constants were obtained by observing the waves while their amplitude was between 70 and 5 percent of its limiting value. For tests showing two distinct decay rates, the initial rate was used to calculate the decay constant on the basis of the argument presented above.

By examining the test records in the manner outlined here, the data presented in the tables of Appendix A were obtained. A number of

tests were exploratory in nature and involved rather singular test conditions and, hence, could not be included in the tables. However, in such cases where significant results were obtained, the individual test will be discussed in the text itself.

V. SOME T-BURNER PROPERTIES IN NON-DIMENSIONAL FORM

Like the properties of many other devices, those of the T-burner can be presented perhaps most clearly in terms of non-dimensional variables. In addition to providing a better feeling for the various quantities involved, such groupings also lay the foundation for discussions that will follow. Most of the features of the T-burner are associated with either the mean flow or the oscillations. Thus, it is appropriate to characterize these two aspects of the burner in terms of non-dimensional variables first, and then relate the other properties to these.

The mean flow itself is best described by the Mach numbers at the burning surface and vent. These represent, respectively, the minimum and maximum values attained by the flow. In Section II, the Mach number at the burning surface was found to be

$$M_b = \frac{\rho_s \bar{r} a_b}{\gamma P}. \qquad (5.1)$$

Taking the following values as typical of those encountered in T-burner tests,

$\rho_s = 1.5$ cm/cm^3 $\qquad$ $\gamma = 1.28$

$\bar{r} = 0.5$ cm/s $\qquad$ $P = 2 \times 10^7$ dynes/cm^2 (300 psia)

$a_b = 10^5$ cm/s

we find by the above equation that the Mach number at the burning sur-

face is only about 0.003. Multiplying this by the speed of sound, a_b, we find that the velocity there is typically 3 meters/sec.

Because the flow area at the vent is considerably smaller than at the burning surface, the Mach number there, denoted as M_v, is substantially greater. For one-dimensional isentropic flow, the mass flow per unit area, expressed as a function of the Mach number M, is

$$m = P_o \sqrt{\frac{\gamma}{RT_o}}\, M \left(\frac{1}{1 + \frac{\gamma-1}{2} M^2} \right)^{\frac{\gamma+1}{2(\gamma-1)}} , \qquad (5.2)$$

where P_o and T_o are the stagnation pressure and temperature. If the flow in the burner is taken as steady, the total mass flow at the vent, $m_v S_v$, is equal to the sum of the total mass flows at the two ends of the burner. Applying equation (5.2) at both burning surfaces as well as the vent and taking the preceding condition into account, it follows that

$$\frac{S_v}{2S_b} = \frac{M_b}{M_v} \left(\frac{1 + \frac{\gamma-1}{2} M_v^2}{1 + \frac{\gamma-1}{2} M_b^2} \right)^{\frac{\gamma+1}{2(\gamma-1)}} \qquad (5.3)$$

where, of course, S_v and S_b are the areas of the vent and the burning propellant surface, respectively. For a propellant diameter of 1.5 inch and a vent diameter of 0.4 inch, $S_v/2S_b = 0.036$. Assuming the value for M_b found earlier, this equation shows that the Mach number at the vent is about 0.08, considerably greater than M_b but still far

from unity. With a speed of sound of 10^5 cm/sec, the flow velocity at the vent would be 80 meters/sec. Thus, the flow never approaches choked conditions within the burner or vent. Naturally, when a surge tank is used to provide the pressurization, the vent diameter is chosen to assure subsonic conditions there.

Just as the mean flow can be described in terms of appropriate Mach numbers, so can the oscillations be characterized by an oscillatory Mach number, defined as

$$M' = \frac{|u'|}{a} \quad , \tag{5.4}$$

where $|u'|$ is the maximum magnitude of the velocity oscillations. For a sinusoidal wave it can be shown that $|u'|$ is related to the pressure amplitude, p', by

$$\frac{|u'|}{a} = \frac{p'}{\gamma P} \tag{5.5}$$

where P is the mean pressure. Thus, the oscillatory Mach number is

$$M' = \frac{p'}{\gamma P} \quad . \tag{5.6}$$

Since the oscillations grow and decay during the test, this number obviously varies from zero to some maximum value determined by the limiting amplitude, $\overline{p'}$. Often the limiting amplitude reaches 15 to 20 percent of the mean pressure. Under such conditions, equation (5.6) indicates an oscillatory Mach number on the order of 0.1. This, in turn, implies a maximum velocity of 100 meters/sec, some 30 times greater than the axial velocity of the mean flow. Naturally,

when the oscillatory velocity is greater than the mean velocity, the flow will undergo reversal in direction twice each cycle. Since the acoustic velocity all but vanishes at the ends of the chamber, it is appropriate to determine, for a given amplitude of oscillation, over what portion of the burner length does this reversal occur. If $|u'|$ denotes the maximum value of the acoustic velocity, then the oscillatory velocity along the chamber is approximately

$$u'(x) = |u'| \sin \frac{\pi x}{L} \quad , \tag{5.7}$$

where x is the distance from one end of the chamber and L the chamber length. For flow reversal to occur, u' must equal the mean velocity, $\bar{u}$, which, by definition, is just aM_b. With equation (5.5) and the above, we find this condition is met when

$$\frac{p'}{\gamma P} \sin \frac{\pi x}{L} = M_b \quad . \tag{5.8}$$

Taking p' as five percent of the mean pressure and M_b as 0.003, we find from the above that

$$x/\tfrac{1}{2}L = 0.05 \quad .$$

Thus, for a wave of only 5 percent of the mean pressure, the acoustic velocity exceeds the mean velocity for more than 95 percent of the chamber. For all practical purposes then, it can be assumed that the flow undergoes reversal all the way from the burning surface to the vent.

The number of reversals for a particular fluid particle is obviously the length of time required for the flow to travel half the chamber length multiplied by twice the number of cycles per unit time which, of course, is the frequency. If $\bar{u}$ is the mean flow velocity and N the number of reversals for each particle, then

$$N = 2 \frac{\frac{1}{2}L}{\bar{u}} f \quad . \tag{5.9}$$

However, by equation (2.1), $a = 2Lf$; and by equation (2.20), $\bar{u} = aM_b$. With these relations, the above expression becomes

$$N = \frac{1}{2M_b} \quad . \tag{5.10}$$

Taking M_b as 0.003 again, we find that a given fluid particle undergoes approximately 160 reversals in flow direction before it reaches the vent. Needless to say, with such processes occurring, it is doubtful if a normal mean flow boundary layer develops on the wall of the burner. This point will be taken up again in the discussions of the acoustic losses of the T-burner.

However, with regard to boundary layer considerations and, in particular, to heat transfer processes, it is appropriate to estimate the Reynolds number associated with both the steady and oscillatory flow. For the former, the Reynolds number based on chamber diameter is

$$Re = \frac{\rho \bar{u} D}{\mu} \quad . \tag{5.11}$$

However, it was shown in equation (2.21) that by continuity $\rho u = \rho_s \bar{r}$, where ρ_s is the solid propellant density and $\bar{r}$ the steady linear burning rate. Using this relation, the mean flow Reynolds number becomes

$$Re = \frac{\rho_s \bar{r} D}{\mu} \quad . \tag{5.12}$$

For typical mixtures of combustion gases, the viscosity coefficient, μ, is approximately 4×10^{-4} gm/cm-sec for temperatures in the range of 1000 to 1500°K. Using the previously assumed values for the other terms, this equation shows that the Reynolds number for the mean flow is typically 7500. If the flow were steady, one would expect it to be turbulent on the basis of this Reynolds number.

Of course, as was demonstrated earlier, the dominant velocity in the T-burner is generally that associated with the oscillations. If one uses this velocity to calculate an "acoustic Reynolds number," Re_a, then

$$Re_a = \frac{\rho u' D}{\mu} \quad , \tag{5.13}$$

where again the characteristic length has been taken as the chamber diameter. With equations (5.4) and (2.20) it is easy to show that

$$Re_a = Re \frac{M'}{M_b} \quad . \tag{5.14}$$

Using previously determined values for the quantities on the right side of this equation, we find that the acoustic Reynolds number is about 10^5. Although the relevance of this acoustic Reynolds number

is not presently apparent, it will later be shown that it is indeed significant with regard to the surface heat transfer in the burner.

Despite the fact that the oscillations often attain large amplitudes, the energy associated with the waves is still very small compared to the thermal energy of the combustion gases. This is easily demonstrated by realizing that for a standing sinusoidal wave of amplitude p', the acoustic energy per unit volume is

$$e_a = \frac{1}{4} \frac{p'^2}{\rho a^2} \quad . \tag{5.15}$$

Likewise, for a perfect gas at temperature T, the internal energy per unit volume is

$$e_T = \rho c_v T \quad . \tag{5.16}$$

Dividing, and realizing that for a perfect gas $a^2 = \gamma P/\rho$, $P = \rho RT$, and $R = (\gamma-1)c_v$, we find

$$\frac{e_a}{e_T} = \frac{\gamma-1}{4\gamma} \left(\frac{p'}{P} \right)^2 \quad . \tag{5.17}$$

Taking the amplitude as 30 percent of the mean pressure, which is about the maximum observed, we find that the acoustic energy is at most only one-half of one percent of the mean thermal energy. Thus, if even a very small fraction of the energy of the combustion gases becomes coupled with the acoustic field, very sizable oscillations can result. It is precisely because of this fact that the propellant, despite its small acoustic admittance and low mean flow velocity, can drive such large oscillations in the T-burner and rocket motors.

VI. A COMPARISON OF VARIOUS IGNITION PROCEDURES

Since an instantaneous ignition and burnout are implicitly assumed in the T-burner theory, a poor ignition resulting later in a slow, uneven burnout of the two propellant disks could certainly have an adverse effect on the test results. Consequently, during the studies four different ignition techniques were tried and their effects on the data compared.

In all four cases, a pyrotechnic "ignition paste" was used to some extent, the major distinction among the four techniques being the type and amount of paste used. Applied to the propellant face, this paste was ignited by passing a 28-volt d. c. signal through a half-inch length of 34-gauge Nichrome wire. Copper leads, fed through a connection in the vent and passed along inside the burner to the propellant, connected the power supply to the Nichrome "hot-wire." The paste, burning rapidly with a hot flame, ignited the propellant in turn. Tests conducted in transparent burners showed that the entire process occurred in a few hundredths of a second.

Of two types of ignition paste used, the first, supplied by the Naval Weapons Center, was denoted as X-225 and consisted of

polyisobutylene	6.0 wt. percent
boron powder	6.9 wt. percent
titanium powder	14.8 wt. percent
potassium perchlorate	72.3 wt. percent

Because of concern over possible attenuation effects arising from metal particles in the combustion products of this paste, another, denoted as CIT-1, was also used and contained the following:

polyisobutylene	10.0 wt. percent
ammonium perchlorate	90.0 wt. percent

The four ignition procedures are briefly described below. In all four cases, Carter's Rubber Cement was used to attach the hot-wire, or tablet containing the hot-wire, to the propellant.

Method 1: X-225 paste was applied to the entire propellant face, forming a layer approximately 0.01 inch thick. To this layer was attached a small tablet of X-225, weighing roughly 0.5 gram, containing the hot-wire.

Method 2: X-225 was applied as above to the propellant. The hot-wire was attached directly to the layer of paste with no tablet being used.

Method 3: X-225 was applied only to a small spot in the center of the propellant face. The hot-wire, which had been coated with X-225 paste by dipping it briefly in the paste, was attached to the spot of paste.

Method 4: CIT-1 paste was applied to the entire propellant face. To this was attached the hot-wire, coated with X-225 as in the previous case.

Of the four methods the first was definitely the best, according to the test data. It produced burn times that were not only highly reproducible but also consistent with known strand burning rates. In tests using this method, the frequency generally decreased almost at the instant when the amplitude started to decay at the end of the firing. This was interpreted as an indication that burnout had occurred not only rapidly, but also very evenly over the entire propellant face. Transparent burner tests showed that the tablet of X-225, upon being ignited, sprayed burning particles over the propellant surface, igniting the paste wherever contact was made. Since this occurred quickly, so did ignition of the propellant face.

Method 2, while yielding fair test reproducibility, was judged generally inferior to the first method. The burn times were, on the whole, longer and the decays less well defined, indicating probably a slower burnout. Again, the transparent burner, to be discussed more fully later, proved most useful in understanding the quality of the second method. The paste near the hot-wire ignited very soon after the firing command had been given. However, a considerable time often elapsed before ignition of the entire surface occurred. Without the igniter tablet used in the first method, ignition depended more on the flame spread speed of the paste itself, which apparently is reasonably slow. There were instances, however, when a rapid ignition was observed using this method, but this appeared to be somewhat random,

depending on burning particles bouncing off the chamber wall and other particles back onto unignited regions. Clearly, the igniter tablet of Method 1 produced a more dependable spray of hot particles across the propellant surface.

Of the four methods, the third was by far the worst, resulting in long burn times and very poor decays of amplitude and frequency. In general, the oscillations were delayed for a considerable time and grew slowly in tests using this method. Although no transparent burner tests were obtained with this procedure, it is clear that ignition in this case depended on the flame spread of the propellant itself, which, with no flow parallel to the propellant surface, was probably very slow.

Finally, the fourth method provided data comparable to that obtained from tests using Method 2, indicating the absence of effects arising from metal particles in the ignition paste. The transparent burner studies showed that most of the products of the ignition paste are flushed out of the chamber by the propellant gases before the oscillations begin. This would explain the lack of influence of the metallized ignition paste on the test data.

In Figure 10, the oscillatory pressure and frequency are shown for two tests which differed only in the ignition procedure followed, the upper test using Method 1 and the lower Method 3. From the preceding remarks it is clear that the tests represent the two ex-

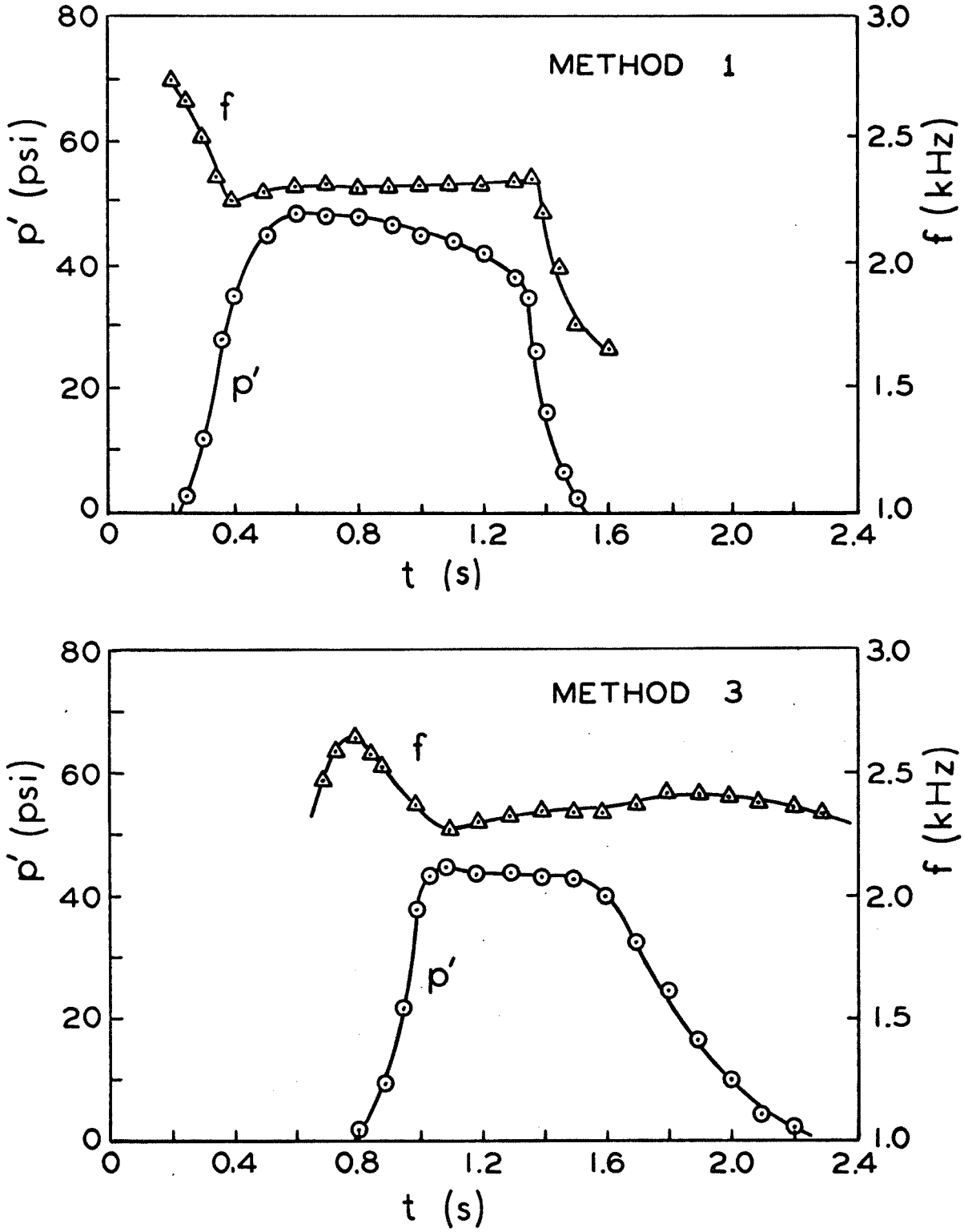

Figure 10. Comparison of Two Tests Which Differed Only in the Ignition Method Used.

tremes as far as quality of ignition is concerned. Using A-13 propellant at a chamber pressure of 300 psig, the tests were conducted in 1.5-inch diameter chambers measuring 7.0 inches in length.

Of the many differences observed in the two test records, a few are readily apparent. First, in the upper test, using Method 1, the oscillations appear approximately 0.2 sec after ignition, but in the lower test almost 0.8 sec elapses before any oscillations develop. This is presumably because in the second case a considerable length of time is required before enough propellant is burning to drive the waves. Burnout occurs at about 1.35 sec in the upper test and at 1.55 sec in the lower, if burnout is taken as that instant when the pressure amplitude begins to decay. Clearly, the frequency does not decrease in the lower test until the oscillations have all but disappeared. Apparently a portion of the propellant continues to burn long after the rest has burned out. In the upper test, however, the frequency decreases immediately after the oscillations start to decay.

These qualitative differences take on greater significance when their quantitative effects become apparent. Below are some of the data derived from the two tests of Figure 10:

	Upper Test (Method 1)	Lower Test (Method 3)
burn time, t_b (s)	1.35	1.55
delay time (s)	0.2	0.8

	Upper Test (Method 1)	Lower Test (Method 3)
growth constant (s^{-1})	33	17
decay constant (s^{-1})	20	10
limiting amplitude, $\bar{p}'$ (psi)	49	43
admittance real part, A_b^r	.0035	.0014

From these results it is apparent that ignition procedures alone can account for errors on the order of 100 percent in measurements of the growth and decay constants, leading to even larger errors in the values inferred for the admittance. This certainly emphasizes the importance of establishing a rapid and even ignition, and indicates that much of the disagreement between various laboratories conducting T-burner tests may arise from significant differences in the ignition procedures followed.

Since ignition plays such an important role in T-burner tests, it is fortunate that faulty ignition procedures can often be detected from certain aspects of the test records. By far the easiest means of detecting a poor ignition is to examine the record after burnout has supposedly occurred. The first indication of poor ignition is the absence of a frequency decrease accompanying the amplitude decay. This can only mean that some propellant is continuing to burn, since otherwise the gases would cool very rapidly.

Of course, a frequency decrease accompanying the amplitude

decay still does not signify a good ignition; it simply means that the ignition was at least fair. In the present tests, the qualitative behavior of the amplitude decay seemed to be the best indicator of ignition quality. Examples of this are afforded by Figure 11, in which the decaying oscillatory pressure of the two tests in the preceding figure is plotted semi-logarithmically against time. Clearly, in the upper test, using Method 1, the pressure decay begins very rapidly and continues at a constant rate for the entire period of time shown. In the second test, on the other hand, burnout is not at all obvious and never does the decay become truly exponential with a constant decay rate. Instead, the decay rate increases slowly with time, probably as a result of more and more propellant burning out. But, even after a significant length of time, the decay constant of the second test is still only half that observed in the other case. This is despite the fact that the only difference between the two firings was the ignition method used. This "rounded" decay exhibited in the second test is typical of that observed in tests where poor ignition occurred and is probably the best indication of such ignition faults.

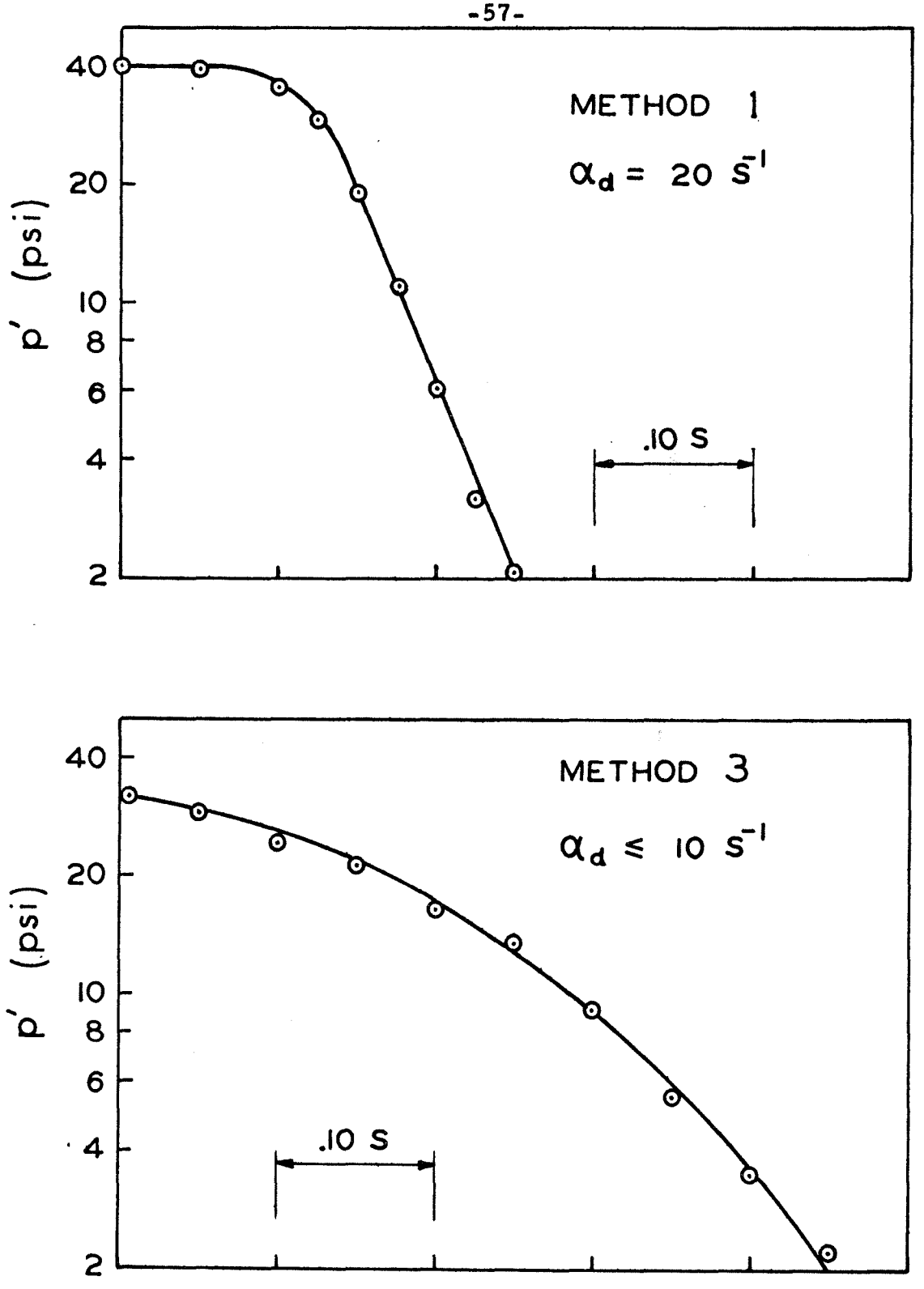

Figure 11. Comparison of the Decay Periods of the Two Tests Shown in Figure 10.

VII. TRANSPARENT T-BURNER STUDIES

Since certain aspects of the T-burner, such as the nature of the flow field, are difficult to determine from the usual test records, a few firings were conducted in transparent Lucite chambers to permit high-speed cinematography of the tests. The latter was provided by a Hycam Model 400 motion picture camera operating at a rate of 8000 frames per second, which, since the oscillation frequency was on the order of 1 kHz, permitted several frames during each cycle. The Lucite chambers had an inner diameter of 1.5 inch and a wall thickness of 0.25 inch. Their lengths ranged from 7.0 to 13.0 inches.

Lucite was selected after initial attempts to use Pyrex had resulted in problems associated with providing an adequate pressure seal between the chamber and vent. Because the Lucite performed so well, further attempts to use Pyrex were abandoned. The only problem found with the Lucite was a tendency for the inner walls of the chamber to become frosted during the test. However, this occurred very slowly, and the rugged nature of this material far outweighed this one disadvantage.

One of the transparent burners used is shown in Figure 12. For this particular test, the chamber length was 10.0 inches and Method 2 ignition procedures were used. As can be seen, bolt-together end caps were used as was a saddle arrangement for the vent connection.

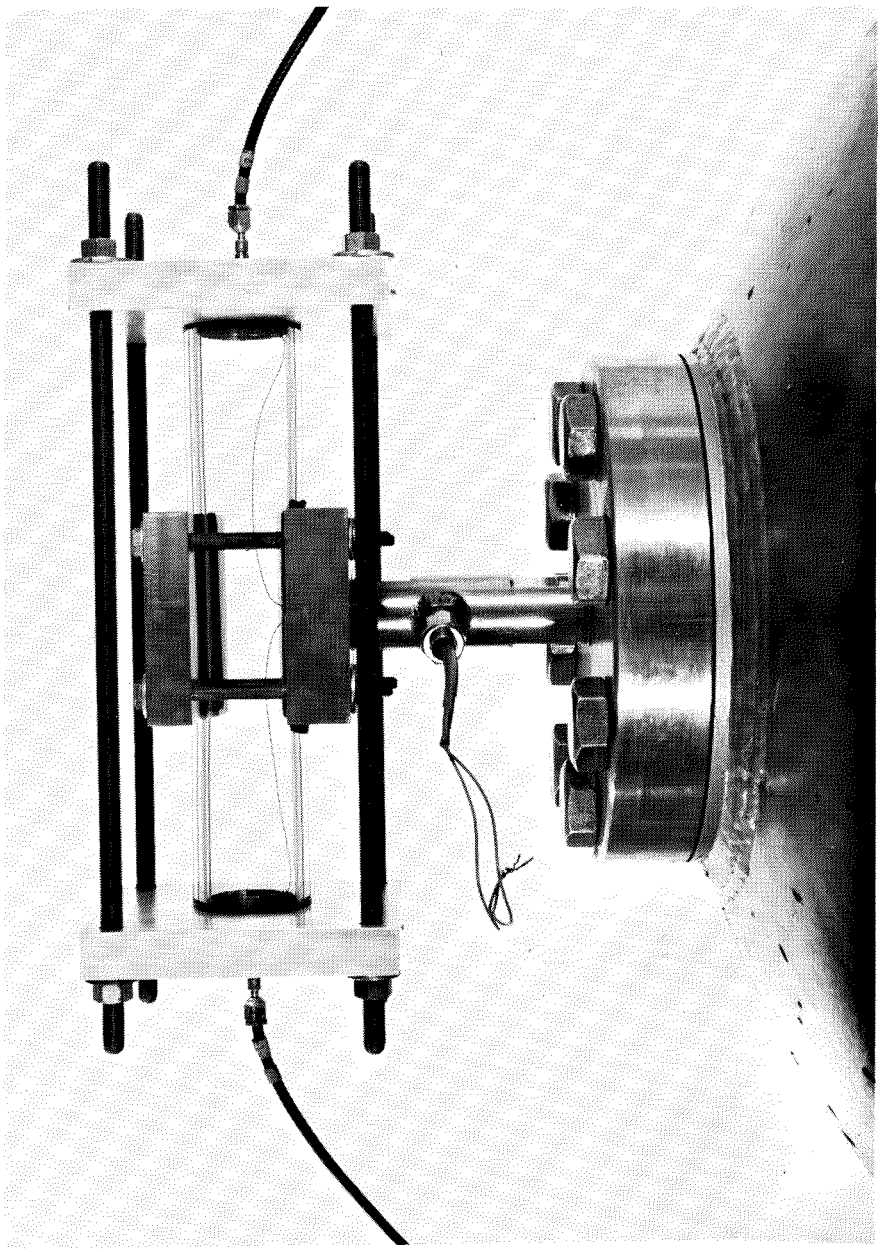

Figure 12 . The Transparent T-Burner.

The main difficulty encountered was the tendency of most burning propellants to form dark deposits on the chamber walls during the test which, of course, obscured the view considerably. Fortunately, T-17 propellant is very clean burning and exhibited none of this behavior. Consequently, it was used for most of the tests. Besides being clean burning, T-17 also was unstable enough to drive sizable pressure oscillations. Often the limiting amplitude exceeded 20 percent of the mean pressure, which was arbitrarily chosen as 115 psia.

There was some initial concern that the Lucite chambers, being less rigid and having thinner walls than their steel counterparts, might adversely affect the test results. These fears were soon allayed by comparisons of data obtained in both types of chambers. Below are the results of one such comparison. For these two tests, the chamber length was 13.0 inches and the propellant was T-17.

	Steel Chamber	Lucite Chamber
growth constant (s^{-1})	22.2	22.9
decay constant (s^{-1})	10.5	10.0
mean frequency (kHz)	1.06	1.04
limiting amplitude (psi)	29	26

The excellent agreement observed here is representative of that found in other comparisons and indicates that the transparent burner is as useful a device for normal tests as is the steel T-burner, ex-

cept, of course, at high pressures where the former obviously cannot be used.

Naturally, the real value of the transparent burner lies in the motion pictures obtained from tests conducted in it. Because of the many frames involved to cover even a short span of time, these do not lend themselves well to display here. However, Figure 13 shows a single frame obtained during one test, which demonstrates rather clearly the important finding that the flow in the T-burner is essentially one dimensional, as assumed. Naturally, near the vent, three-dimensional effects appear, but this region comprises a relatively small portion of the burner. This particular photograph was obtained shortly before the oscillations appeared. Although the flow underwent reversal after the onset of oscillations, it still remained basically one dimensional. No circulating secondary flows were observed at all. Pulsations of light, out of phase at the two ends of the burner, were clearly visible and presumably arose from temperature oscillation.

In addition to providing these interesting observations, which certainly helped to establish the validity of several assumptions regarding the burner itself, the transparent burner proved most useful in comparing and evaluating the various ignition procedures discussed in Section VI. Some of the differences between the methods are rather subtle and would have been difficult to understand without the

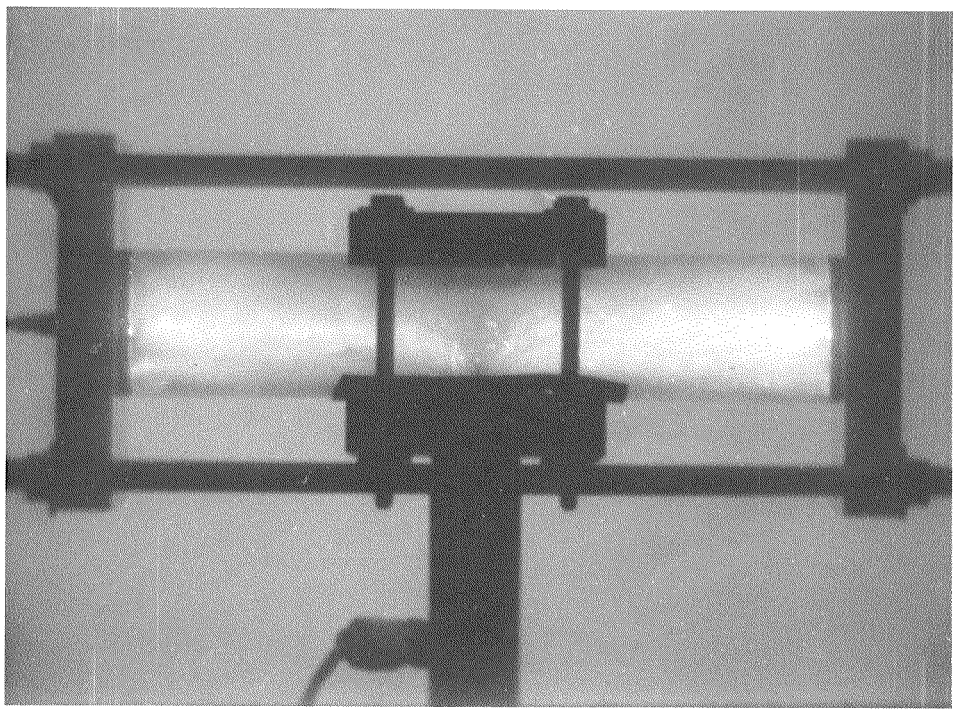

Figure 13. The Transparent T-burner During a Firing.

photographic records. For instance, it was abundantly clear from the motion pictures that the igniter tablet used in ignition Method 1 provided a very rapid and reliable ignition by spraying hot particles across the propellant face. From the films it also became apparent why Method 2 sometimes produced a good ignition and sometimes did not. If hot particles of burning paste happened to collide just right and bounce back onto unlit portions, then a rapid ignition could be obtained by this method also. Because of the random nature of this process, this method proved less reliable than the former. Thus, with the transparent T-burner,not only the effects of the various ignition procedures could be observed but also the causes behind these effects.

These observations and comparisons, while important in themselves, serve only to indicate the many applications which exist for a burner of this type. Of the many studies, those conducted with the transparent T-burner certainly provided some of the most interesting and enlightening insights into the nature of the burner.

VIII. HEAT TRANSFER IN THE T-BURNER

It has been mentioned several times in previous sections that because of heat transfer to the chamber walls the combustion gases are considerably cooler by the time they reach the vent than they were upon leaving the burning surface. Although a few direct temperature measurements were made, this is usually inferred from the fact that the observed frequency is lower than would be expected from calculations based on the adiabatic flame temperatures of the propellants used. Since the frequency is related to the mean speed of sound by

$$f = \bar{a}/2L \ , \qquad (8.1)$$

where L is the distance separating the burning propellant surfaces, measurements of the frequency can easily be interpreted as measurements of the mean speed of sound in the burner. Since, for a perfect gas

$$\bar{a}^2 = \gamma R \bar{T} \ , \qquad (8.2)$$

these latter values can be used to determine the mean temperature of the combustion gases present.

In Figure 14 the mean speed of sound, as inferred from such measurements, is shown as a function of chamber length for A-13 propellant at 300 psig in 1.5 inch diameter chambers. Clearly, the mean speed of sound, and hence the temperature, decreases with increasing chamber length. Far more interesting, however, is the fact

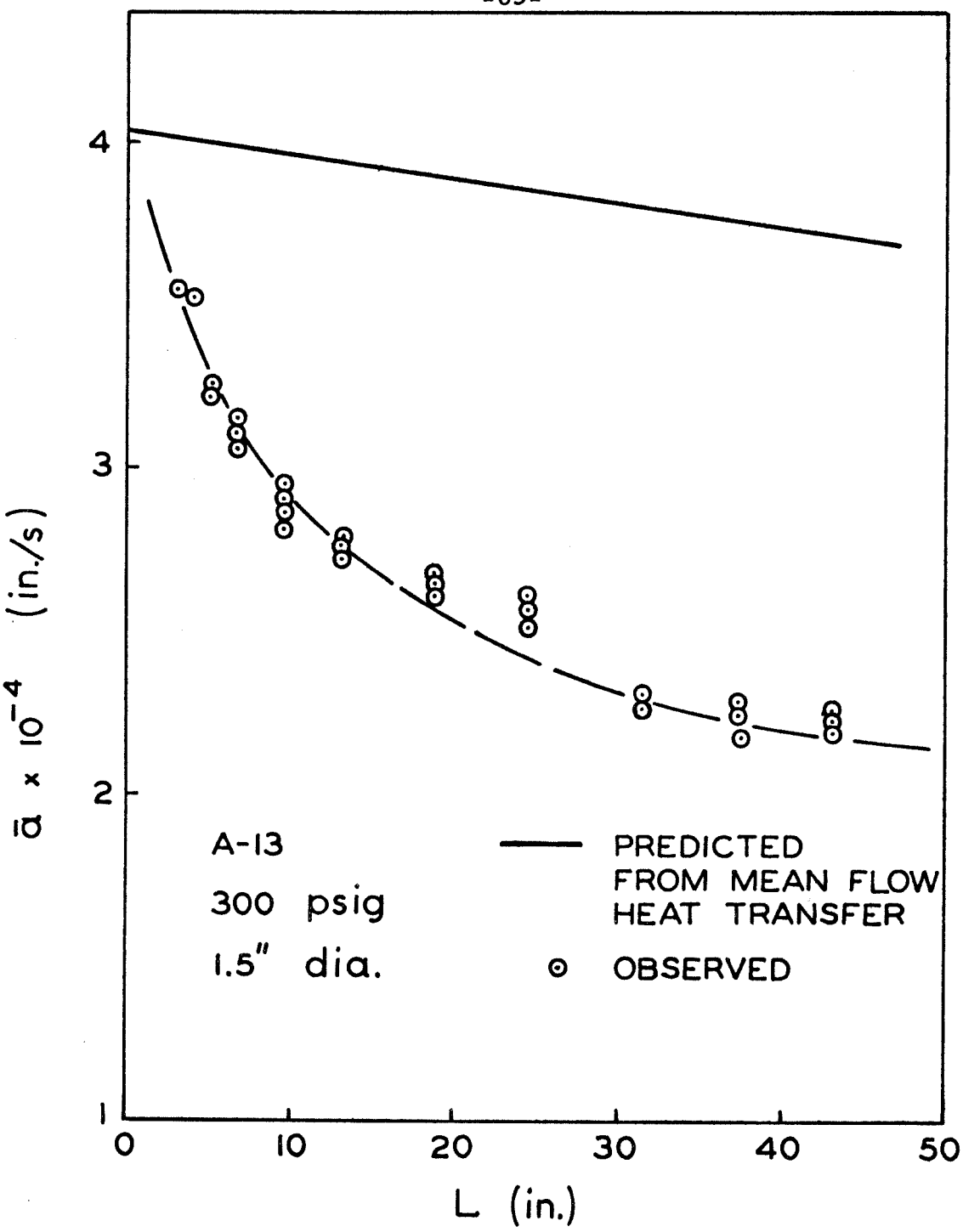

Figure 14. Average Speed of Sound as a Function of Chamber Length.

that the speed of sound is considerably lower than would be expected from heat transfer calculations based on the mean flow. The latter values are shown as the solid line near the top of the figure and will be discussed more fully somewhat later. Such significant differences can only imply that the heat losses from the gases to the chamber walls are considerably greater than would be expected. With the large oscillations being a distinctive feature of the flow in the T-burner, it was decided to investigate the heat transfer as a function of the oscillatory amplitude.

Although other studies[12] have been made of heat transfer under oscillatory conditions, very few have dealt with oscillations as large as those encountered in the T-burner, where the oscillatory velocity is often one to two orders of magnitude larger than the mean velocity. In one case[13], however, the T-burner was actually used to calculate heat transfer rates in the presence of such large oscillations. Although that study involved a completely different approach from the one which follows, and interpreted the results in a significantly different way, it did conclude that in general the oscillations increase the heat transfer to the walls. The present studies certainly support this conclusion and, perhaps more importantly, have resulted in a good correlation between the heat transfer rate and the amplitude of the oscillations. Consequently, it now may be possible to predict the increases of heat transfer in rocket motors which have long been

known[14] to accompany combustion instability. In fact, it is conceivable that the T-burner could become an important tool for studying heat transfer under such conditions and thereby assume an even broader role.

In the past, considerable attention has been given to the problem of determining the heat transfer from gases flowing inside tubes. The heat transfer is often characterized by a convective heat transfer coefficient, h, defined by

$$h = \frac{\dot{q}_w}{T_g - T_w} \quad , \tag{8.3}$$

where $\dot{q}_w$ is the heat transfer rate per unit wall area and T_g and T_w are the temperatures of the gas and wall, respectively. In general, h depends on the geometry involved as well as the nature of the flow.

In Section V it was noted that the Reynolds number based on mean velocity and chamber diameter is about 7500 for the flow inside the T-burner. Likewise, the Reynolds number based on the acoustic velocity was found to be about 10^5. A steady flow with either of these Reynolds numbers would most likely be turbulent. For fully-developed turbulent flows, many attempts have been made to correlate observed values for the heat transfer coefficient with the various fluid dynamic variables. Perhaps the best known, and certainly one of the most satisfactory, correlations is[15]

$$\frac{hD}{k} = 0.023 \left(\frac{\rho u D}{\mu}\right)^{0.8} \left(\frac{\mu c_p}{k}\right)^{0.4} \quad . \tag{8.4}$$

The dimensionless combination hD/k is recognized as the Nusselt number, $\rho uD/\mu$ as the Reynolds number, and $\mu c_p/k$ as the Prandtl number, where k is the thermal conductivity and μ the viscosity coefficient. Using these dimensionless variables, the above can be written more simply as

$$Nu = 0.023\, Re^{0.8} Pr^{0.4} . \qquad (8.5)$$

In rocket motors, very large temperature differences usually exist between the hot combustion gases and the cool chamber walls. Consequently, the fluid properties can vary greatly, depending on what temperature is used to evaluate them. Quite often, the arithmetic mean between the gas and wall temperature is used. As an example, Bartz[14] found the following semi-empirical equation described rather well the heat transfer coefficients determined in one series of rocket motor firings:

$$h = 0.026 \left(\frac{\mu^{0.2} c_p}{Pr^{0.6}}\right) \frac{(\rho u)^{0.8}}{D^{0.2}} \left(\frac{\rho_{am}}{\rho}\right)\left(\frac{\mu_{am}}{\mu_o}\right) . \qquad (8.6)$$

Here, the fluid properties with the subscript 'am' were evaluated at the arithmetic mean temperature.

Since the T-burner in many ways resembles a rocket motor, it was initially felt that the above equation might also apply to the heat transfer in the burner. Of course, for the most part, only indirect measurements were available for the temperature of the gases in the chamber. However, by the following analysis it will be shown how

these measurements were able to establish not only that the values predicted by the above were far too low but also what the appropriate correlation is for the heat transfer in the T-burner.

To determine the heat transfer coefficient for the gas flow in the T-burner, consider a gas flowing at temperature T and velocity u through a tube of diameter D whose wall temperature, T_w, is constant. For simplicity, assume that the temperature is a function only of the distance, x, the gas has traveled since entering the tube at temperature T_c. As the gas flows a distance dx, an amount of heat dq is transferred per unit time to each unit area of wall surface. For a cylinder of diameter D and length dx, the wall area is obviously $\pi D\,dx$. From equation (8.3) then the rate of heat transfer, $\dot{dq}$, is

$$\dot{dq} = h(T-T_w)\pi D\,dx. \tag{8.7}$$

Naturally, this transfer of heat results in a decrease of the gas temperature. The principle of conservation of energy applied to the cylindrical control volume used above shows that

$$\dot{dq} = -\rho u c_p S_c \frac{dT}{dx}\,dx\ , \tag{8.8}$$

where c_p is the specific heat of the gas and S_c is the cross-sectional area of the tube, which in the present case is simply $\frac{1}{4}\pi D^2$. Combining the two preceding equations, we find

$$\frac{dT}{dx} = -\frac{4h}{\rho u D c_p}(T-T_w)\ . \tag{8.9}$$

If h is approximated by its mean value along the length of the tube, $\bar{h}$, this equation can be integrated directly to give the temperature as a function of distance:

$$\frac{T(x)-T_w}{T_c-T_w} = e^{-x/\lambda} \quad . \tag{8.10}$$

Here, the condition $T(0) = T_c$ has been applied, and the length constant, λ, is defined as:

$$\lambda = \frac{\rho u D_c}{4\bar{h}} \quad . \tag{8.11}$$

For the T-burner, λ can be expressed in terms of propellant properties by noting that $\rho u = \rho_s \bar{r}$ by conservation of mass, as was shown in Section II. Thus, for the T-burner,

$$\lambda = \frac{\rho_s \bar{r} D_c}{4\bar{h}} \quad . \tag{8.12}$$

If the mean temperature in the chamber, $\bar{T}$, is taken as the mass averaged value, then this implies

$$\bar{T} = \frac{\int_0^{L/2} \rho(x)T(x)dx}{\int_0^{L/2} \rho(x)dx} \quad , \tag{8.13}$$

where the integration is taken only to $x = \frac{1}{2}L$, since that is the distance the gas flows in the burner before reaching the vent. For a perfect gas, the product $\rho(x)T(x)$ is directly proportional to the mean pressure $P(x)$, which, for the very low Mach numbers involved, is

essentially constant. Likewise, the integrand in the lower integral is proportional to $1/T(x)$, and hence the mean temperature is

$$\overline{T} = \frac{\int_0^{L/2} dx}{\int_0^{L/2} \frac{dx}{T(x)}} , \qquad (8.14)$$

which, after using equation (8.10) and carrying out the integrations, becomes

$$\overline{T} = \frac{T_w}{1 - \frac{L}{2\lambda} \ell n\left(\frac{1 + c_1}{1 + c_1 e^{-L/2\lambda}}\right)} , \qquad (8.15)$$

where the constant c_1 is defined as $(T_c - T_w)/T_w$. Thus, if the propellant properties are known and a value for the mean heat transfer coefficient assumed, the mean temperature in the T-burner can be calculated.

For A-13 propellant at 300 psig, the combustion temperature T_c has been calculated[16] as 2100°K, and the specific heats ratio, γ, as 1.28. The density of the solid is 1.54 and the mean burning rate is 0.49 cm/sec. By assuming a wall temperature of 450°K and using the heat transfer coefficient predicted from equation (8.6), values for the mean temperature and hence the mean speed of sound were calculated for various chamber lengths. Naturally, since the heat transfer coefficient depends on the temperature, an iterative approach had to be used. The results are shown as the solid line in Figure 14 re-

ferred to earlier. Clearly, the values predicted on the basis of mean flow heat transfer coefficients are much higher than those observed. As mentioned earlier, since the main difference between the flow in the T-burner and that present in other long tubes is the oscillations, one is inclined to feel that the latter are responsible for the increased heat transfer. Considering that at times the mean flow velocity is only a fraction of the oscillatory velocity, it is not particularly surprising that this could be the case.

Since measurements of the mean speed of sound in the burner can be related to the mean temperature by equation (8.2), the former can be used to infer values for the mean heat transfer coefficient by working backwards with equation (8.15). Again, because of the nature of the latter equation, iterative approaches must be used to solve for $\bar{h}$ once $\bar{T}$ and the various propellant properties are given.

When such calculations were performed, it was found, as expected, that the heat transfer coefficients in the T-burner are indeed much greater than would be predicted from mean flow considerations alone. In fact, the inferred values were often 10 to 20 times greater than would have been expected. The most interesting feature was the fact that the calculated values for $\bar{h}$ showed a definite dependence on the amplitude of the oscillations. This is demonstrated quite clearly in Figure 15, where $\bar{h}$ is shown as a function of oscillatory amplitude for several propellants and chamber diameters. All of these tests

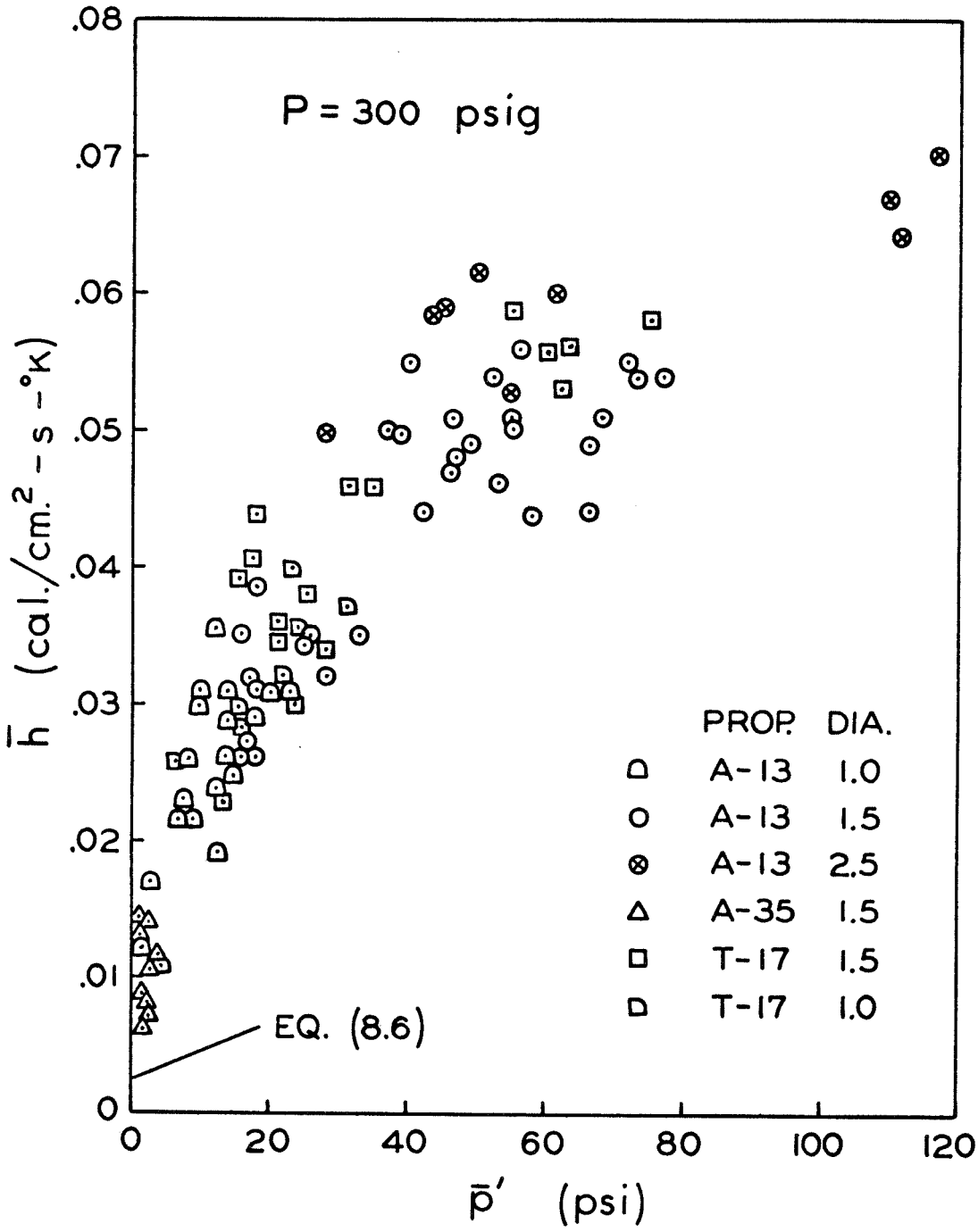

Figure 15. Mean Heat Transfer Coefficient as a Function of Oscillation Amplitude.

were conducted at a mean pressure of 300 psig. Although the tests covered a frequency range of from 0.4 to 3.0 kHz, the mean heat transfer coefficients showed only a dependence on the amplitude of the oscillations.

The value predicted on the basis of the mean flow velocity by equation (8.6) is also indicated in the figure. Clearly, as the amplitude of the oscillations goes to zero, the heat transfer coefficient tends toward this value, as one would expect.

Similar results were obtained at other mean pressure levels and are presented in dimensionless form in Figure 16. Here, the mean Nusselt number, $\overline{Nu}$, is defined as $\bar{h}D/k$ where k is the thermal conductivity of the gas evaluated at the mean temperature. The acoustic Reynolds number, Re_a, is defined as $\rho u'D/\mu$, where ρ and μ are the density and viscosity coefficients of the gas, again evaluated at $\bar{T}$. The acoustic velocity, u', was obtained from the limiting pressure amplitude, $\bar{p}'$, by assuming that the waves were isentropic and sinusoidal. Under these assumptions, u' is

$$u' = \frac{\bar{p}'}{\gamma P}\,\bar{a} \quad . \tag{8.16}$$

From the figure it is apparent that the data are correlated very well in these dimensionless variables by the following;

for $\quad 2.5 \times 10^4 < Re_a < 2.5 \times 10^6$

$$\overline{Nu} = 1.25\, Re_a^{0.5} \quad . \tag{8.17}$$

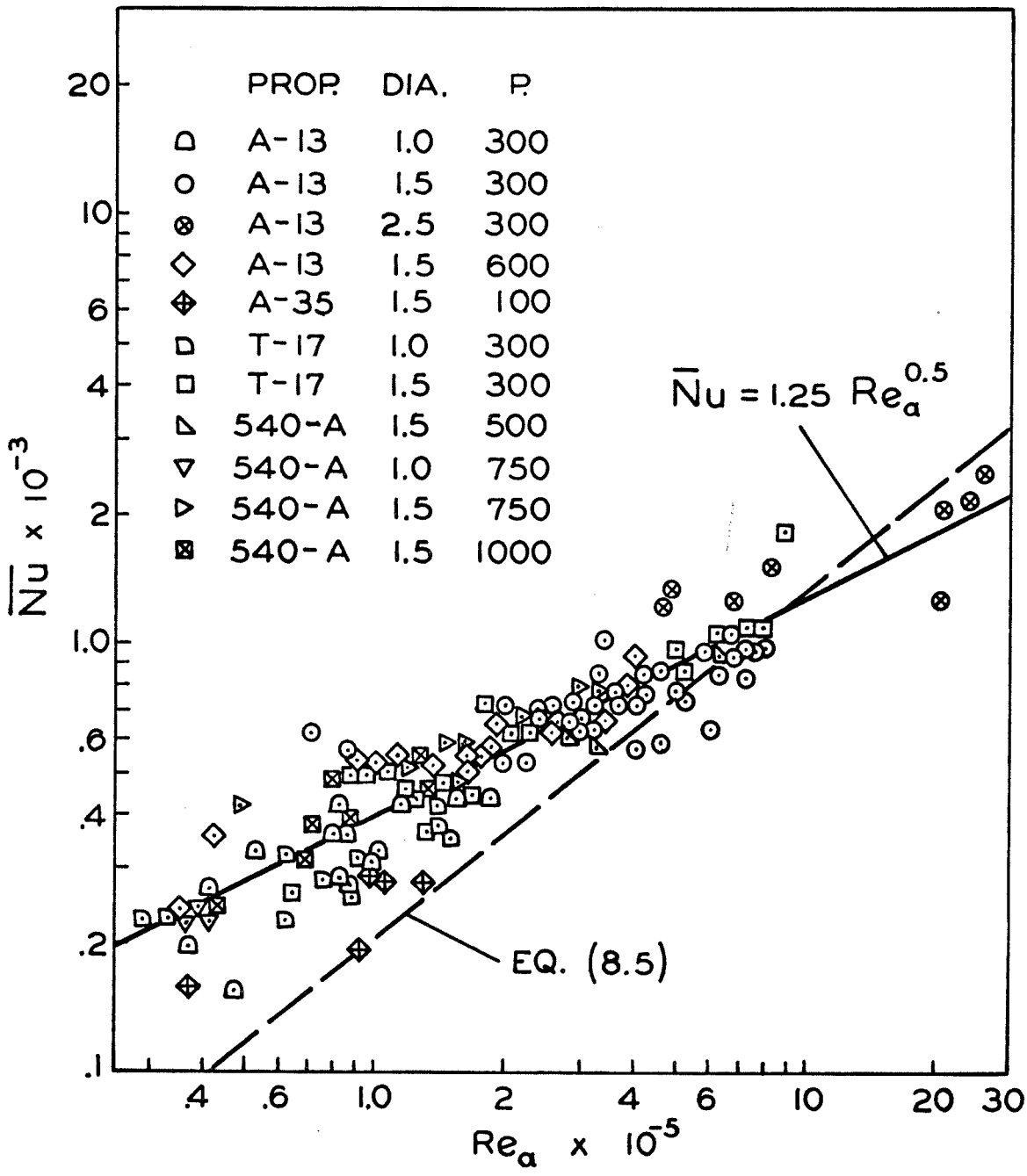

Figure 16. Mean Nusselt Number as a Function of Acoustic Reynolds Number.

Although the form of this equation differs from that of equation (8.5), the values predicted by the two agree reasonably well if the acoustic velocity is used in place of the flow velocity in the latter. This is shown in the figure, where equation (8.5), using the acoustic Reynolds number, is represented by the dashed line. This reasonable agreement is somewhat surprising since equation (8.5) applies normally to fully-developed, turbulent flows. Certainly, the high frequency oscillations present in the T-burner could lend turbulence to the flow. Also, the heat transfer should depend on the speed of the gases and not on their direction. Hence, it is possible that the oscillating flow in the T-burner resembles a high-speed turbulent flow in one direction. In any case, the results obtained by this indirect approach indicate that the heat transfer coefficient depends on the amplitude of the oscillations in a definite and predictable way.

Despite the convincing nature of these results, they were admittedly obtained by indirect means and involved several simplifying assumptions. For this reason a second, more direct, approach was also taken in an attempt to support the earlier findings. This second approach consisted of temperature measurements of the inner wall of the chamber during the firing. From these, the heat flux into the wall as a function of time was determined and, in turn, the heat transfer coefficient itself.

To obtain these measurements, a thermocouple probe manu-

factured by the Nanmac Corporation was used. This device, described in reference 17, uses two thin ribbons of dissimilar metals, in the present case Chromel and Alumel. These ribbons are separated by an even thinner layer of mica insulation. Upon grinding off the end of the assembly, many tiny junctions are formed. For the T-burner tests a Nanmac Model G thermocouple probe was used, which had a main body assembly fabricated from 0.125-inch diameter stainless steel tubing. Upon being inserted into a hole of the same diameter in the T-burner wall and soldered into place, the thermocouple body became an integral part of the wall itself. Being of the same material as the chamber, it presumably caused only a small disturbance of the thermal environment surrounding it. After being seated in place, the end of the thermocouple was ground off flush with the inner wall. Generally, the thermocouple was mounted midway between the ends of the burner and at right angles to the vent. In a few tests, however, other axial locations were chosen. The former location, of course, placed the thermocouple at the anti-node of the oscillatory velocity, the site of maximum heat transfer if the indirect measurements have been interpreted correctly.

To transform the temperature measurements into heat flux rates, the analysis suggested by Howard[18] was used. This procedure, based on a set of heat balance equations, employs a finite difference computing technique. The wall is assumed one-dimensional

and is divided into a number of thin blocks. A set of equations can then be written to take into account the amount of heat entering, leaving, and being stored in each block during each interval of time. With initial conditions and the wall temperature as a function of time given, this set of equations can be solved to obtain the heat flux at the wall. By assuming a value for the gas temperature, the heat transfer coefficient itself can be determined from equation (8.3). Naturally, the results obtained will be sensitive to the value assumed for the gas temperature. However, since the purpose of these tests was to provide only approximate values for the heat transfer coefficient, this presented no particular problem. Rather than use the adiabatic flame temperature, the value indicated by the mean speed of sound measurements was used for the gas temperature. For the finite difference computations, the wall was divided into twenty sections whose thickness varied from 0.01 cm at the inner side to 0.1 cm at the cold side of the wall. Taking very thin sections at the inner wall provided better accuracy in this region of large temperature gradients.

Since the heat transfer coefficient determined in this way represented a local value, as opposed to the average value obtained in the indirect measurements, it would obviously depend on location along the chamber wall. As mentioned earlier, most of the tests were conducted with the thermocouple located at the oscillatory velocity maximum, where the velocity is $|u'|$. If the spatial dependence

of the acoustic velocity is assumed sinusoidal, then the mean value over each half-length of the chamber is obviously

$$\langle u' \rangle = \frac{2}{L} \int_0^{L/2} |u'| \sin \frac{\pi x}{L} \, dx = \frac{2}{\pi} |u'| . \qquad (8.18)$$

If the indirect measurements are indeed valid, then by equation (8.17) the heat transfer coefficient should vary approximately as the square root of the acoustic velocity. If h_d denotes the value obtained directly for the local heat transfer coefficient at the velocity maximum and $\bar{h}_i$ the value obtained indirectly for the mean coefficient in the chamber, then from equation (8.17) and the above we would expect

$$h_d = \sqrt{\pi/2} \; \bar{h}_i \qquad (8.19)$$

if, again, the indirect measurements are correct.

In Figure 17, values for h_d obtained from thermocouple measurements are plotted against the indirect values, $\bar{h}_i$, inferred for the same tests. The values clearly agree with equation (8.19) very well, indicating that the indirect method discussed earlier is a valid means of obtaining the average heat transfer coefficient.

Values for h_d obtained at other axial locations indicate that the local heat transfer coefficient decreases as one proceeds toward the acoustic velocity node. This, of course, supports the contention that the acoustic velocity is responsible for the observed heat transfer increases.

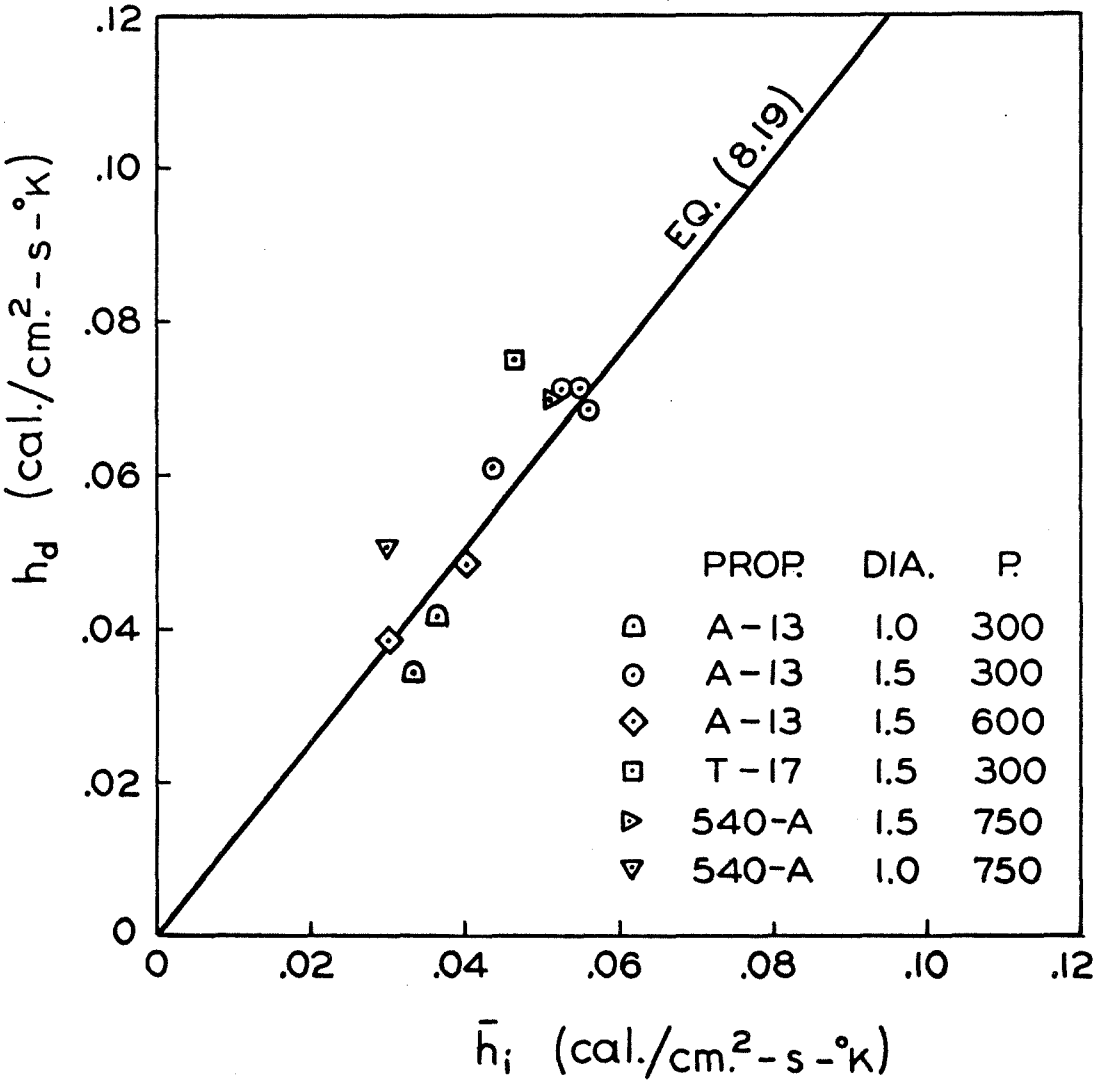

Figure 17. Comparison of Heat Transfer Coefficients Determined by Direct and Indirect Means.

Thus, by both a direct and indirect approach, the heat transfer coefficient in the T-burner has been related to the amplitude of the oscillations. Naturally, to understand more fully the observed increases in the heat transfer, additional measurements of the local transfer rate would be desirable. However, the present results certainly indicate in a most quantitative manner the reasons why combustion instability is usually accompanied by increases in heat transfer to the rocket motor. If the amplitude of the instability can be estimated, then the present results should provide quantitative estimates of these heat transfer increases. Because of this, the T-burner may, in time, become a useful tool in the study of heat transfer in rocket motors under oscillatory combustion conditions. More important, however, is the fact that in subsequent sections it will be shown that the results discussed here help explain several observed features of the T-burner itself.

IX. THE ACOUSTIC LOSSES OF THE T-BURNER

Long before the present studies, it was realized that the acoustic losses of the burner could play an important role in the tests. It will be recalled from Section II that one of the essential assumptions of the basic T-burner method is that the losses measured after burnout are the same as those present during growth. Naturally, if the losses change during the test, this assumption is incorrect and the values inferred for the admittance are wrong. To avoid some of these difficulties, another T-burner method, described in Section X, was introduced which uses only growth rate measurements. However, like the original method, it too depends on assumptions made concerning the damping in the chamber. Thus, it is obvious that a thorough understanding of the T-burner is dependent upon a proper understanding of its acoustic losses.

For this reason, considerable attention was given in the present investigations toward obtaining a better understanding of these losses. In fact, probably no other feature of the burner was examined more closely. However, it appears that this effort was well justified, for in examining the chamber damping, several important results emerged. The first is that, contrary to common opinion, the losses of the T-burner now appear to be non-linear. If this is true, then the present interpretation of T-burner data obtained by the basic "growth-decay" method is incorrect, since the wrong value is used for the de-

cay constant. In the next section it will be shown that this generally produces large errors in the values inferred for the admittance. Another important consequence is that on the basis of these non-linear losses, the behavior observed in the limiting amplitude of the oscillations can be explained reasonably well. Section XI will deal more specifically with this point. Consequently, it appears that the losses play an even more important role than was first thought. Indeed, they seem to be responsible for a number of observations which have heretofore gone unexplained.

Experimental Observations of the Losses

In Section IV it was shown that the losses are measured in terms of a decay constant, which is a convenient way of expressing the decay rate observed after burnout. In Figure 18 decay constants measured using A-13 and T-17 propellants at a pressure of 300 psig are shown as a function of frequency for different chamber diameters. Two important aspects of the T-burner losses are apparent from these results, which are typical of those obtained under other chamber conditions. First, the decay constant varies as the square root of the frequency, as indicated by the straight lines passing through the data. Second, the losses measured after burnout are nearly independent of chamber diameter.

Of course, one is interested in the losses, mainly because of

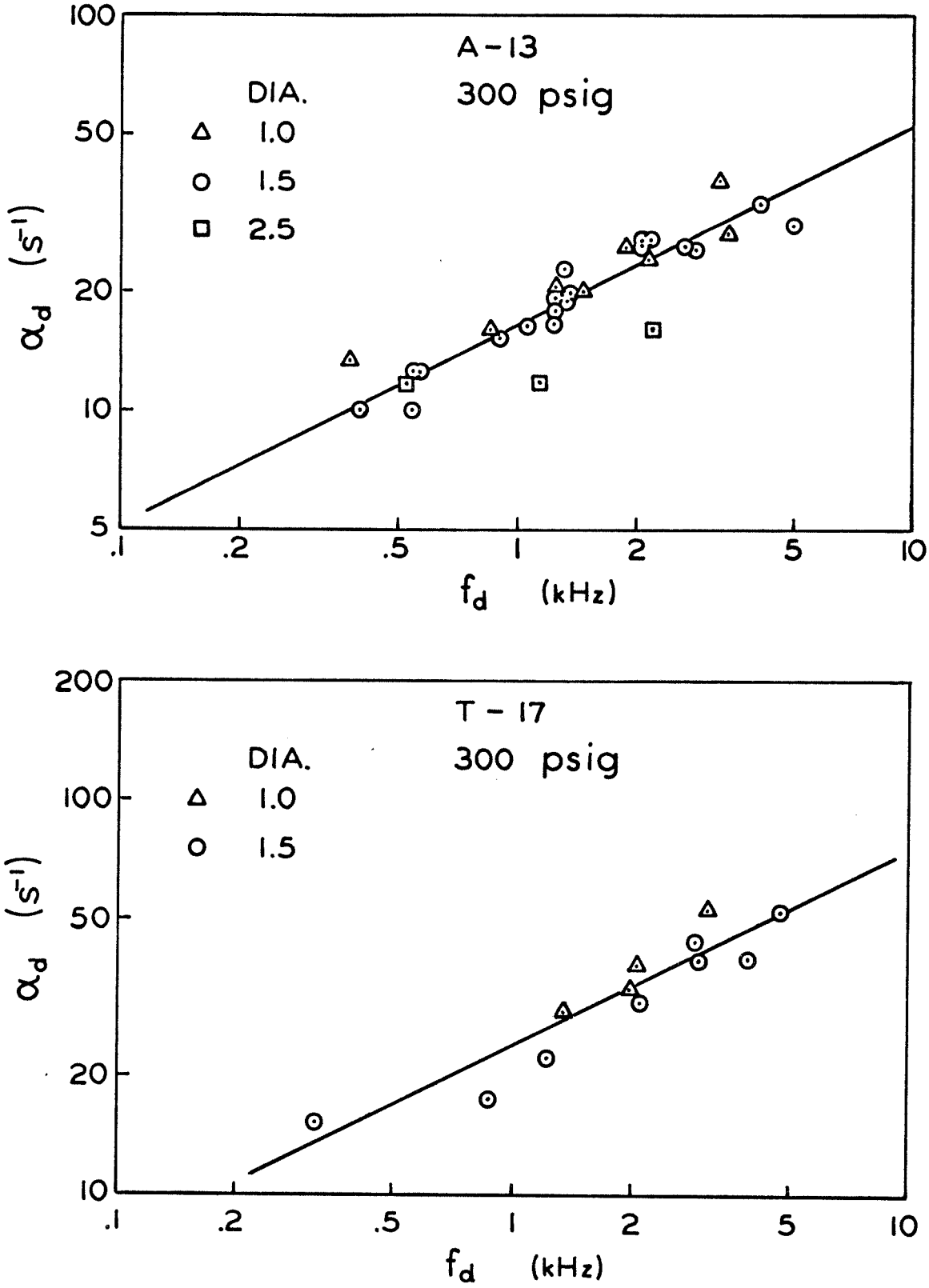

Figure 18. Decay Constants Measured as a Function of Frequency for Different Chamber Diameters.

their effects on the growth rates. In Figure 19, growth constants for A-13 at 300 psig are shown as a function of frequency for the three diameters used. Like the losses, the growth constants show little dependence on diameter. This same observation was made in at least one other instance[19]. One possible explanation for this behavior is that the losses remain constant during the entire test. Since the results of Figure 18 showed that the losses present at the end of the test are independent of diameter, then, if the damping is constant, the growth rates should also be independent of chamber diameter. This commonly held opinion is the basis of the "growth-decay" T-burner method which was outlined earlier, and will be described more fully in the next section. However, another explanation for the behavior of the growth constants is that the losses present during growth are too small to affect the growth rate seriously. For reasons to be given below, this latter interpretation appears to be the correct one.

The Acoustic Boundary Layer and T-Burner Losses

The square root dependence of the losses on frequency shown in Figure 18 is strongly suggestive of the wall losses normally associated with acoustic waves traveling through tubes. It has long been known that the major source of acoustic damping in tubes is the viscous and thermal energy dissipation occurring in a thin region, known as the "acoustic boundary layer," next to the tube wall. It can be

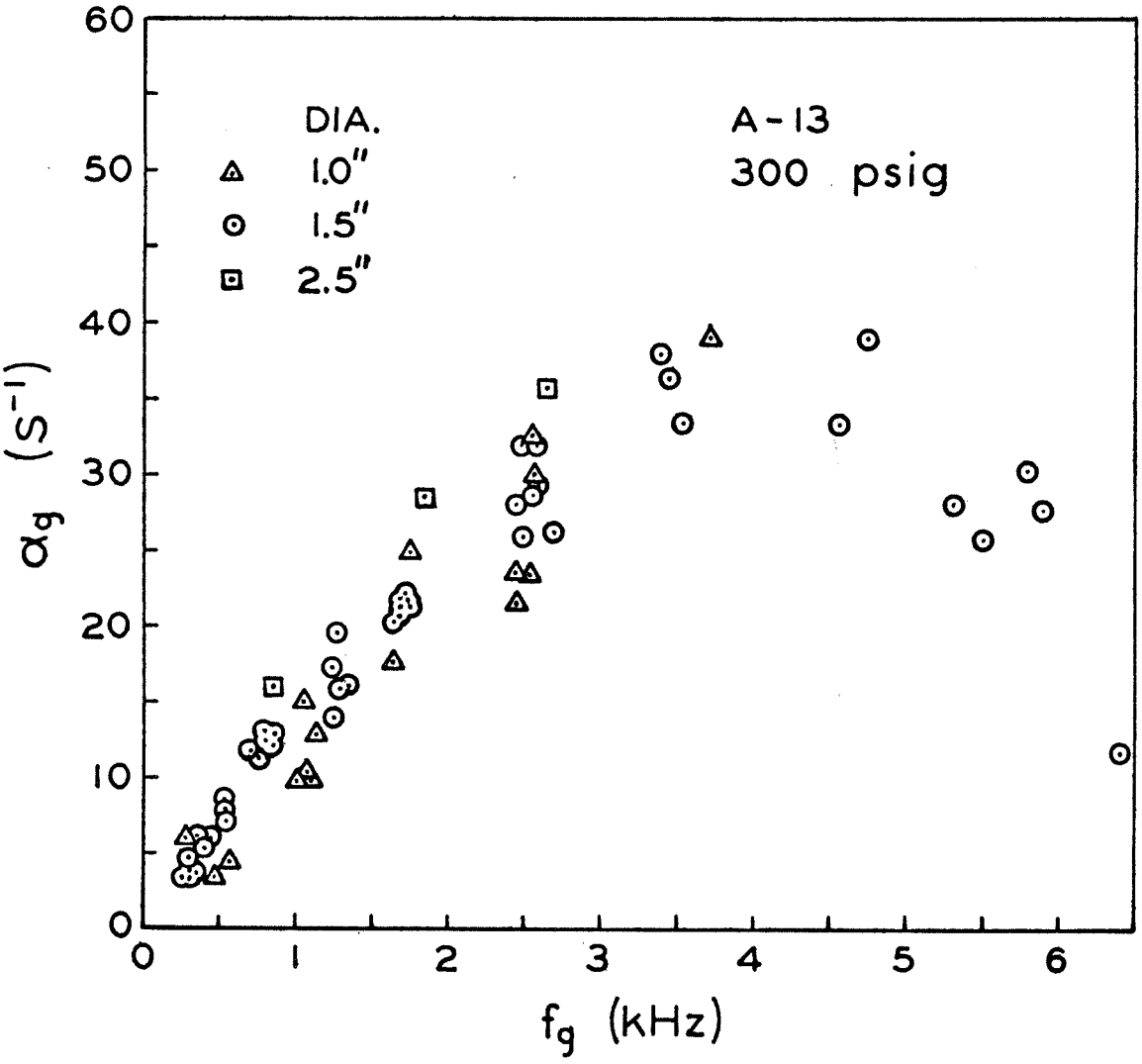

Figure 19. Growth Constants Measured as a Function of Frequency for Different Chamber Diameters.

shown that[20] the thickness, δ, of this layer is approximately

$$\delta = \left(\frac{\nu}{\pi f}\right)^{\frac{1}{2}} , \tag{9.1}$$

where ν is the kinematic viscosity and f the frequency. For a 1 kHz sound wave traveling through a tube filled with air at ambient conditions, the acoustic boundary layer is less than a tenth of a millimeter thick. The amplitudes of both the acoustic velocity and temperature vary from their full values at the outer edge of this thin layer to zero at the wall. The energy dissipation results from these steep gradients in velocity and temperature.

If the mean temperature of the gas and wall are equal, then the decay constant associated with this dissipation in a tube of diameter D is[21]

$$\alpha_d = 2\sqrt{\pi\nu}\left(1 + \frac{\gamma - 1}{\sqrt{Pr}}\right)\frac{\sqrt{f}}{D} \tag{9.2}$$

where Pr is the Prandtl number of the gas. Considering again a 1 kHz sound wave traveling through a tube filled with air at ambient conditions, we find the decay constant for a 1.5-inch diameter tube is 16 s^{-1}. This means that in 1/16 of a second, the amplitude of the wave decays by a factor of 1/e.

Returning to Figure 18, we see that the decay constants at 300 psig for A-13 and T-17 at a frequency of 1 kHz are 16 s^{-1} and 21 s^{-1}, respectively. Although T-burner conditions are far from ambient, the similarity in numerical value and frequency dependence

between the T-burner decay constants and those arising from acoustic boundary layer dissipation certainly raises the possibility that the two are one and the same.

Because of the observed frequency dependence, this possibility was suggested early in the investigations[22]. However, the weak dependence on diameter found in subsequent tests seemed to rule out this explanation and presented a dilemma regarding the true nature of the damping in the burner.

However, to explore the possibility of wall damping further, and to examine the T-burner losses under ideal conditions, measurements of the decay constants were obtained under cold chamber conditions. By "cold" it is meant that the T-burners contained neither burning propellant nor a mean flow; they were used simply as passive acoustic cavities. Oscillations were maintained in the chambers by an external sound driver linked to the burner interior by a small hole, packed with steel wool to provide a high acoustic impedance, in one end cap. At the opposite end was a quarter-inch diameter type 4136 Brüel and Kjaer microphone. By turning off the driver very quickly and watching the decay of the waves on a storage oscilloscope, the decay constants were determined. The tests, conducted at ambient conditions, used chamber lengths ranging from 3.5 to 31.5 inches and diameters of 1.0, 1.5, and 2.5 inches. Decay constants were measured only for the first mode oscillations, which are generally the only

ones present to any extent in the T-burner.

The results of these cold acoustic tests are shown in Figure 20, where the product $D\alpha_d$ is given as a function of frequency. By multiplying the decay constant by D, the dependence on diameter suggested by equation (9.2) is removed. The values predicted by this latter equation are shown as the solid line and fall about 30 percent below the observed values. This lack of numerical agreement is not particularly disturbing since other investigators[23], using very careful experimental techniques, have found the observed wall losses to be higher than theory indicates. More important is the fact that the decay constants show the predicted dependence on both frequency and diameter. Thus, under these ideal conditions, the T-burner losses are definitely due to dissipation within the acoustic boundary layer.

To study possible contributions by the vent to the chamber damping, additional cold acoustic tests were conducted using vents of different diameters. In one series, the vent was completely closed off. Just as in the case of actual test firings, mentioned in Section III, no effect whatsoever was observed upon changing the vent size. Thus, it may be assumed that the vent plays a very small role in the T-burner losses. One possible exception will be given in Section XI with regard to the sinusoidal appearance of the waves.

Although these tests demonstrated that under ideal conditions the losses of the burner are easily explained, they did nothing to re-

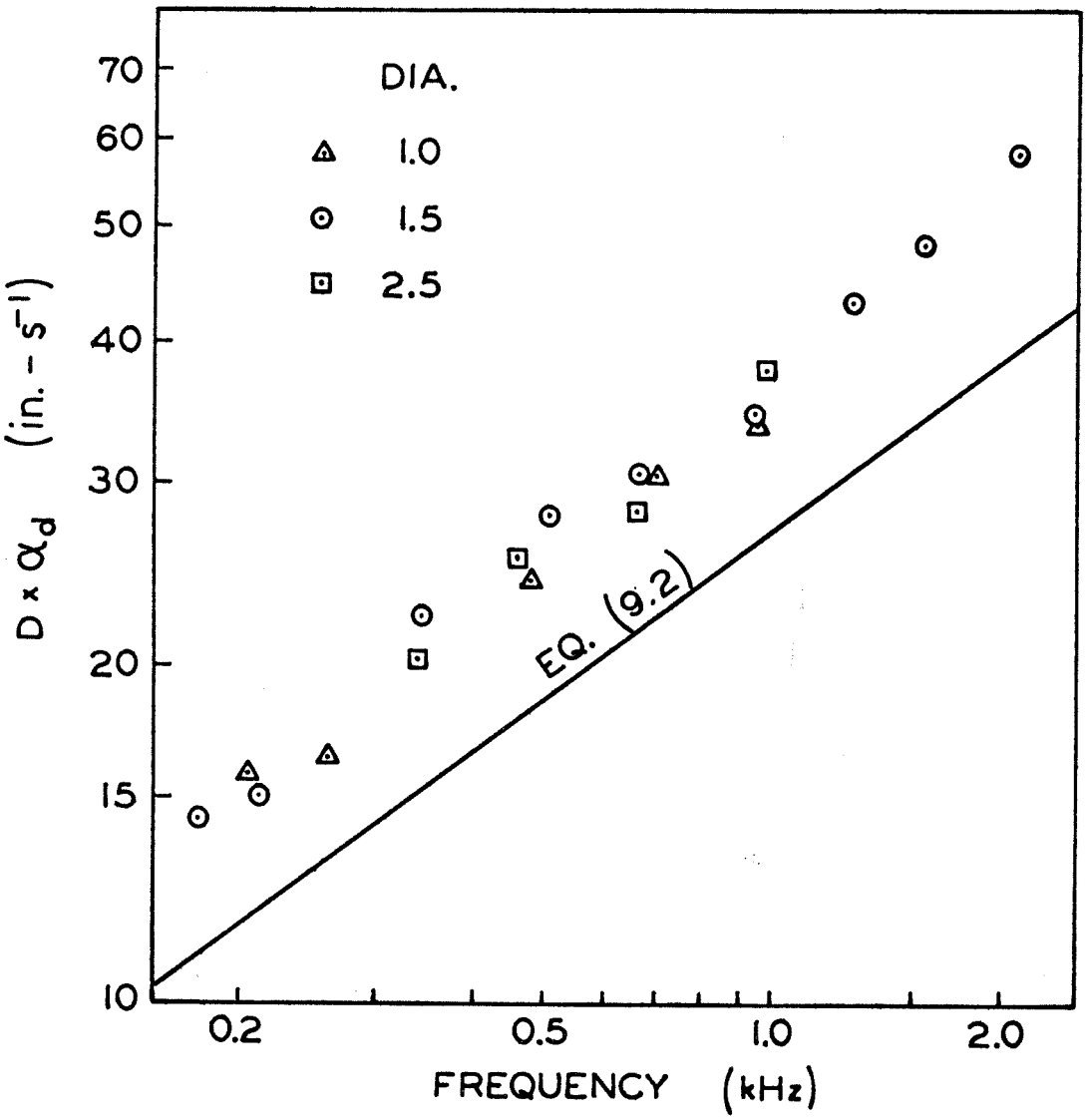

Figure 20. Results of Cold Acoustic Tests.

solve the dilemma presented by the lack of a dependence on diameter observed in the decay constants measured in actual test firings. One important clue, however, was provided by the analysis of Cantrell, McClure, and Hart[24], who considered the acoustic damping in cavities that contain a mean flow with a temperature considerably different from that of the walls. The basic assumption of that analysis was that the acoustic boundary layer is at least an order of magnitude thinner than the boundary layer due to the mean flow. Consequently, the temperature of the former was assumed to be the same as that of the wall. Under this assumption, the dissipation occurs in a region whose temperature is T_w. Since the major part of the acoustic energy is associated with the central core of the gas at temperature $\bar{T}$, the decay constant, obtained by dividing the energy dissipation by the total energy, was shown to be

$$\alpha_d = 2\sqrt{\pi \nu_w}\left(\frac{T_w}{\bar{T}} + \frac{\gamma - 1}{\sqrt{Pr}}\right)\frac{\sqrt{f}}{D} \qquad (9.3)$$

where ν_w is the kinematic viscosity evaluated at the wall temperature, T_w. Obviously, if T_w increases with diameter, the dependence of the decay constant on the latter will be lessened. It was in recognition of this fact that the heat transfer studies described earlier were begun. However, from the thermocouple measurements of wall temperature obtained during those investigations, it became apparent that observed wall temperature variations were insufficient to account

for the behavior of the losses. The wall temperature was observed to rise at most to only about 500°K from an initial value of 300°K. Since some rise always occurred, obviously the variations between tests using different diameters could not be very large.

In addition, for such cool wall temperatures, the values predicted by equation (9.3) are almost an order smaller than those observed. For example, assume a wall temperature of 500°K and a mean flow temperature of 1500°K. For A-13 propellant, the mole fractions of CO, H_2, H_2O, $HC\ell$, N_2, and CO_2 in the combustion gases are approximately[16] .30, .27, .19, .14, .06, and .04, respectively. By the methods described in Appendix C, the kinematic viscosity at the wall can be shown to be approximately 0.02 cm^2/s at a pressure of 300 psig. If a γ of 1.28 and a Prandtl number of 0.73 are assumed, then according to equation (9.3) the decay constant for a 1 kHz wave in a 1.5-inch diameter tube is 2 s^{-1}, compared to the observed value of 16 s^{-1}.

Thus, it is clear that either equation (9.3) is incorrect, or the T-burner losses arise from a mechanism other than acoustic boundary layer dissipation. Since that equation was derived under the assumption that the acoustic boundary layer is at the wall temperature, it is interesting to see the results of relaxing this restriction. In Figure 21 the decay constants observed for A-13 at 300 psig are

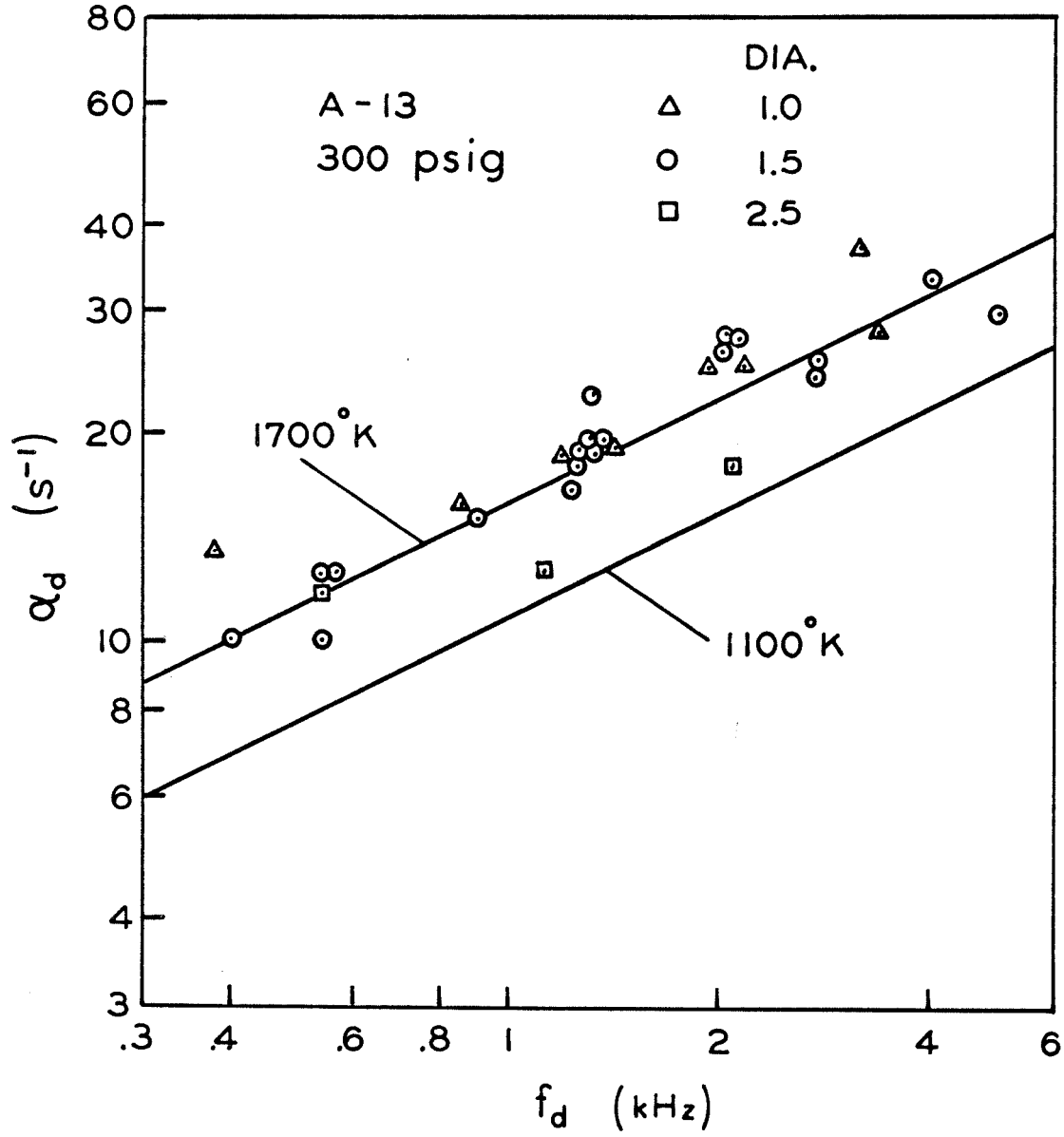

Figure 21. Decay Constants as a Function of Frequency. Solid Lines Indicate Values Predicted by eq. (9.3) if T_w Is Replaced by the Temperatures Shown.

shown again, along with values predicted by equation (9.3) where, instead of T_w, the temperatures indicated were used to calculate the properties in the acoustic boundary layer. In both cases, the mean flow and acoustic boundary layer were taken to be at the same temperature. The kinematic viscosity was calculated using the gas composition given earlier.

Clearly, the values for a temperature of 1700°K agree very well with those observed. The decay constants for a temperature of 1100°K fall 30 percent below the experimental values and correspond to the relation found in the cold acoustic tests between theory and experiment. Both of these temperatures, while far above observed wall temperatures, are still well below flame temperatures, which were shown earlier to be between 2000°K and 3000°K for the propellants used. Consequently, they are physically possible.

From these calculations we see that if the acoustic boundary layer is at a sufficiently high temperature, the dissipation occurring there is large enough to account for the T-burner losses. In addition, if this temperature increases for some reason with chamber diameter, then the losses of the burner will show a weaker dependence on the latter than would be expected. Thus, the analysis of reference 24 provided a possible mechanism for explaining the T-burner losses if, instead of the wall temperature taken there, a much higher value is assumed for the acoustic boundary layer.

The heat transfer measurements described in the previous section provided the first indication that the acoustic boundary layer might be at a significantly higher temperature than the wall. The high rates of heat transfer found there were taken as an indication of very steep temperature gradients in the gas next to the wall. Depending on the size of these gradients, the acoustic boundary layer temperature could vary considerably. If such a variation depended in just the right way on chamber size, then the losses would be independent of diameter. In the following analysis, it will be shown that this now seems to be the case, with the temperature variation arising from changes in the oscillation amplitude with chamber diameter.

If $\dot{q}_w$ denotes the average rate of heat transfer to the wall, then we know it is related to the mean radial temperature gradient in the gas at the wall by

$$\dot{q}_w = -k_w \left(\frac{dT}{dr}\right)_w \tag{9.4}$$

where k_w is the thermal conductivity of the fluid next to the wall. Because the acoustic boundary layer is so thin, it is reasonable to assume that the temperature gradient remains constant through it. Under this assumption the temperature midway through the acoustic boundary layer, T_{BL}, is approximately

$$T_{BL} = T_w + \frac{1}{2} \frac{\dot{q}_w}{k_w} \delta \ , \tag{9.5}$$

where δ is the thickness of the acoustic boundary layer given by

equation (9.1). Obviously, if the heat transfer rate is large enough, T_{BL} can be much higher than T_w. Thus, by prescribing a value for $\dot{q}_w$ and T_w, the above equation can be used to calculate the acoustic boundary layer temperature. Since δ depends on T_{BL}, iterative methods must be used.

Once T_{BL} is determined, the acoustic losses can be calculated using equation (9.3) with T_w replaced by T_{BL}. Thus, the decay constant should be given by

$$\alpha_d = 2\sqrt{\pi \nu_{BL}} \left(\frac{T_{BL}}{\overline{T}} + \frac{\gamma - 1}{\sqrt{Pr}} \right) \frac{\sqrt{f}}{D} , \tag{9.6}$$

where ν_{BL} is the viscosity evaluated at T_{BL}.

To compare the values predicted by this equation with those observed, an expression relating the heat flux at the wall to the other test variables must be given. In Section VIII it was shown that the heat flux could be correlated very well by equation (8.17). Noting that the heat transfer coefficient is defined in terms of $\dot{q}_w$ by equation (8.1), the correlation can be written:

$$\frac{\dot{q}_w D}{k(T - T_w)} = 1.25 \left(\frac{\rho u' D}{\mu} \right)^{\frac{1}{2}} . \tag{9.7}$$

Using equation (5.5) to relate u' and $\overline{p}'$, and assuming that $a^2 = \gamma P/\rho$, the above becomes

$$\dot{q}_w = 1.25 k(\overline{T} - T_w) \left(\frac{\overline{p}'}{\mu a D} \right)^{\frac{1}{2}} . \tag{9.8}$$

Clearly, if the wave amplitude increases sufficiently with di-

ameter, then the heat transfer to the wall, and hence the temperature of the acoustic boundary layer, will also increase with chamber size. This, of course, is exactly the behavior required to produce the observed losses.

To carry out the calculations, a wall temperature of 450°K was assumed. The mean temperature of the gas in the chamber was found from the speed of sound measurements discussed earlier. For the gas composition given above, it is shown in Appendix C that the viscosity should vary with temperature approximately as

$$\mu = 3.2 \times 10^{-6} T^{0.7} , \qquad (9.9)$$

where the temperature is in degrees Kelvin and the viscosity in gm/cm-s. Likewise, for the wall temperature assumed, the thermal conductivity of the gas at the wall should be approximately 1.1×10^{-4} cal/cm-s-°K.

Using these values along with observed values of the limiting amplitude, $\bar{p}'$, the temperature in the acoustic boundary layer was calculated for a number of tests and used to determine the theoretical chamber losses indicated by equation (9.6). The results are shown in Figure 22, where the predicted decay constants are plotted against the observed values. Despite the scatter, which, considering the approximations made is not excessive, the predicted values correlate reasonably well those observed. The solid line passing through the points represents simply the best fit and shows that the predicted

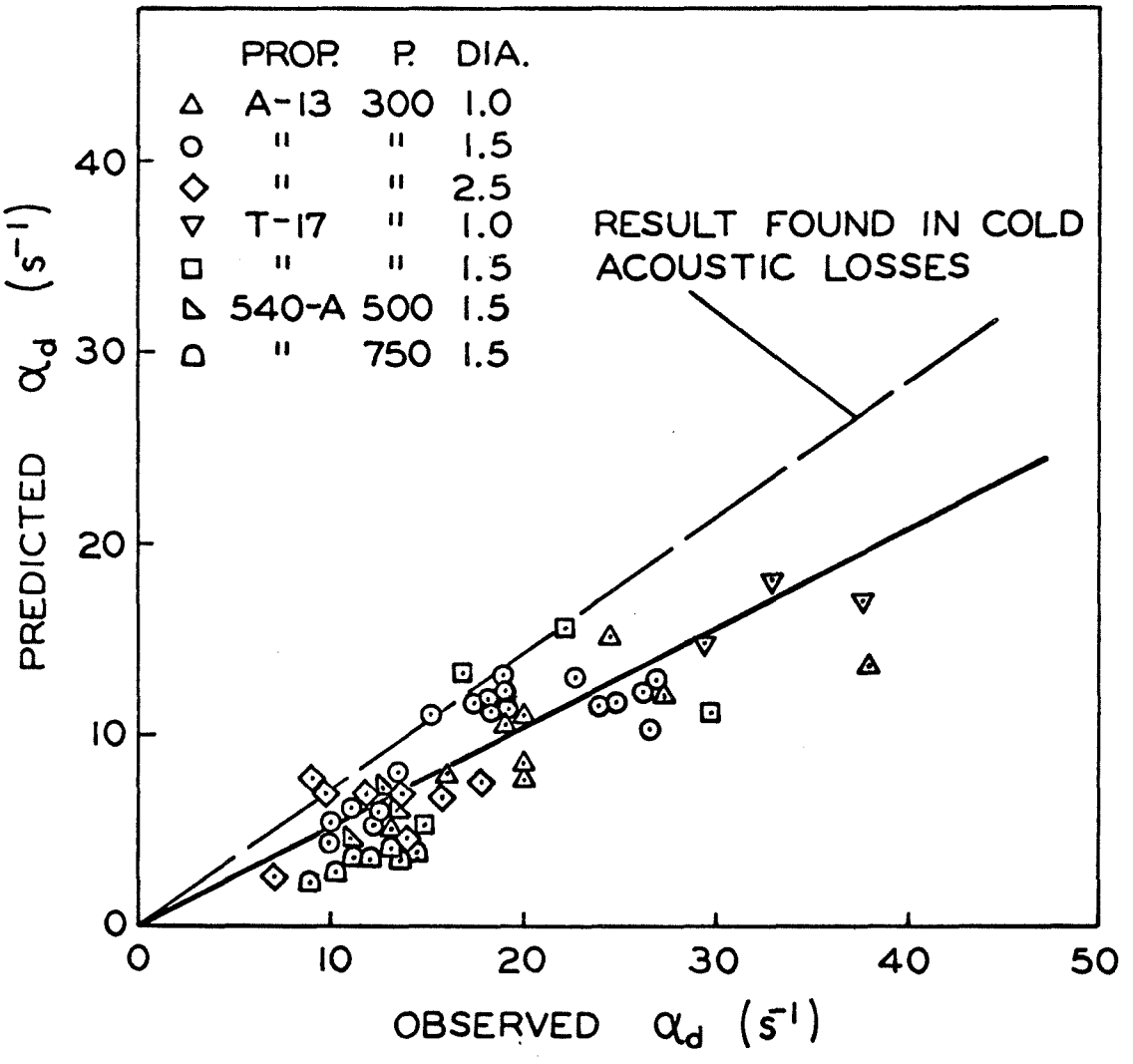

Figure 22. Comparison of Predicted and Observed Decay Constants.

values are about half the size of the experimental values. However, recalling that even in the cold acoustic tests the theoretical values were only about 70 percent as large as the measured decay constants, the present lack of numerical agreement is not surprising. The relation found in the cold acoustic tests between theory and experiment is indicated by the dashed line.

More important than the absence of good numerical agreement is the fact that these results show that the observed lack of a dependence on diameter is expected for losses arising in this manner. In addition, since the tests shown in the figure covered frequencies ranging from 0.5 to 3.0 kHz, we see that the observed frequency dependence is also predicted. The following comparison of values calculated for two tests which differed only in chamber diameter will make it even clearer that the proposed loss mechanism does produce decay constants which are essentially independent of diameter.

The two tests used A-13 at 300 psig in chambers 10.0 inches long. In the first test, conducted in a 1.0-inch diameter chamber, the mean frequency was 1.52 kHz and the wave amplitude 17 psi. In the second test, which used a 1.5-inch burner, the values were 1.50 kHz and 51 psi, respectively. Using this information, the following values were calculated:

	Test 1 (1.0" dia.)	Test 2 (1.5" dia.)
$\overline{T}$ (^{o}K)	1120	1090
T_{BL} (^{o}K)	770	1000
Predicted α_d (s^{-1})	11.1	11.5
Observed α_d (s^{-1})	20.0	19.5

The 30 percent higher boundary layer temperature in the second case just exactly offsets the effect of diameter. In Section XI we shall see that this is no coincidence, but that, in fact, the decay constant measured at the end of the test should be essentially independent of diameter, for it is precisely because of this fact that we observe the amplitude limitation that we do.

Although equation (9.8), which related the heat transfer at the wall to the wave amplitude, was obtained from steady-state measurements, there is no reason to assume that it does not apply equally well to cases where the amplitude is changing slowly compared to the period of the oscillations. This, of course, would mean that the losses increase with the amplitude of the waves. Because of the nature of equations (9.5) - (9.8), a simple and yet accurate expression for α_d as a function of p' cannot be given. However, it is obvious that the decay constant should increase with amplitude.

Naturally, if the losses are non-linear, then several consequences must follow. The first is that the decay constant measured

after burnout is different from that present during the growth of the oscillations since the amplitudes at the two times are different. A second result is that eventually an amplitude will be reached where the losses just equal the gains provided by the burning propellant. Thus, non-linear losses offer an explanation for the observed behavior of the limiting amplitude. In the following two sections it will be shown that experimental evidence indicates that both of these effects are, in fact, observed and that, therefore, the losses described here can account for a number of other observations.

X. A COMPARISON OF TWO COMMON T-BURNER METHODS

The method outlined in Section II is one of two conventional ways of conducting T-burner tests. Because it involves measurements of both the growth and decay rates of the oscillations, that technique is usually referred to as the "growth-decay" T-burner method. Another approach, known as the "variable-area" method, uses only growth rate measurements and derives its name from the fact that the propellant area is varied from test to test. Presumably, by measuring the growth rate as a function of this area, the real part of the admittance can be determined.

Despite their many similarities, these two techniques have nevertheless been the subject of a continuing debate for a number of years. Unfortunately, few experimental comparisons of the two methods have appeared. Since differences in experimental procedures, such as the ignition techniques described earlier, can definitely play an important role in the test results, only a direct comparison using the same procedures for both methods may be meaningful.

For this reason such a comparison was undertaken, maintaining, insofar as possible, identical experimental procedures. The comparison revealed among other things that with the usual interpretation of growth-decay data, the two methods produce results which

agree very poorly. However, if the T-burner losses are assumed to be those predicted in Section IX, then the two methods agree extremely well. Although these results cannot be taken as proof of the validity of the arguments given in that section, they certainly support it and possibly explain why results obtained by the two methods have been in disagreement in the past.

Description of the Two T-burner Methods

In Section II it was shown that if the T-burner were free of losses, the oscillations would grow at a rate proportional to the sum, $A_b^r + M_b$. Because of losses present, however, the growth rate is less than this ideal figure. If the propellant completely fills both ends of the burner, then by equation (2.18), the observed growth constant, α_g, is

$$\alpha_g = \frac{2a_b}{L}(A_b^r + M_b) - \alpha_d' \quad , \tag{10.1}$$

where α_d' represents the decay constant that would be observed if the propellant instantly burned out. In reality, of course, the propellant continues to burn for some time after the initial growth period. During that time the oscillations reach a limiting amplitude which is often five to ten times larger than the amplitude present when the growth constants are measured. Finally, burnout occurs, and the waves begin to decay at a rate measured by the observed decay constant, α_d. As discussed in Section IV, this value is usually obtained

immediately after burnout, since if one waits for the amplitude to become very small, chamber conditions will have changed drastically as a result of the rapid cooling of the gases.

The crucial assumption of the growth-decay method is that the losses remain constant during the entire test, which means that $\alpha_d' = \alpha_d$. With this assumption, equation (10.1) can be rearranged to provide the following expression for the sum, $A_b^r + M_b$, in terms of the observed growth and decay constants:

$$A_b^r + M_b = \frac{\bar{a}}{a_b} \frac{\alpha_g + \alpha_d}{4f} , \qquad (10.2)$$

where equation (2.1) has been used to relate $\bar{a}$ to the frequency. Since M_b and a_b can be calculated from known propellant properties, (10.2) is essentially an equation for calculating the real part of the admittance.

If the losses are linear in the wave amplitude, then the assumption that they are constant during the test is reasonably valid. Naturally, since the growth and decay frequencies differ, one might expect the losses to vary some even if they are linear. However, such effects should not be extremely important and, in any case, can be allowed for[7].

On the other hand, if the losses are non-linear, this assumption would be completely wrong, since the amplitudes present when the growth and decay constants are measured are usually quite dif-

ferent. In particular, if the arguments developed in Section IX are basically correct, then the normal interpretation of T-burner data obtained by the growth-decay method is wrong. Fortunately, even if this is true, the method can still be used by calculating the losses present during growth theoretically and using those values instead of the observed growth constant. It will later be shown that generally the theoretical losses based on the discussion of Section IX are rather small, and hence theoretical inaccuracies should not strongly affect the results.

To avoid completely the problems associated with the growth-decay method, the variable-area technique was introduced[25]. In this method, the ratio of propellant area to chamber cross-section area is varied from test to test. This ratio, denoted here by S_b/S_c, is usually less than one, which means that the propellant does not completely cover the ends of the chamber. However, through use of cup-shaped propellant samples[25], values greater than one have been employed. This latter procedure, which, of course, could also be used in growth-decay tests, is particularly useful in testing metallized propellants, which often oscillate weakly at best in the usual T-burner configuration.

Since the propellant is the driving mechanism for the oscillations, the greater its area, the greater the rate of energy input to the acoustic field. Naturally, this implies higher growth rates for larger

area ratios. In equation (2.18), it was shown that the growth constant is related to the area ratio by

$$\alpha_g = \frac{2a_b}{L}\left(A_b^r + M_b\right)\frac{S_b}{S_c} - \alpha'_d \quad , \tag{10.3}$$

where again α'_d is the decay constant which would be observed if the propellant instantly burned out.

According to this equation, if α'_d is independent of area ratio, then a plot of α_g against S_b/S_c should result in a straight line whose slope is proportional to $A_b^r + M_b$. Since growth constants for the different area ratios are all obtained while the amplitude is very small, then even if the losses are non-linear, they should not seriously affect the results of this method. Thus, the variable-area method is less sensitive to the nature of the acoustic losses, which is certainly a desirable feature.

Experimental Comparison of the Two Methods

For the experimental comparison, A-13 propellant was used at a mean pressure of 300 psig. Chamber lengths ranging from 3.5 to 25.5 inches were used in the growth-decay tests along with diameters of 1.0, 1.5, and 2.5 inches. All of the variable-area tests were conducted in 1.5-inch diameter burners. For the latter tests, only three chamber lengths, 19.0, 10.0, and 5.5 inches, were used since several firings had to be conducted at each frequency to establish the growth constant versus area ratio plot. At each chamber length, a

minimum of two tests were conducted at each of the three area ratios of 0.43, 0.72, and 1.00. The first two ratios were obtained by bonding 1.0- and 1.3-inch diameter propellant disks into stainless steel rings which were in turn bonded to the chamber walls.

The results were first calculated using the normal interpretation for the growth-decay data; that is, the observed decay constants were used in equation (10.2). These results are presented in Figure 23, where the inferred values for $A_b^r + M_b$ are shown as a function of frequency. Two important conclusions can be drawn from these results. First, the values obtained by the growth-decay method are independent of the chamber diameter. This, of course, is a direct consequence of the observations discussed in the previous section that the growth and decay constants show no dependence on diameter. However, it is a most encouraging finding, since any other result would case doubt on the entire T-burner method.

A second conclusion is that the values obtained by the growth-decay method are considerably higher than those found from variable-area measurements. The bars on the latter data indicate the range of values which could be inferred since the growth constant plots did not give straight lines. However, the spread is not significantly greater than the scatter in the growth-decay data. More importantly, the two methods agree very poorly in predicting the admittance. Since the two are reasonably independent, good agreement would lend support

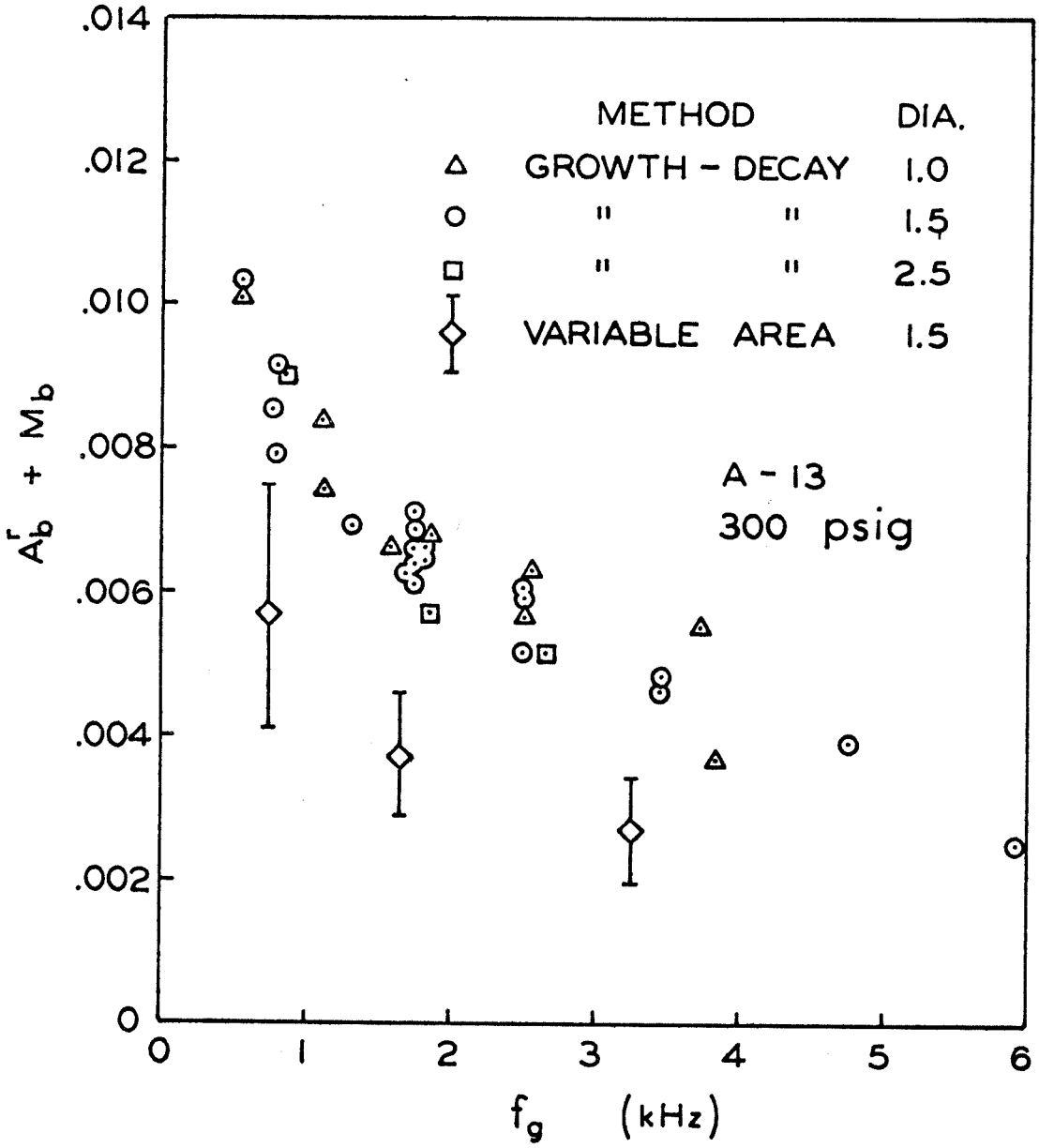

Figure 23. Comparison of Results Obtained from the Two T-burner Methods Using Observed Decay Constants.

to the validity of both methods. Thus, the observed lack of agreement was received initially as a very discouraging result.

However, when evidence began to mount that the losses might be non-linear, it was realized that this lack of agreement could be due to incorrect interpretation of the growth-decay data. Consequently, the latter values were recalculated, this time using the theoretical decay constants predicted by equation (9.6) with an assumed boundary layer temperature equal to the initial wall temperature. The latter assumption was based on the fact that initially the boundary layer is still very cool. Only after the oscillations appear does the heat transfer to the wall begin to raise the boundary layer's temperature.

These results are shown in Figure 24 where, again, $A_b^r + M_b$ is plotted against frequency. Clearly, the results obtained by the two methods are in very good agreement if the predicted, rather than the observed, decay constant is used in equation (10.2).

In general, the decay constants predicted by equation (9.6) are small if the acoustic boundary layer is assumed to be at the wall temperature. This point was also made in the previous section. Typical values lie in the range of 1 to 4 s^{-1}. Usually, the growth constant is considerably greater than these values. Thus, as a first approximation, $A_b^r + M_b$ can be calculated from equation (10.2) by neglecting the decay constant completely and using only the observed growth con-

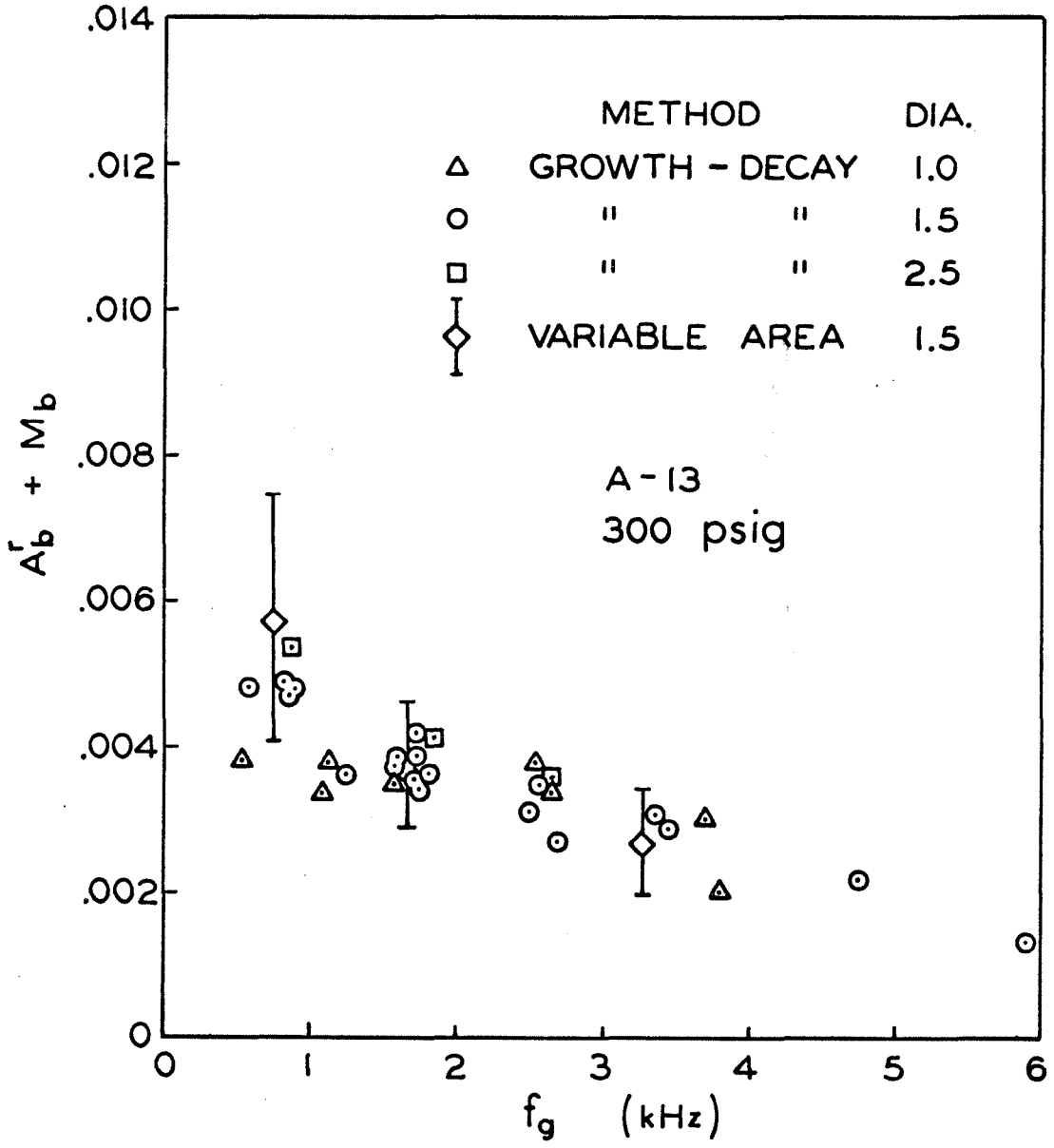

Figure 24. Comparison of Results Obtained from the Two T-burner Methods Using Theoretical Decay Constant.

stant. Naturally, if α_g is very small, this would not be a very accurate procedure. Another exception is in the case where metallized propellants are used. There, the losses may be due to particles present in the combustion products rather than to the wall dissipation assumed here. In such instances, account will have to be taken of the observed damping.

Conclusions Regarding the Two Methods

Naturally, the results of Figure 24 cannot be taken as proof that the usual interpretation of growth-decay data is incorrect. Likewise, they do not establish the existence of non-linear losses. However, they do support both contentions and provide an explanation of why growth-decay data often lie above variable-area data. Thus, the arguments presented in Section IX not only account for the observed losses reasonably well but also bring about a very good agreement between two independent T-burner methods which heretofore has been lacking. In the next section it will be shown that these same arguments can also be used to predict the limiting amplitude.

With regard to the methods themselves, there appears to be no real advantage of either method over the other, if the predicted losses are used in place of the observed ones. The accuracy of the two appears to be approximately the same. There is one point, however, which, depending on the situation, could be important. Under

ideal conditions, the variable-area method requires more experimental effort. Ideally, only one growth-decay test needs to be performed to determine the admittance. However, since the variable-area method depends on determining the slope of a line, a minimum of two tests are required. Naturally, in both cases, more than the minimum number of tests would be done in most instances. However, there are occasions when the extra effort required by the variable-area method might be considered a definite disadvantage.

Perhaps the best approach to T-burner testing is to conduct at least two tests at each frequency. The first, using an area ratio of unity, naturally provides data for both methods. The second, conducted at a ratio different from unity, also provides data for both methods if equation (2.19), using the theoretical decay constant, is used to calculate the results from the growth-decay method. In this way, three data points are obtained, two by the growth-decay and one by the variable-area method. If careful procedures are followed, then the results shown in this section indicate that good agreement should be observed in the three values inferred.

XI. THE LIMITING AMPLITUDE OF THE OSCILLATIONS

Of the many aspects of the T-burner examined during these studies, certainly one of the most interesting is the nature of the limiting amplitude of the oscillations. In nearly every test the wave amplitude reached a limiting value which was as reproducible as any other feature of the firing. The only exceptions were those few tests conducted at very low frequencies where the growth rate was so low that the amplitude increased throughout the test without ever reaching a very large value. These, however, comprised a small fraction of the total number of firings.

Despite the fact that the limiting amplitude must reflect certain non-linear features of the T-burner or the propellant admittance, this particular aspect has received very little attention in the past[26]. During the present studies, however, it was examined as a function of frequency, chamber diameter, and mean pressure for the different propellants. From these observations it is now apparent that the amplitude limitation results mainly from non-linear losses in the burner rather than from non-linearities in the response of the propellant. Moreover, it will be shown also that the acoustic losses described in Section IX can account very well for the observed behavior of the limiting amplitude. Thus, additional support is given the arguments presented there.

General Aspects of the Limiting Amplitude

One characteristic of the waves in the T-burner is that, despite

their large amplitude, they are generally very sinusoidal in appearance. This behavior is quite different from that observed when large acoustic waves are driven by a piston vibrating in the end of a closed tube. There, shock waves are generally encountered when resonance is approached[27].

Figure 25a shows a waveform which is typical of that observed in the majority of the tests. Clearly, the wave is very sinusoidal. Although for this particular test the limiting amplitude was only about 5 percent of the mean pressure, a similar behavior was observed in cases where the amplitude reached 10 to 15 percent of the chamber pressure. At still higher amplitudes, however, the waveform became distorted, as shown in Figure 25b. Nevertheless, even in these cases the harmonic content of the waveform was relatively small. As an example, for the wave shown here, where the amplitude is 23 percent of the mean pressure, by graphical procedures it has been determined that the amplitudes of the second through the fifth harmonics total less than 31 percent of that of the first harmonic. For a sawtooth waveform, the amplitude of the n^{th} harmonic is proportional to $1/n$. Thus, the amplitudes of the second through the fifth harmonics total about 128 percent of that of the fundamental. Clearly then, the waves in the T-burner, even in their most distorted form, are far from being sawtooth-shaped shock waves.

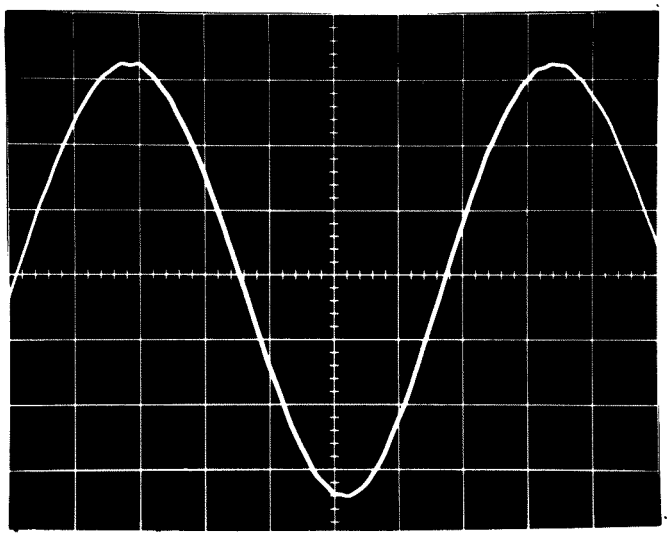

A-13 propellant

$\overline{p'}$ = 34 psi

P = 600 psig

$\overline{f}$ = 1.36 hKz

Figure 25a. Example of the Nearly Sinusoidal Waveform Observed in the Majority of the Tests.

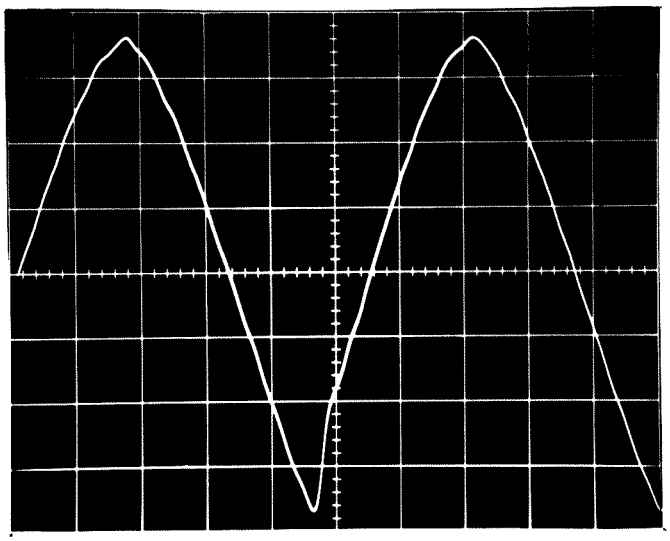

A-13 Propellant

$\overline{p'}$ = 72 psi

P = 300 psig

$\overline{f}$ = 1.44 kHz

Figure 25b. Distorted Waveform Observed in a Few Tests Where the Amplitude Was Very Large.

The sinusoidal nature of the T-burner oscillations is probably the result of several effects. First, for all of the even harmonics, the vent is located at a pressure anti-node and, therefore, damps these modes strongly. Second, the acoustic losses of the burner definitely increase with frequency, which again implies large damping for the higher harmonics. The effects of damping were very apparent after burnout, when even the most distorted waveform quickly returned to a nearly perfect sine wave. Finally, the response of the propellant itself decreases at higher frequencies. Thus, the higher harmonics are both more heavily damped and less effectively driven, with the result being a waveform relatively free of harmonic distortion.

Two other characteristic features of the limiting amplitude are evident in Figure 26, where results obtained from tests using A-13 propellant in chambers of different diameters are shown. For a given diameter, it is clear that the limiting amplitude reaches a maximum for a frequency in the range of 1 to 2 kHz. Gould[26] observed a similar dependence on frequency. In addition, a similar behavior was observed with the other propellants examined in the present studies. Another feature obvious from the figure is that, for a particular frequency, the limiting amplitude increases with chamber diameter. This, of course, must be related to characteristics of the burner itself and indicates that non-linearities in the propellant response alone

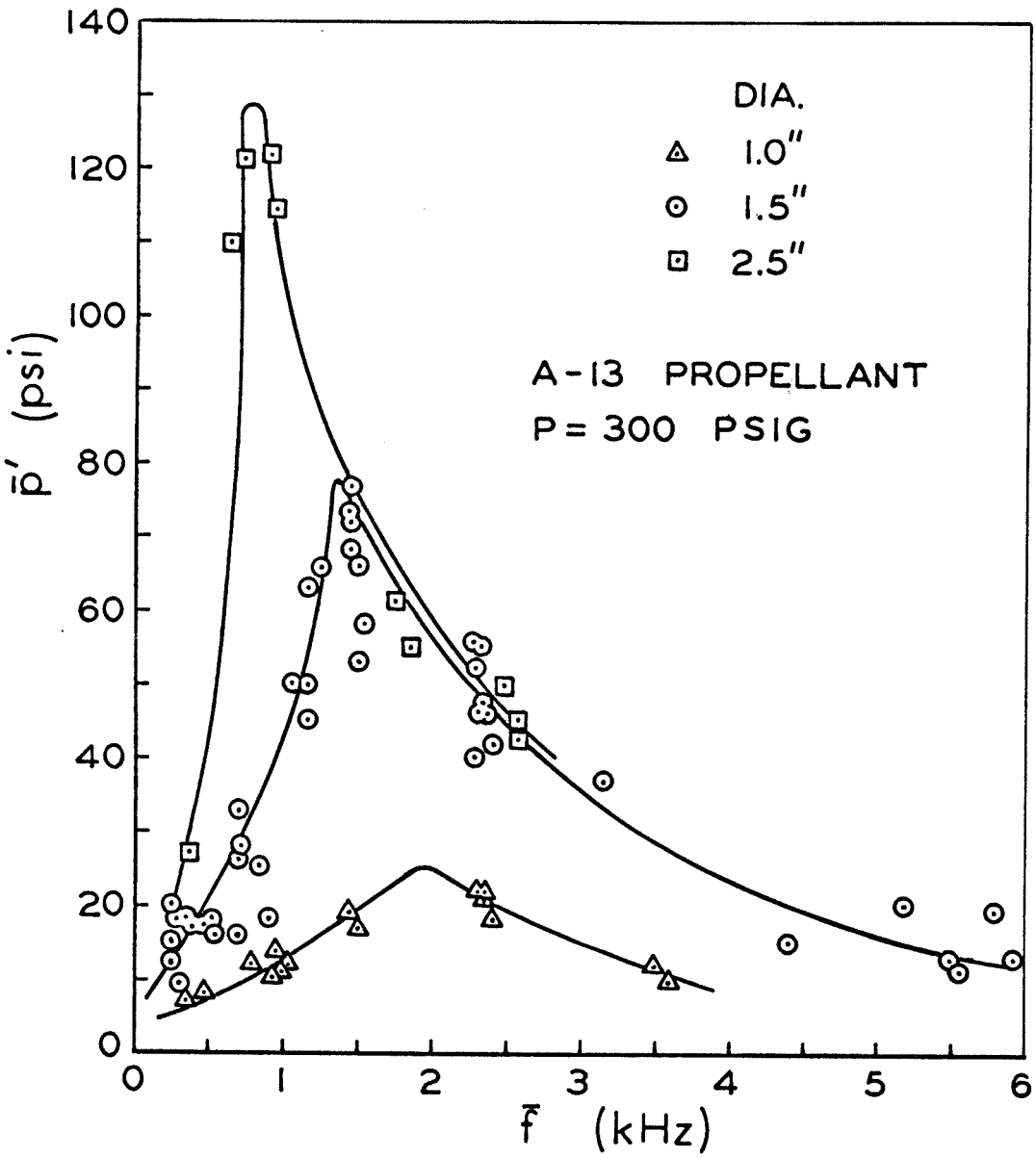

Figure 26. Limiting Amplitude as a Function of Frequency for Different Chamber Diameters.

cannot account for the observed amplitude limitation. Thus, non-linear losses dependent on diameter must be present in the T-burner.

The final aspect examined was the effect of chamber pressure on the limiting amplitude. Results obtained are shown in Figure 27 for a chamber diameter of 1.5 inch. For a given frequency, we see that the limiting amplitude reaches a maximum near a pressure of 300 psig. A similar behavior was observed with T-17 and 540-A propellants, although in the latter case the maximum occurred near a mean pressure of 500 psig.

The nature of the limiting amplitude is similar to that of the propellant response, which also passes through maxima with respect to frequency and pressure. Thus, qualitatively, the behavior of the limiting amplitude is probably just a reflection of the propellant's ability to drive the oscillations. However, we see that the actual value attained by the amplitude is strongly dependent on the diameter of the burner. Thus, although one can say that, in general, the limiting amplitude will be large when the response is large, a quantitative description requires knowledge of the effects of the burner itself.

Predictions of Limiting Amplitude Based on Non-linear Losses

It was mentioned in Section IX that if the losses are non-linear, then a possible explanation for the limiting amplitude is provided. Obviously, if the losses increase sufficiently with amplitude, then as the oscillations grow, a point will be reached where the losses just

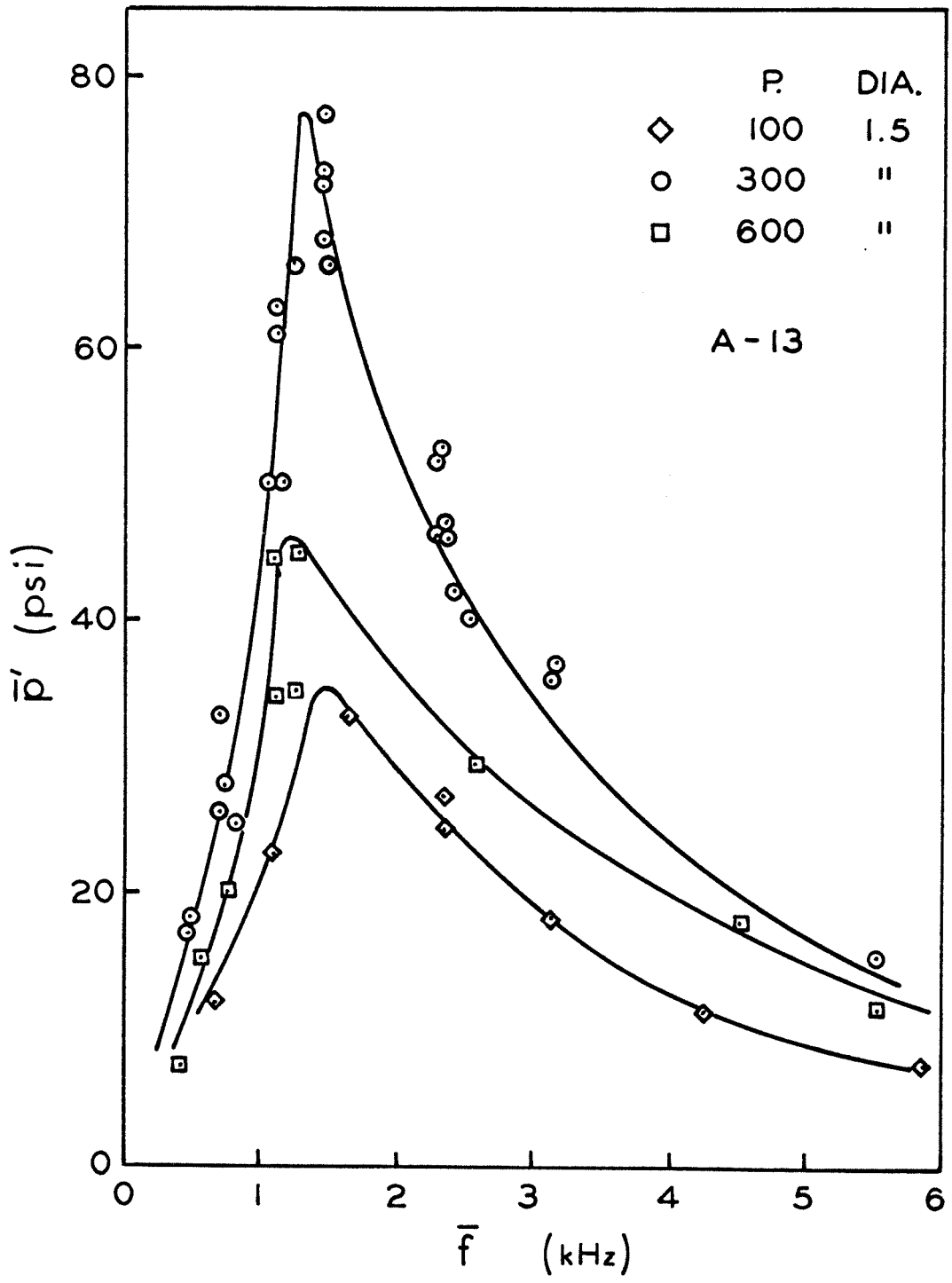

Figure 27. Limiting Amplitude for Different Chamber Pressures as a Function of Frequency.

balance the gains provided by the propellant.

For small amplitudes, the acoustic losses described in Section IX are almost negligible compared to the driving by the propellant. The initial growth rate is therefore nearly equal to the ideal value given in equation (2.16). With non-linear losses present, the growth rate decreases as the waves grow until finally it becomes zero when limiting amplitude is reached. If the propellant response is linear, then obviously the difference between the decay constant at limiting amplitude and its value at zero amplitude must equal the initial growth constant. As a first approximation, the decay constant at zero amplitude can be neglected. Also, the decay constant observed immediately after burnout is essentially that present at limiting amplitude. Thus, if the amplitude limitation arises completely from non-linear losses, then the observed growth and decay constants should be equal. In Figure 28, growth and decay constants obtained for the same test are plotted against each other for a variety of chamber conditions. Clearly, for most of the tests, α_g and α_d are nearly equal. The latter observation is not new, but in the past it has generally been viewed as a matter of coincidence. Now, however, we see that it provides evidence that the amplitude limitation arises primarily from non-linear losses and not from non-linearities in the admittance. In addition to its importance to the present considerations, this conclusion has other significant consequences, among which

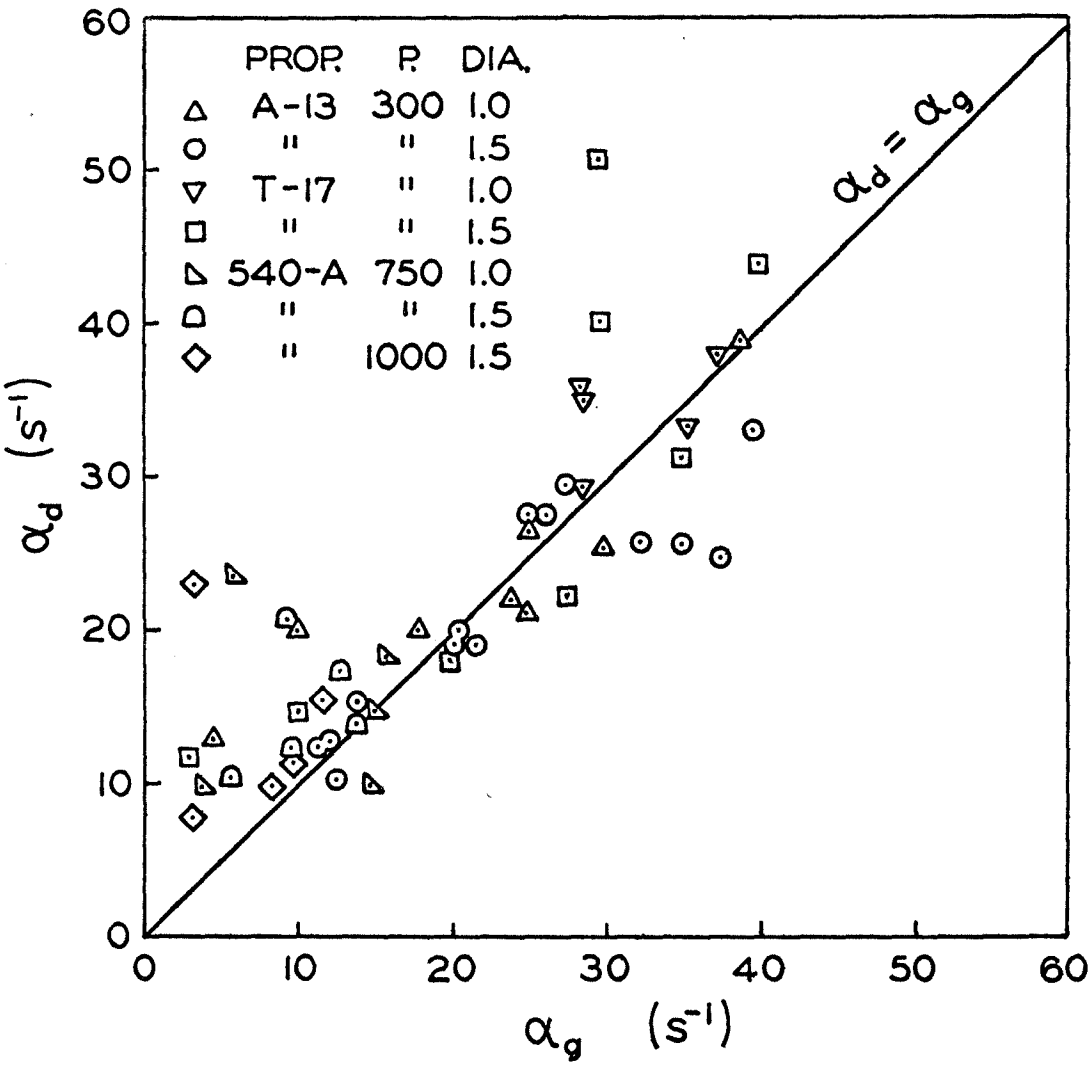

Figure 28. Observed Decay Constant Plotted Against Growth Constant.

is the fact that apparently the linear description of the admittance is valid even for reasonably large amplitudes. Since most descriptions of the admittance are based on linear approximations, it is encouraging to find evidence that they may be valid over a larger range of amplitudes than has generally been assumed.

Having shown that the amplitude limitation appears to arise from non-linear losses, the next step is to determine if the acoustic losses described in Section IX can account for the observed behavior. It was mentioned in that section that a simple, and yet valid, expression for the decay constant in terms of the amplitude could not be given. Consequently, an equation explicitly relating the limiting amplitude to the other test measurables cannot be obtained. However, this does not prevent numerical calculation of the limiting amplitude.

From Section IX it will be recalled that by specifying the wave amplitude, the heat flux at the wall can be calculated. From these calculations follow a value for the temperature of the acoustic boundary layer which, in turn, permits determination of the decay constant through equation (9.6). By following this procedure for various amplitudes, α_d can be determined as a function of p'. Ideally, for a given test, the limiting amplitude is obtained by finding that value of p' where the change in α_d from its value at zero amplitude just equals

the observed growth constant. However, it was shown earlier that the predicted decay constants are only about half the magnitude of those observed. Hence, to be consistent, the predicted decay constants should be multiplied by two. With this condition, the limiting amplitude is given when

$$\alpha_d(\bar{p}') - \alpha_d(0) = \tfrac{1}{2}\alpha_g \quad ,$$

where the decay constants are calculated from equations (9.5) - (9.8) and α_g is the observed growth constant.

This procedure was followed for a number of tests and the results are presented in Figure 29, where the predicted limiting amplitude is plotted against the observed value. For the calculations a wall temperature of 375°K was assumed, which is halfway between the initial wall temperature of 300°K and the typical final value of 450°K. From the figure it is apparent that the predicted and observed values agree very well. In fact, the agreement is better than ± 10 psi for over two-thirds of the tests. Considering the approximations made and the fact that, as mentioned in Section IV, the limiting amplitude itself was not always a well-defined quantity, the agreement is remarkably good.

Thus, we see that the behavior of the limiting amplitude over a wide range of frequencies, chamber diameters, mean pressures, and propellant formulations can be predicted rather accurately on the

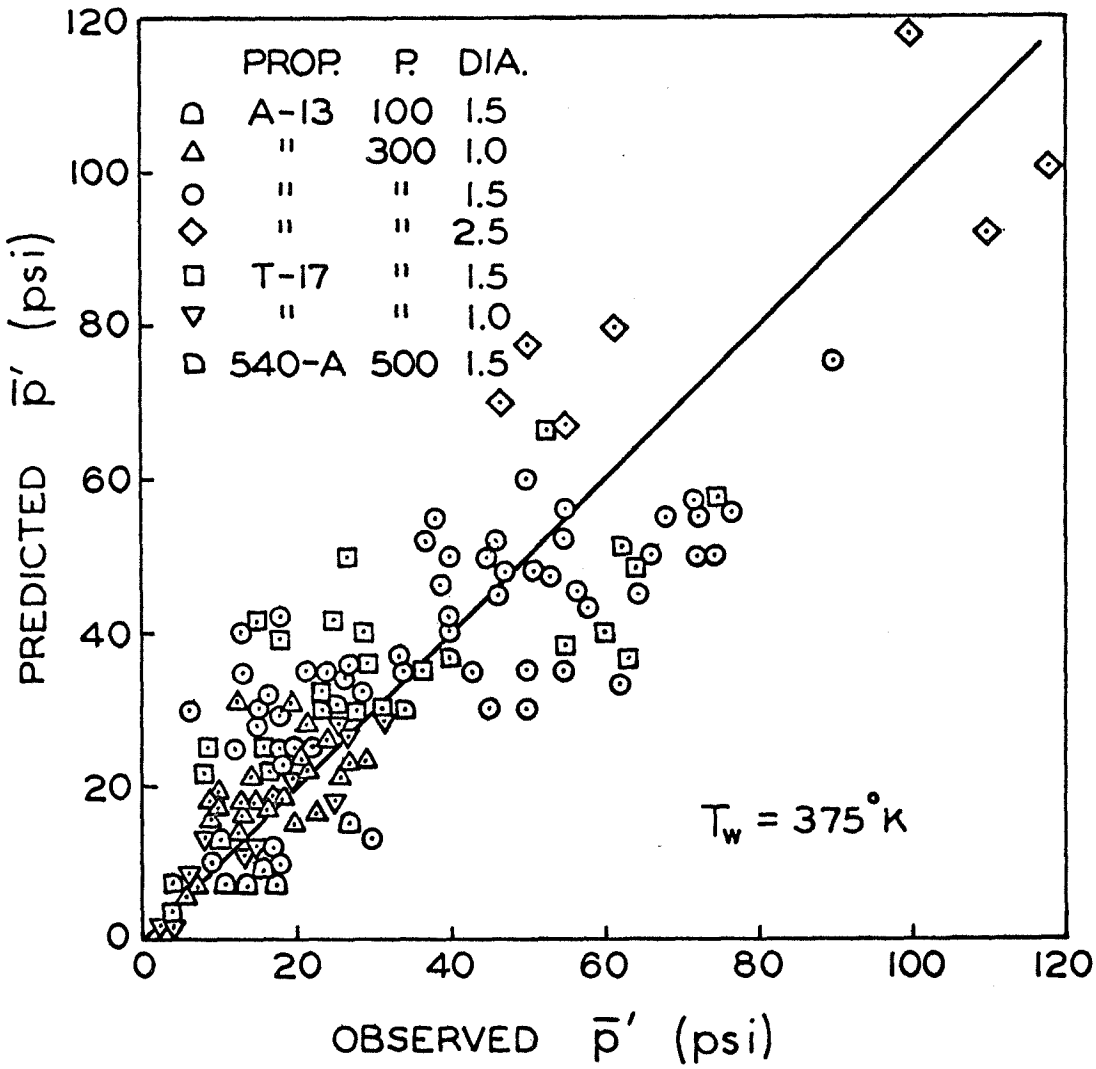

Figure 29. Comparison of Predicted and Observed Limiting Amplitude.

basis of the acoustic losses described earlier. Since considerable experimental evidence supports the description of those losses, there can be little doubt but that the arguments presented there are at least basically correct.

XII. T-BURNER DATA AND ROCKET MOTOR INSTABILITY

Although the T-burner has been involved in many prior studies of solid propellant instability, little effort has been given to establishing the relevance of T-burner data to predictions of combustion instability in rocket motors. Ideally, for a given motor design, one would like to be able to construct a stability map based on T-burner measurements and other pertinent factors, such as the nature of the flow field and the various damping mechanisms present in the motor. Even a crude prediction of the stability characteristics would be an improvement over the usual approach.

The most comprehensive study of solid rocket instability is that of Brownlee and Marble[28], which involved over 400 test firings of cylindrically perforated, case-bonded motors using a single propellant formulation. The instability, occurring as the first tangential mode of the chamber whenever it appeared, was examined as a function of motor geometry, chamber pressure, and initial grain temperature.

Those studies produced a stability map for one propellant operating in such a motor configuration. The stability map was presented in several ways, most often in the K_n-D_p plane, where K_n is the ratio of initial burning area to throat area and D_p the initial diameter of the grain port. Since K_n is related to the chamber pres-

sure and D_p to the frequency of the observed mode, the stability map is easily transformed into the P-D_p and the P-f planes. For discussion of T-burner data, the latter form is probably the most useful since pressure and frequency are the usual T-burner test variables.

The feature of most interest in the stability map was the stability boundary itself, which separated the region where small oscillations would grow from that where they would decay. Although several chamber lengths were used in the Brownlee-Marble studies, the majority of the motors were 31.0 inches long. For these, the stability boundary was given quite well over a wide range by

$$K_n = 66.1\, D_p \,, \tag{12.1}$$

with the stable region lying above this line. The stability boundary shifted downward in the K_n-D_p plane as the motor length was decreased. Since in the K_n-D_p plane a given firing would proceed along a straight line whose slope depended on the throat diameter, the boundary given by the above equation indicates that the motor's stability characteristics depended very much on the throat size.

Subsequent to those studies, the stability of acoustic oscillations in solid rocket motors was examined analytically[2], and the following expression was found for the growth constant for small pressure disturbances, where the present notation has been adopted:

$$\alpha_g = \left(\frac{A_b^r}{1-m_1^2} - M_b \Lambda \right) \frac{2\bar{a}}{D_p} - (\beta + \sigma) \,. \tag{12.2}$$

The term $M_b \Lambda$, where Λ depends on the nature of the flow, represents the contribution of the mean flow to the driving of the waves. It will be shown that for the first tangential mode Λ is negative. From the above equation it is apparent that this implies that the mean flow tends to drive the waves. Thus, even if the admittance is negative, oscillations may still be unstable if the mean flow contribution is large enough. This, of course, is not particularly surprising, since it is also true in the T-burner where equation (2.18) corresponds to the above equation. However, it is important to realize that the stability of a rocket motor depends on both the mean flow and the propellant response.

Returning to equation (12.2), β and σ represent attenuation effects arising, respectively, from losses in the gas phase and at the head end of the chamber. The former are presumably due to the presence of solid particles in the combustion products and the latter to viscous dissipation at the head wall of the motor. Finally, m_1 is a mathematical constant, approximately equal to 0.543, and is related to the mode shape.

If the growth rate is set equal to zero, then (12.2) is an equation for the stability boundary. From this results the following expression for the admittance at the stability boundary:

$$A_b^r = \frac{(1-m_1^2)(\beta+\sigma)D_p}{2\bar{a}} + (1-m_1^2)M_b\Lambda \quad . \tag{12.3}$$

For given chamber conditions, if the admittance is greater than this value, the motor will presumably be unstable. Obviously, by increasing the damping, larger values for the admittance are acceptable.

The term Λ has been calculated[29] for the potential flow field in the motor as well as for a rotational field. For these two cases we have,

$$\Lambda_{potential} = - \frac{m_1^2}{1 - m_1^2} \tag{12.4a}$$

$$\Lambda_{rotational} = \Lambda_{potential} + \left(\frac{\pi \beta_r}{2} - 1 \right) \tag{12.4b}$$

where β_r is an integral expression evaluated in reference 29. For numerical purposes, these two values are

$$\Lambda_{potential} = -0.418 \tag{12.5a}$$

$$\Lambda_{rotational} = -0.154 \tag{12.5b}$$

for the first tangential mode of the motor.

Returning to equation (12.2), it is obvious that the stability boundary of a rocket motor is reached when the contributions from the combustion, mean flow, and chamber damping just balance. Since the contribution from the mean flow is positive, this balance can occur for either positive or negative values of the admittance, depending on the amount of damping present.

For non-metallized propellants it has been argued[2] that the attenuation from solid particles in the exhaust, represented by β, can

be neglected since the only particles present are smoke particles, which contribute very little to the damping. The transparent T-burner revealed that the T-17 propellant used in the Brownlee-Marble studies produces very little smoke. Thus, for this propellant it can be assumed that β is zero. Naturally, for metallized propellants, this would be an invalid assumption. In such cases, explicit attention would have to be given the solid particle attenuation effects.

If σ is assumed to arise from viscous effects at the head end of the chamber, then by a simple calculation[2] it can be shown that

$$\sigma = \frac{21.4}{L\sqrt{D_p}} , \tag{12.6}$$

where σ is expressed in s^{-1} and both L and D_p in inches. This result follows from dividing the energy dissipated at the head end by the total energy in the chamber and corresponds to that given in equation (9.2) for the wall losses in the T-burner.

Using this expression and the assumption that β is zero, equation (12.3) becomes

$$A_b^r = 0.705 M_b \Lambda + \frac{6.5\sqrt{D_p}}{\bar{a} L} , \tag{12.7}$$

where the value for m_1 given earlier has been used.

In the Brownlee-Marble investigations, D_p was at most 5.5 inches, the diameter of the motor case itself. If L is taken as 31.0 inches and $\bar{a}$ is 3085 ft/sec, the second term on the right hand side of

this equation never exceeds 1.3×10^{-5}. Using the larger of the two values given for Λ in equation (12.5) and assuming M_b is 0.003, as found in Section V, the first term on the right hand side is equal to 3.0×10^{-4}. Thus, the attenuation effects are at least an order of magnitude smaller than the contribution from the mean flow. If the former are neglected, then the stability boundary takes on a very simple form indeed:

$$A_b^r / M_b = 0.705 \Lambda \quad . \tag{12.8}$$

This equation predicts the stability boundary when damping effects are small, or, more specifically, when

$$\frac{(\beta+\sigma)D_p}{2\bar{a}M_b\Lambda} \ll 1 \quad . \tag{12.9}$$

To compare the stability boundary predicted by equation (12.8) with that observed, the admittance of the T-17 propellant used by Brownlee and Marble was measured at chamber pressures of 200, 300, and 400 psig over a frequency range of from 0.5 to 6.0 hKz. The tests were conducted in T-burners of 1.0 and 1.5 inch diameter. An initial temperature of 160°F, corresponding to that used in the Brownlee-Marble studies, was closely achieved by conditioning the assembled burners overnight in an oven maintained at 170°F.

Because T-17 is not sufficiently unstable to drive oscillations well at reduced area ratios, the variable-area method could not be

employed. Therefore, the growth-decay method was used, but the admittance was calculated by assuming a theoretical decay constant instead of the observed value for the reasons given in Section X.

The results obtained at a pressure of 300 psig are given in Figure 30, where the ratio A_b^r/M_b is shown as a function of frequency. The solid line is simply a curve fitted to the data. The dashed lines, however, correspond to equation (12.8) for rotational and potential flows. The stability boundary for the rocket motor at 300 psig should be given by the points where the solid and dashed lines intersect. For a rotational flow field, we see from the figure that this occurs at a frequency of 2.8 hKz, and for the potential flow at 3.8 hKz.

From similar plots obtained at the other pressures, the stability boundaries shown as the dashed curves in Figure 31 were determined for the two flow fields. The solid line is the boundary observed by Brownlee and Marble and clearly lies well above the predicted curves. Obviously, the agreement is too poor to make quantitative predictions of the motor's stability characteristics on the basis of the T-burner measurements. At best, the latter provide only a crude estimate of the actual stability boundary.

Although the reason for this lack of agreement is not clear, there are several possibilities. First, there is no certainty that the T-17 propellant used here was identical to that used in the motor firings. The batch to batch reproducibility of this propellant is not as

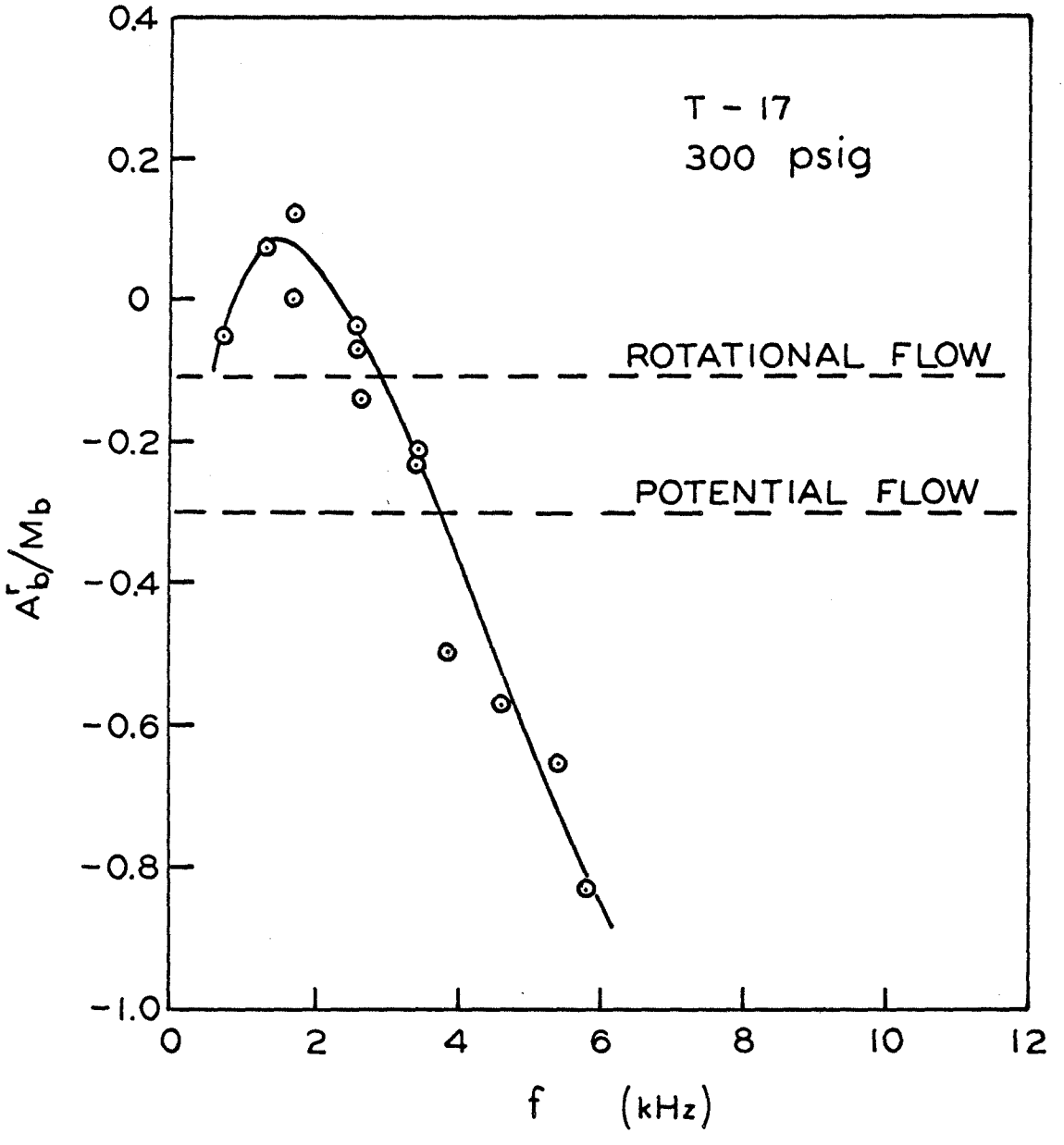

Figure 30. The Ratio A_b^r/M_b for T-17 Propellant at 300 psig. Dashed Lines Represent Eq. (12.8) for Rotational and Potential Flows.

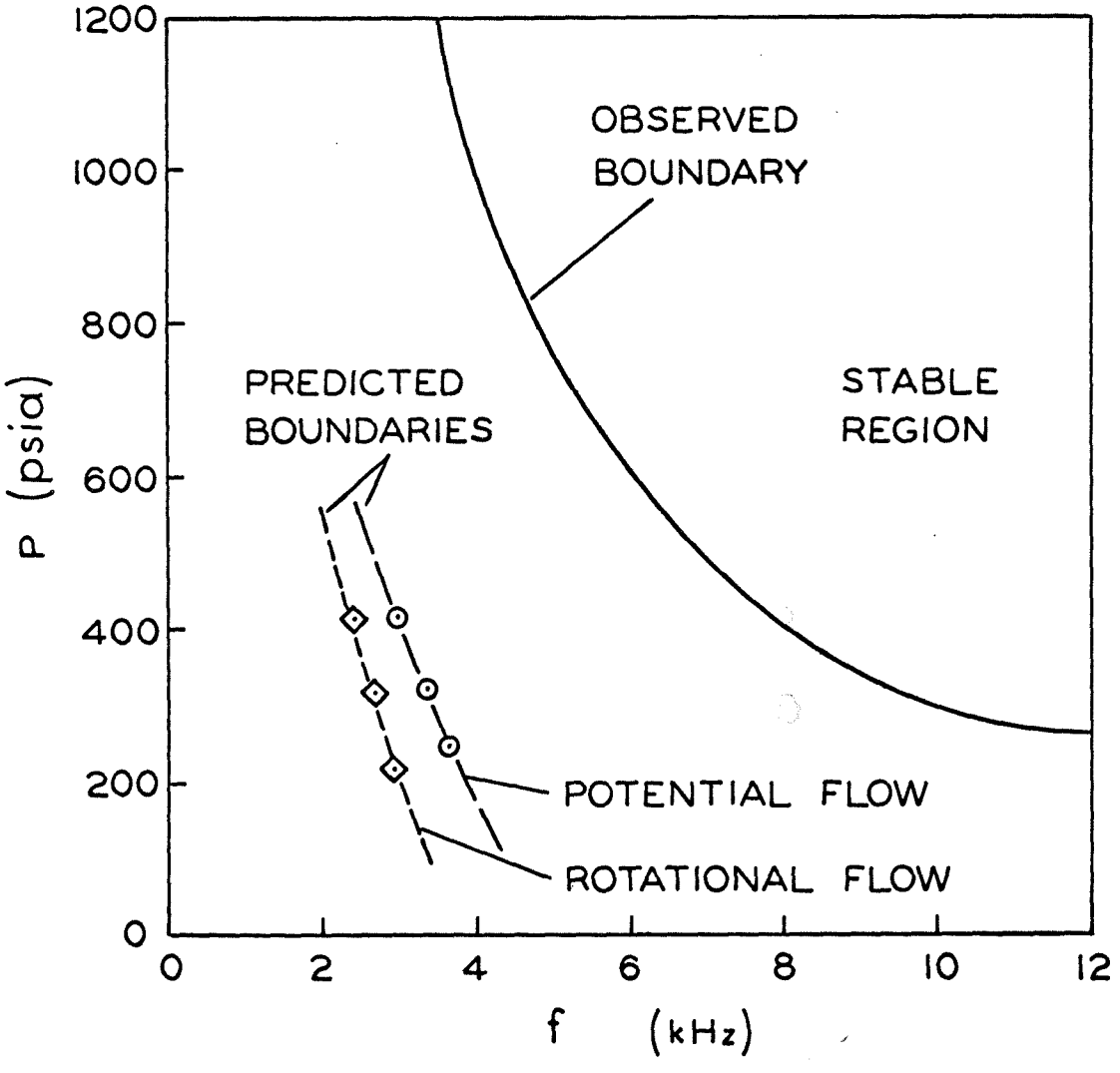

Figure 31. Predicted and Observed Stability Boundaries for the Rocket Motors Used in Ref. 28.

good as one would like. In fact, the propellant used in the T-burner tests had to receive additional high-temperature curing before it hardened sufficiently to use. The effects of this extra curing on the propellant response are unknown, but could be responsible for the observed behavior.

Another possibility is that the analysis of reference 2 is incomplete in some way. As an example, that analysis, which resulted in the equation for the predicted stability boundary, neglected effects on the propellant response arising from acoustic velocities parallel to the burning surface. Although in the T-burner the acoustic velocity is normal to the propellant surface, in the rocket motor the velocity of the tangential mode is parallel to the combustion zone. Thus, the admittance inferred from T-burner measurements may be different from that associated with the propellant in the motor. However, since little is known about the effects of "velocity coupling," no quantitative estimates of the errors involved in neglecting them can be given.

Finally, one cannot overlook the possibility that the T-burner measurements themselves are incorrect. For instance, if the observed decay constant had been used in reducing the data instead of the theoretical values, better agreement between the predicted and observed stability boundaries would have resulted. However, good agreement would still have been lacking, and from the arguments presented in Section X, it appears that the use of the observed decay constants is

incorrect. In any case, it is doubtful if the errors in the T-burner measurements are large enough to account for the observed disagreement since the present studies have shown that most of the basic assumptions of the T-burner method are valid.

At present, the only conclusion which can be drawn is that more comparisons of this type are needed in order to determine the role of the T-burner in studies of instability in rocket motors.

XIII. SUMMARY OF MAJOR CONCLUSIONS

Because of the length of the previous sections, it seems appropriate to summarize briefly the major conclusions drawn from the investigations.

Certainly, one of the most significant findings is that, on the basis of a number of different observations, the acoustic losses of the T-burner appear to be non-linear. As a result, the losses measured after burnout are larger than those present when the waves first begin to grow. This, in turn, implies that the usual interpretation of the growth-decay T-burner method is incorrect. Instead of using the observed decay constant, one should use a theoretical value based on the amplitude present when the growth constant is measured. Since, for low amplitudes, the theoretical losses are small, a first approximation for the admittance can be obtained by neglecting the losses completely. In any case, agreement between the growth-decay and the variable-area T-burner methods is not obtained when the observed decay constant is used, but is observed when the theoretical value is employed.

By both direct and indirect means, it was found that the heat transfer from the combustion gases to the chamber wall is dependent on the amplitude of the oscillations. In addition, a good correlation was obtained from the heat transfer data.

From the transparent burner studies it is clear that the T-

burner is basically a one-dimensional device with three-dimensional effects confined primarily to a small region near the vent.

The ignition studies provided further evidence that a rapid, even ignition is essential to obtaining reproducible and meaningful test data.

Finally, predictions of rocket motor instability based on T-burner measurements were found to be in poor agreement with actual observations. Although several possible reasons for this disagreement were offered, it is apparent that only through further such comparisons can the role of the T-burner in such studies be defined.

LIST OF SYMBOLS

a	speed of sound
a_1	burning rate coefficient
A_b	admittance of burning propellant
c_1	$(T_c - T_w)/T_w$
c_p	specific heat at constant pressure
c_v	specific heat at constant volume
D	chamber diameter
D_p	port diameter of rocket motor grain
e_a	acoustic energy
e_T	thermal energy
f	frequency
h	heat transfer coefficient
h_d	directly determined heat transfer coefficient
h_i	indirectly determined heat transfer coefficient
k	thermal conductivity
K_n	ratio of propellant area to nozzle throat area in rocket motor
L	chamber length
m	mass flux
m_1	constant related to mode shape
m_p	mass of propellant burned
M	Mach number

M_i	mass of nitrogen in surge tank
n	burning rate exponent
N	number of flow reversals
Nu	Nusselt number
p'	acoustic pressure
$\bar{p}'$	limiting amplitude
P	mean chamber pressure
Pr	Prandtl number
$\dot{q}_w$	heat flux at wall
r	burning rate
R	gas constant
R_b	response function of burning propellant
Re	Reynolds number
Re_a	acoustic Reynolds number
S_b	area of burning propellant
S_c	cross-sectional area of chamber
S_v	cross-sectional area of vent
t	time
t_b	burn time
T	temperature
T_c	combustion temperature
T_{BL}	temperature of acoustic boundary layer
T_w	wall temperature

u	velocity
u'	acoustic velocity
V	surge tank volume
W	work done by burning propellant on the oscillations
α_d	observed decay constant
α'_d	instantaneous value of decay constant
α_g	observed growth constant
β	measure of acoustic losses due to solid particles
γ	specific heats ratio, c_p/c_v
δ	thickness of acoustic boundary layer
λ	defined in equation (8.11)
Λ	contribution of mean flow to the acoustic driving
μ	viscosity coefficient
ν	kinematic viscosity coefficient
ρ	density
ρ_s	density of solid propellant
σ	acoustic damping due to viscous attenuation

Subscripts

$(\ )_{am}$	arithmetic mean
$(\ )_b$	evaluated at burning surface
$(\ )_{BL}$	evaluated at temperature T_{BL}
$(\ )_c$	evaluated at combustion zone

$( )_f$ final value

$( )_g$ pertains to combustion gases

$( )_i$ initial value

$( )_o$ stagnation value

$( )_w$ value at wall

Superscripts

$( )^i$ imaginary part

$( )^r$ real part

$\overline{( )}$ mean value of steady quantities, limiting value of fluctuating quantities

$( )'$ fluctuating part of

REFERENCES

1. Bird, J.F., McClure, F.T., and Hart, R.W., "Acoustical Instability in the Transverse Modes of Solid Propellant Rockets," Twelfth International Astronautical Congress, pp. 459-473 (1963).

2. Culick, F.E.C., "Acoustic Oscillations in Solid Rocket Chambers," Astronautica Acta, Vol. 12, No. 2, pp. 113-126 (1960).

3. Price, E.W. and Sofferis, J.W., "Combustion Instability in Solid Propellant Rocket Motors," Jet Propulsion, Vol. 28, No. 3, pp. 190-192 (1958).

4. Horton, M.D., "One-Dimensional Solid Propellant Oscillatory Burner," ARS Journal, Vol. 31, No. 11, pp. 1596-1597 (1961).

5. Krier, H., Mathes, H.B., Price, E.W., and Summerfield, M., "Entropy Waves Produced in Oscillatory Combustion of Solid Propellants," AIAA Paper 68-499, presented at the ICRPG/AIAA Third Solid Propulsion Conference, Atlantic City, N.J. (1968).

6. Horton, M.D. and Rice, D.W., "The Effect of Compositional Variables upon Oscillatory Combustion of Solid Rocket Propellants," Combustion and Flame, Vol. 8, No. 1, pp. 21-28 (1964).

7. "T-Burner Manual," prepared by the Committee on Standardization of Combustion Instability Measurements in the T-Burner of the ICRPG Working Group on Solid Propellant Combustion, Chemical Propulsion Information Agency Publication No. 191 (1969).

8. Culick, F.E.C., "A Review of Calculations for Unsteady Burning of a Solid Propellant," AIAA Journal, Vol. 6, No. 12, pp. 2241-2255 (1968).

9. Cantrell, R.H. and Hart, R.W., "Interaction between Sound and Flow in Acoustic Cavities: Mass, Momentum, and Energy Considerations," Journal of the Acoustical Society of America, Vol. 36, No. 4, pp. 697-706 (1964).

10. Eisel, J.L., Horton, M.D., Price, W.E., and Rice, D.W., "Preferred Frequency Oscillatory Combustion of Solid Propellants," AIAA Journal, Vol. 2, No. 7, pp. 1319-1323 (1964).

11. Stepp, E. E., "Effect of Pressure and Velocity Coupling on Low-Frequency Instability," AIAA Journal, Vol. 5, No. 5, pp. 945-948 (1967).

12. Bogdonoff, D. W., "A Study of the Mechanisms of Heat Transfer in Oscillating Flow," Tech. Report No. 483-f, Dept. of Aerospace and Mechanical Sciences, Princeton University (1967).

13. Horton, M. D., Eisel, J. L., and Dehority, G. L., "Heat Transfer Coefficients for a Hot Gas Oscillating at High Amplitudes in a Cylindrical Chamber," A. I. Ch. E. Journal, Vol. 10, No. 4, pp. 580-583 (1964).

14. Bartz, D. R., "A Simple Equation for Rapid Estimation of Rocket Nozzle Convective Heat Transfer Coefficients," Jet Propulsion, Vol. 27, No. 1, pp. 49-51 (1957).

15. McAdams, W. H., Heat Transmission, 3rd edition, McGraw-Hill, New York, p. 219 (1954).

16. Mathes, H. B., Naval Weapons Center, China Lake, Calif. (private communication).

17. Sellers, J. P., "Thermocouple Probes for Evaluating Local Heat Transfer Coefficients in Rocket Motors," in Temperature, Its Measurement and Control in Science and Industry, Vol. III, Part 2, Reinhold Publishing Co., New York, pp. 673-679 (1962).

18. Howard, F. G., "Single-Thermocouple Method for Determining Heat Flux to a Thermally Thick Wall," NASA TN D-4737 (1968).

19. Horton, M. D., "Testing the Dynamic Stability of Solid Propellants: Techniques and Data," NOTS Tech. Pub. 3610, China Lake, Calif., pp. 4-5 (1964).

20. Lambert, R. F., "A Study of the Factors Influencing the Damping of an Acoustical Cavity Resonator," Journal of the Acoustical Society of America, Vol. 25, No. 6, pp. 1068-1083 (1953).

21. Landau, L. D. and Lifschitz, E. M., Fluid Mechanics, Addison-Wesley Publishing Co., Reading, Mass., p. 303 (1959).

22. Perry, E. H., "T-Burner Studies," Space Programs Summary 37-51, Vol. III, Jet Propulsion Laboratory, Pasadena, Calif., pp. 105-108 (1968).

23. Parker, J. G., "Effect of Adsorption on Acoustic Boundary-Layer Losses," Journal of Chemical Physics, Vol. 36, No. 6, pp. 1547-1554 (1962).

24. Cantrell, R. H., McClure, F. T., and Hart, R. W., "Acoustic Damping in Cavities with Mean Velocity and Thermal Boundary Layers," Journal of the Acoustical Society of America, Vol. 35, No. 4, pp. 500-509 (1963).

25. Coates, R. L., Horton, M. D., and Ryan, N. W., "T-burner Method of Determining the Acoustic Admittance of Burning Propellants," AIAA Journal, Vol. 2, No. 6, pp. 1119-1122 (1964).

26. Gould, R. D., "Combustion Instability Studies with Plastic Propellant," AIAA Paper 69-478, presented at the AIAA 5th Propulsion Joint Specialist Conference, U. S. Air Force Academy, Colorado Springs, Colorado (1969).

27. Chester, W., "Resonant Oscillations in Closed Tubes," Journal of Fluid Mechanics, Vol. 18, p. 44 (1964).

28. Brownlee, W. G. and Marble, F. E., "An Experimental Investigation of Unstable Combustion in Solid Propellant Rocket Motors," in Progress in Astronautics and Rocketry, Vol. 1, Academic Press, New York, pp. 455-494 (1960).

29. Culick, F. E. C., "Rotational Axisymmetric Mean Flow and Damping of Acoustic Waves in a Solid Propellant Rocket," AIAA Journal, Vol. 4, No. 8, pp. 1462-1464 (1966).

30. Hirschfelder, J. O., Curtiss, C. F., and Bird, R. B., Molecular Theory of Gases and Liquids, John Wiley and Sons, New York, pp. 528-534, 570, 599, 1110-1129 (1954).

APPENDIX A. Data Tables

In the following tables are found data obtained from many of the tests. Unless mentioned explicitly in the table heading, the area ratio S_b/S_c is unity. The tests using T-17 propellant had an initial grain temperature of 160°F. All other tests were conducted at 80°F. Below is a list of the tables, giving the major variables.

Table	Propellant	Pressure (psig)	Diameter (in.)	Area Ratio
1	A-13	100	1.5	1.00
2	A-13	300	1.0	1.00
3	A-13	300	1.5	1.00
4	A-13	300	1.5	0.72
5	A-13	300	1.5	0.43
6	A-13	300	2.5	1.00
7	A-13	600	1.5	1.00
8	T-17	300	1.0	1.00
9	T-17	300	1.5	1.00
10	T-17	300	2.5	1.00
11	T-17	400	1.5	1.00
12	540-A	500	1.5	1.00
13	540-A	750	1.0	1.00
14	540-A	750	1.5	1.00
15	540-A	1000	1.5	1.00
16	540-A	1250	1.5	1.00

TABLE 1. A-13 Propellant at 100 psig in 1.5-Inch Diameter Chambers.

Run No.	Ignition Method	L (in)	$\bar{r}$ (in/s)	$\bar{f}$ (kHz)	$\bar{p}'$ (psi)	f_g (kHz)	α_g (s^{-1})	f_d (kHz)	α_d (s^{-1})
70	1	31.5	0.109	0.35	14	0.38	4.0	0.33	3.7
85	1	31.5	0.122	0.35	10	0.40	6.8	0.31	5.0
69	1	19.0	0.091	0.68	19	0.66	7.7	0.62	3.5
82	1	19.0	0.080	0.68	12	0.67	7.7	0.65	3.9
91	1	19.0	0.117	0.68	16	0.72	11.7	0.62	6.4
66	1	13.0	0.104	1.08	23	1.06	5.6	1.00	5.6
67	1	7.0	0.106	2.32	25	2.33	11.5	2.10	7.4
81	1	7.0	0.122	2.34	28	2.40	30.8	2.15	14.8

TABLE 2. A-13 Propellant at 300 psig in 1.0-Inch Diameter Chambers.

Run No.	Ignition Method	L (in)	$\bar{r}$ (in/s)	$\bar{f}$ (kHz)	$\bar{p}'$ (psi)	f_g (kHz)	α_g (s^{-1})	f_d (kHz)	α_d (s^{-1})
54	1	32.5	0.198	0.36	8	0.28	5.9	0.33	6.6
50	1	25.5	0.198	0.77	12	0.48	3.4	0.40	8.5
322	1	25.5	0.188	0.48	8	0.56	4.5	0.38	13.2
48	1	14.0	0.192	1.04	12	1.06	15.1	0.98	12.3
51	1	14.0	0.208	0.96	23	1.04	9.8	0.92	13.8
80	1	14.0	0.188	1.00	11	1.10	10.0	0.95	12.4
303	1	14.0	0.184	0.96	14	1.14	12.9	0.85	16.0
315	1	14.0	0.185	0.96	10	1.10	10.2	0.80	20.0
316	1	10.0	0.189	1.52	17	1.65	17.7	1.45	20.0
421	1	10.0	0.201	1.44	19	1.75	25.0	1.28	19.2
46	1	7.0	0.180	2.36	21	2.45	23.5	2.25	16.0
49	1	7.0	0.187	2.52	9	2.53	23.5	2.45	16.9
52	1	7.0	0.192	2.40	18	2.45	21.6	2.32	14.3
416	1	7.0	0.191	2.34	22	2.58	30.2	2.16	24.2
420	1	7.0	0.198	2.32	22	2.55	32.5	2.10	26.6
319	1	5.0	0.190	3.60	10	3.83	25.8	3.39	27.5
343	1	5.0	0.185	3.50	12	3.72	39.0	3.20	38.0
107	4	25.5	0.190	0.49	9	0.55	10.9	0.44	7.4
112	4	25.5	0.181	0.49	6	0.53	3.8	0.46	10.2
104	4	14.0	0.188	0.99	15	1.05	13.3	0.90	7.9

TABLE 2 (continued)

Run No.	Ignition Method	L (in)	$\bar{r}$ (in/s)	$\bar{f}$ (kHz)	$\bar{p}'$ (psi)	f_g (kHz)	α_g (s^{-1})	f_d (kHz)	α_d (s^{-1})
110	4	14.0	0.178	0.95	13	1.07	10.5	0.97	8.4
113	4	14.0	0.174	0.94	21	1.04	13.3	0.93	10.5
103	4	7.0	0.185	2.48	15	2.54	24.2	2.44	8.8
114	4	7.0	0.183	2.38	26	2.55	25.4	2.15	18.4
119	4	7.0	0.172	2.36	26	2.44	26.2	2.28	16.0
109	4	7.0	0.181	2.37	20	2.46	17.4	2.20	11.1
100	4	7.0	0.184	2.36	29	2.48	27.6	2.26	14.9

TABLE 3. A-13 Propellant at 300 psig in 1.5-Inch Diameter Chambers.

Run No.	Ignition Method	L (in)	$\bar{r}$ (in/s)	$\bar{f}$ (kHz)	$\bar{p}'$ (psi)	f_g (kHz)	α_g (s^{-1})	f_d (kHz)	α_d (s^{-1})
18	1	43.5	0.181	0.24	12	0.30	3.7	0.21	9.1
23	1	43.5	0.192	0.23	20	0.28	3.4	0.21	6.3
26	1	43.5	0.187	0.25	15	0.30	3.6	0.21	7.4
27	1	43.5	0.187	0.25	15	0.30	3.6	0.21	7.4
47	1	43.5	0.196	0.30	9	0.31	4.5	0.23	6.0
12	1	37.5	0.191	0.32	17	0.35	3.2	0.27	8.5
17	1	37.5	0.192	0.29	18	0.35	5.9	0.24	9.2
8	1	31.5	0.192	0.38	18	0.40	5.1	0.37	7.1
22	1	31.5	0.187	0.36	18	0.45	5.9	0.30	8.1
6	1	25.5	0.182	0.52	18	0.55	7.7	0.38	8.7
21	1	25.5	0.184	0.52	16	0.56	8.5	0.45	10.0
362	1	25.5	0.190	0.49	17	0.55	7.1	0.40	10.0
5	1	19.5	0.188	0.91	18	0.76	11.1	0.66	7.6
13	1	19.0	0.181	0.70	16	0.72	11.4	0.68	8.0
24	1	19.0	0.182	0.70	33	0.80	12.8	0.57	10.8
306	1	19.0	0.188	0.84	25	0.84	11.8	0.56	12.5
309	1	19.0	0.188	0.72	28	0.82	12.1	0.55	12.5
311	1	19.0	0.189	0.70	26	0.84	12.5	0.54	10.0
10	1	13.0	0.195	1.16	45	1.30	15.7	1.00	18.6
15	1	13.0	0.188	1.15	50	1.24	17.2	0.99	12.2

TABLE 3 (continued)

Run No.	Ignition Method	L (in)	$\bar{r}$ (in/s)	$\bar{f}$ (kHz)	$\bar{p}'$ (psi)	f_g (kHz)	α_g (s^{-1})	f_d (kHz)	α_d (s^{-1})
16	1	13.0	0.184	1.05	50	1.28	19.6	0.85	13.3
43	1	13.0	0.187	1.14	63	1.35	16.0	1.04	16.3
307	1	13.0	0.192	1.24	66	1.24	13.8	0.90	15.1
301	1	10.0	0.185	1.44	77	1.70	21.6	1.23	16.6
302	1	10.0	0.189	1.52	58	1.75	21.6	1.30	22.8
305	1	10.0	0.191	1.46	68	1.75	21.6	1.24	19.1
308	1	10.0	0.192	1.44	73	1.75	20.5	1.24	19.1
310	1	10.0	0.192	1.44	72	1.70	20.5	1.32	19.0
337	1	10.0	0.189	1.50	53	1.70	20.9	1.35	19.5
339	1	10.0	0.188	1.48	66	1.65	20.0	1.24	17.9
7	1	7.0	0.187	2.29	52	2.48	23.5	2.24	18.6
14	1	7.0	0.189	2.27	56	2.44	28.0	2.10	10.8
19	1	7.0	0.192	2.35	47	2.60	29.2	2.15	13.9
20	1	7.0	0.193	2.33	55	2.50	32.0	2.10	13.3
25	1	7.0	0.188	2.36	46	2.58	28.6	2.15	16.6
340	1	7.0	0.195	2.28	40	2.50	25.8	2.05	27.5
342	1	7.0	0.191	2.32	46	2.60	32.0	2.02	26.2
347	1	7.0	0.188	2.40	42	2.70	26.2	2.10	27.5
313	1	5.5	0.194	3.15	37	3.45	36.3	2.78	25.4
330	1	5.5	0.197	3.16	36	3.40	37.8	2.72	24.2

TABLE 3 (continued)

Run No.	Ignition Method	L (in)	$\bar{r}$ (in/s)	$\bar{f}$ (kHz)	$\bar{p}'$ (psi)	f_g (kHz)	α_g (s^{-1})	f_d (kHz)	α_d (s^{-1})
327	1	4.3	0.190	4.40	15	4.75	39.0	4.05	33.3
312	1	3.5	0.195	5.50	13	5.90	27.5	5.05	29.4
87	3	31.5	0.172	0.38	21	0.40	5.0	0.32	3.8
95	3	31.5	0.104	0.37	6	0.41	2.9	0.36	2.3
86	3	13.0	0.172	1.10	24	1.19	12.2	1.10	8.4
94	3	13.0	0.111	1.08	34	1.08	6.0	1.13	3.7
88	3	10.0	0.194	1.52	57	1.57	12.5	1.53	7.7
78	3	7.0	0.127	2.34	43	2.50	17.4	2.38	10.4
96	4	31.5	0.181	0.34	24	0.43	7.9	0.33	6.7
101	4	25.5	0.181	1.39	86	1.72	20.0	1.30	16.0
97	4	19.0	0.182	0.70	26	0.80	12.1	0.60	8.9
99	4	13.0	0.188	1.10	64	1.27	18.6	0.88	12.9
102	4	10.0	0.185	1.39	90	1.72	20.0	1.30	16.0
106	4	10.0	0.181	1.44	72	1.63	16.7	1.35	12.5
111	4	10.0	0.180	1.44	74	1.62	17.4	1.35	10.5
98	4	7.0	0.195	2.44	40	2.66	28.6	2.30	14.8
105	4	7.0	0.180	2.34	55	2.58	17.4	2.14	13.3
143	4	7.0	0.167	2.38	45	2.47	17.8	2.13	10.8
167	4	5.5	0.178	3.20	39	3.55	33.3	2.90	15.4
168	4	3.8	0.173	5.20	21	5.50	25.4	4.72	16.3

TABLE 4. A-13 Propellant at 300 psig in 1.5-Inch Diameter Chambers.

Area Ratio = 0.72

Run No.	Ignition Method	L (in)	$\bar{r}$ (in/s)	$\bar{f}$ (kHz)	$\bar{p}'$ (psi)	f_g (kHz)	α_g (s^{-1})	f_d (kHz)	α_d (s^{-1})
318	1	19.0	0.190	0.64	18	0.80	7.0	0.58	11.7
324	1	19.0	0.187	0.64	16	0.78	6.7	0.55	12.1
328	1	10.0	0.194	1.52	20	1.65	13.5	1.27	14.3
331	1	10.0	0.193	1.48	19	1.65	16.2	1.27	14.8
341	1	10.0	0.194	1.48	18	1.68	13.3	1.15	13.8
326	1	5.5	0.188	3.12	23	3.35	23.8	3.00	31.4
332	1	5.5	0.195	3.12	29	3.40	24.2	2.80	18.2

TABLE 5. A-13 Propellant at 300 psig in 1.5-Inch Diameter Chambers.

Area Ratio = 0.43

Run No.	Ignition Method	L (in)	$\bar{r}$ (in/s)	$\bar{f}$ (kHz)	$\bar{p}'$ (psi)	f_g (kHz)	α_g (s^{-1})	f_d (kHz)	α_d (s^{-1})
321	1	19.0	0.184	0.67	2	0.76	3.8	0.58	9.1
329	1	19.0	0.195	0.68	3	0.76	4.2	0.59	8.9
325	1	10.0	0.196	1.50	4	1.68	8.7	1.35	12.1
346	1	10.0	0.179	1.54	2	1.65	7.4	1.44	17.4
333	1	5.5	0.192	3.20	8	3.30	16.7	3.10	24.2
338	1	5.5	0.188	3.24	3	3.35	16.0	3.20	28.5
108	4	19.0	0.181	0.68	4	0.70	2.4	0.64	4.6
115	4	13.0	0.177	0.95	8	1.13	6.0	0.94	6.7
121	4	13.0	0.180	1.05	7	1.13	7.0	0.95	8.2
116	4	10.0	0.174	1.42	9	1.60	8.3	1.36	10.8
122	4	10.0	0.178	1.50	10	1.59	10.0	1.42	10.5
117	4	7.0	0.183	2.24	10	2.47	9.1	2.18	12.1
120	4	7.0	0.176	2.25	10	2.40	13.9	2.15	14.3
134	4	7.0	0.185	2.16	13	2.37	10.0	2.32	12.7

TABLE 6. A-13 Propellant at 300 psig in 2.5-Inch Diameter Chambers.

Run No.	Ignition Method	L (in)	$\bar{r}$ (in/s)	$\bar{f}$ (kHz)	$\bar{p}'$ (psi)	f_g (kHz)	α_g (s^{-1})	f_d (kHz)	α_d (s^{-1})
361	1	10.0	0.193	1.60	61	1.85	28.6	1.13	11.8
422	1	20.0	0.200	0.63	110	0.85	16.0	0.53	12.1
360	1	7.0	0.192	2.49	45	2.65	35.5	2.20	16.0
278	2	10.0	0.165	1.64	55	1.70	25.4	1.35	13.4
235	2	7.0	0.160	2.50	43	2.60	24.2	2.35	21.6
246	2	7.0	0.172	2.45	50	2.65	28.1	2.15	15.4
136	4	31.0	0.183	0.39	27	0.46	8.1	0.36	7.2
139	4	20.0	0.181	0.72	121	0.84	11.4	0.48	12.1
127	4	15.0	0.152	0.91	123	1.07	16.6	0.82	9.5
135	4	15.0	0.181	0.93	114	1.18	16.0	0.75	7.2

TABLE 7. A-13 Propellant at 600 psig in 1.5-Inch Diameter Chambers.

Run No.	Ignition Method	L (in)	$\bar{r}$ (in/s)	$\bar{f}$ (kHz)	$\bar{p}'$ (psi)	f_g (kHz)	α_g (s^{-1})	f_d (kHz)	α_d (s^{-1})
34	1	31.5	0.253	0.48	7	0.52	2.0	0.42	7.3
38	1	25.5	0.275	0.56	16	0.62	2.6	0.42	9.3
32	1	19.0	0.284	0.69	15	0.70	4.9	0.55	10.5
35	1	19.0	0.271	0.78	20	0.90	5.3	0.65	9.1
30	1	13.0	0.288	1.13	45	1.34	7.5	1.00	12.1
36	1	13.0	0.269	1.20	45	1.35	7.7	1.15	14.3
55	1	13.0	0.257	1.20	33	1.32	5.5	1.05	11.1
393	1	13.0	0.269	1.36	34	1.35	6.8	1.05	13.3
394	1	10.0	0.272	1.68	16	1.84	8.0	1.55	18.1
31	1	7.0	0.288	2.56	29	2.68	8.9	2.45	19.0
37	1	7.0	0.271	2.56	25	2.70	9.5	2.40	18.2
53	1	7.0	0.270	2.52	41	2.66	8.7	2.42	17.8
389	1	7.0	0.275	2.58	24	2.75	11.1	2.30	21.5
390	1	5.5	0.263	3.40	18	3.50	12.1	3.30	25.0
396	1	5.5	0.266	3.32	32	3.50	14.8	3.00	24.2
391	1	4.3	0.278	4.54	17	4.70	17.0	4.00	50.0
392	1	3.5	0.266	5.52	11	5.90	13.8	5.20	43.2

TABLE 8. T-17 Propellant at 300 psig in 1.0-Inch Diameter Chambers.

Run No.	Ignition Method	L (in)	$\bar{r}$ (in/s)	$\bar{f}$ (kHz)	$\bar{p}'$ (psi)	f_g (kHz)	α_g (s^{-1})	f_d (kHz)	α_d (s^{-1})
414	1	10.0	0.308	1.49	25	1.75	28.0	1.35	29.6
411	1	7.0	0.320	2.28	31	2.60	36.4	1.98	33.3
413	1	7.0	0.313	2.33	22	2.65	38.0	2.03	38.1
412	1	5.0	0.321	3.52	16	3.80	29.6	3.10	53.0
261	2	25.5	0.272	0.60	4	0.60	4.1	0.45	13.3
280	2	25.5	0.268	0.60	3	0.60	3.4	0.45	12.3
240	2	14.0	0.278	1.05	15	1.15	10.2	0.90	14.8
255	2	10.0	0.269	1.02	10	1.15	9.1	0.90	14.8
270	2	10.0	0.272	1.44	23	1.65	13.3	1.33	19.3
274	2	10.0	0.269	1.55	15	1.65	10.0	1.35	15.0
247	2	7.0	0.278	2.40	8	2.50	18.6	2.25	22.8
275	2	7.0	0.269	2.40	7	2.50	7.4	2.15	20.5

TABLE 9. T-17 Propellant at 300 psig in 1.5-Inch Diameter Chambers.

Run No.	Ignition Method	L (in)	$\bar{r}$ (in/s)	$\bar{f}$ (kHz)	$\bar{p}'$ (psi)	f_g (kHz)	α_g (s^{-1})	f_d (kHz)	α_d (s^{-1})
404	1	19.0	0.312	0.60	54	0.84	10.5	0.32	15.3
407	1	13.0	0.301	1.04	75	1.34	20.5	0.87	17.7
402	1	10.0	0.312	1.48	62	1.80	27.5	1.22	22.2
403	1	7.0	0.305	2.44	28	2.66	34.8	2.10	30.8
406	1	5.5	0.298	3.18	26	3.46	40.0	2.90	44.4
415	1	5.5	0.296	3.20	24	3.46	39.0	2.97	40.0
405	1	4.3	0.305	4.25	17	4.60	29.1	3.95	40.0
408	1	3.8	0.309	5.07	13	5.38	29.9	4.68	52.5
429	1	3.3	0.294	5.52	7	5.80	10.2	5.28	43.4
229	2	31.5	0.271	0.50	3	0.50	4.0	0.38	7.3
221	2	13.0	0.279	1.05	60	1.28	12.9	0.88	11.1
262	2	13.0	0.269	1.05	63	1.30	11.4	0.85	11.7
264	2	10.0	0.263	1.45	55	1.65	12.3	1.35	14.3
192	2	7.0	0.253	2.35	35	2.55	20.0	2.10	15.5
283	2	7.0	0.275	2.35	31	2.55	14.8	2.25	22.1
211	2	5.5	0.291	3.20	21	3.35	24.2	3.05	17.4
239	2	5.5	0.288	3.25	24	3.20	24.2	3.00	36.4
265	2	5.5	0.275	3.13	17	3.30	12.9	3.05	25.0
273	2	5.5	0.269	3.05	28	3.30	13.3	3.00	27.6
212	2	4.3	0.284	4.25	16	4.40	14.4	4.10	26.7

TABLE 10. T-17 Propellant at 300 psig in 2.5-Inch Diameter Chambers.

Run No.	Ignition Method	L (in)	$\bar{r}$ (in/s)	$\bar{f}$ (kHz)	$\bar{p}'$ (psi)	f_g (kHz)	α_g (s^{-1})	f_d (kHz)	α_d (s^{-1})
287	2	19.0	0.272	0.84	5	0.88	8.3	0.80	9.6
286	2	10.0	0.272	1.72	31	1.80	23.5	1.45	16.0
281	2	10.0	0.278	1.64	40	1.75	20.0	1.45	13.8
282	2	7.0	0.275	2.50	22	2.60	21.0	2.35	21.0

TABLE 11. T-17 Propellant at 400 psig in 1.5-inch Diameter Chambers.

Run No.	Ignition Method	L (in)	$\bar{r}$ (in/s)	$\bar{f}$ (kHz)	$\bar{p}'$ (psi)	f_g (kHz)	α_g (s^{-1})	f_d (kHz)	α_d (s^{-1})
430	1	3.8	0.313	4.70	7	4.90	8.3	4.52	49.5
431	1	5.5	0.309	3.12	26	3.36	22.2	2.75	40.0
232	2	19.0	0.281	0.80	7	0.88	6.0	0.68	12.9
225	2	13.0	0.288	1.18	29	1.33	10.0	1.00	11.9
226	2	10.0	0.301	1.60	25	1.72	10.8	1.40	16.7
223	2	7.0	0.288	2.44	19	2.55	16.0	2.44	16.3
227	2	5.5	0.301	3.16	19	3.35	13.6	2.95	27.6
234	2	5.5	0.301	3.16	15	3.30	10.5	3.10	29.6

TABLE 12. 540-A Propellant at 500 psig in 1.5-Inch Diameter Chambers.

Run No.	Ignition Method	L (in)	$\bar{r}$ (in/s)	$\bar{f}$ (kHz)	$\bar{p}'$ (psi)	f_g (kHz)	α_g (s^{-1})	f_d (kHz)	α_d (s^{-1})
378	1	19.0	0.208	0.72	32	0.87	8.2	0.60	11.1
417	1	19.0	0.205	0.73	22	0.90	9.8	0.60	12.9
419	1	19.0	0.213	0.74	25	0.86	8.6	0.60	10.8
377	1	13.0	0.210	1.04	64	1.38	9.3	0.87	12.9
376	1	10.0	0.214	1.56	40	1.96	11.1	1.28	13.8
367	1	7.0	0.206	2.70	5	2.80	4.2	2.30	21.0

TABLE 13. 540-A Propellant at 750 psig in 1.0-Inch Diameter Chambers.

Run No.	Ignition Method	L (in)	$\bar{r}$ (in/s)	$\bar{f}$ (kHz)	$\bar{p}'$ (psi)	f_g (kHz)	α_g (s^{-1})	f_d (kHz)	α_d (s^{-1})
352	1	14.0	0.201	1.08	8	1.28	14.2	0.96	10.2
357	1	14.0	0.200	1.08	7	1.26	14.2	0.88	9.5
350	1	10.0	0.195	1.64	8	1.86	14.8	1.40	14.3
351	1	7.0	0.208	2.60	7	2.80	15.1	2.25	18.5

TABLE 14. 540-A Propellant at 750 psig in 1.5-Inch Diameter Chambers.

Run No.	Ignition Method	L (in)	$\bar{r}$ (in/s)	$\bar{f}$ (kHz)	$\bar{p}'$ (psi)	f_g (kHz)	α_g (s^{-1})	f_d (kHz)	α_d (s^{-1})
345	1	19.0	0.207	0.72	16	0.90	5.7	0.60	9.5
355	1	19.0	0.211	0.76	19	0.85	5.5	0.64	10.5
348	1	13.0	0.203	1.08	35	1.40	9.5	0.94	12.5
354	1	10.0	0.210	1.55	34	1.80	35.5	1.37	13.8
398	1	10.0	0.200	1.49	36	1.92	12.1	1.25	11.3
353	1	7.0	0.208	2.52	18	2.85	12.9	2.15	17.4
399	1	7.0	0.208	2.44	25	2.84	12.2	2.10	14.8
349	1	5.5	0.206	3.45	11	3.63	9.0	3.10	21.6

TABLE 15. 540-A Propellant at 1000 psig in 1.5-Inch Diameter Chambers.

Run No.	Ignition Method	L (in)	$\bar{r}$ (in/s)	$\bar{f}$ (kHz)	$\bar{p}'$ (psi)	f_g (kHz)	α_g (s^{-1})	f_d (kHz)	α_d (s^{-1})
371	1	25.5	0.210	0.60	5	0.65	2.6	0.48	7.7
375	1	19.0	0.207	0.82	10	0.95	4.5	0.69	8.9
400	1	13.0	0.208	1.24	13	1.45	8.5	1.05	8.0
368	1	10.0	0.215	1.73	13	1.90	9.8	1.50	11.9
374	1	7.0	0.210	2.50	19	2.85	13.3	2.20	18.6
369	1	5.5	0.210	3.36	18	3.80	11.7	2.90	15.4
373	1	4.3	0.205	4.60	11	4.90	6.7	4.15	24.2
380	1	3.5	0.208	5.84	1	5.80	4.1	5.55	28.6

TABLE 16. 540-A Propellant at 1250 psig in 1.5-Inch Diameter Chambers.

Run No.	Ignition Method	L (in)	$\bar{r}$ (in/s)	$\bar{f}$ (kHz)	$\bar{p}'$ (psi)	f_g (kHz)	α_g (s^{-1})	f_d (kHz)	α_d (s^{-1})
385	1	13.0	0.221	1.32	8	1.44	5.1	1.09	7.4
381	1	7.0	0.227	2.64	12	2.86	8.9	2.64	12.5
384	1	5.5	0.221	3.44	12	3.68	6.9	2.95	17.8
382	1	4.3	0.214	4.60	11	4.90	6.2	4.20	25.8
383	1	3.5	0.223	5.30	1	5.50	2.4	5.15	15.6

APPENDIX B. Linear T-burner Analysis

The following analysis of the T-burner is essentially that given in reference 7, although some slight changes have been made. There, it is shown that by writing the pressure and velocity as

$$p = P + p'$$

$$u = \bar{u} + u'$$

where P is the mean pressure, $\bar{u}$ the mean flow velocity, and p' and u' the fluctuations in pressure and velocity; the one-dimensional conservation equations become

$$\frac{\partial u'}{\partial t} + \frac{1}{\bar{\rho}} \frac{\partial p'}{\partial x} = -\frac{\partial}{\partial x} (\overline{uu'}) \quad , \tag{B.1a}$$

$$\frac{\partial p'}{\partial t} + \gamma P \frac{\partial u'}{\partial x} = -(\bar{u} \frac{\partial p'}{\partial x} + \gamma p' \frac{d\bar{u}}{dx}) \quad . \tag{B.1b}$$

By differentiating the first of these with respect to x and the second with respect to t and subtracting, we find

$$\bar{a}^{-2} \frac{\partial^2 p}{\partial x^2} - \frac{\partial^2 p}{\partial t^2} = \frac{\partial}{\partial t} (\bar{u} \frac{\partial p'}{\partial x} + \gamma p' \frac{d\bar{u}}{dx}) - \gamma P \frac{\partial^2}{\partial x^2} (\bar{u} u') , \tag{B.2}$$

where $\bar{a}^{-2} \equiv \gamma P/\bar{\rho}$ is the average speed of sound in the chamber.

If the fluctuations are assumed harmonic, then the time dependence is $\exp(i\Omega t)$ where Ω is the complex frequency given by

$$\Omega \equiv \omega - i\alpha \quad . \tag{B.3}$$

Here, ω is the actual frequency and α the "growth constant" of the oscillations. Under this assumption, equation (B.2) becomes

$$\frac{d^2p'}{dx^2} + k^2 p' = h \ , \tag{B.4}$$

where

$$k \equiv \Omega/\bar{a} \tag{B.5}$$

and

$$h \equiv -\bar{\rho} \frac{d^2}{dx^2}(\bar{u}u') + i\frac{k}{\bar{a}}\left(\bar{u}\frac{dp'}{dx} + \gamma p' \frac{d\bar{u}}{dx}\right) . \tag{B.6}$$

To obtain the growth constant of the oscillations, equation (B.4) must be solved subject to the boundary conditions given by equation (B.1a):

$$\frac{dp'}{dx} = -f \qquad \text{at } x = 0, L \ , \tag{B.7}$$

where

$$f \equiv ik\bar{\rho}\bar{a}u' + \bar{\rho}\frac{d}{dx}(\bar{u}u') . \tag{B.8}$$

To find the values of k that satisfy the above, consider the problem of acoustic waves in a closed tube containing no mean flow. For that problem the equations corresponding to (B.4) and (B.7) are, respectively,

$$\frac{d^2\psi}{dx^2} + k_o^2 \psi = 0 \tag{B.9}$$

and

$$\frac{d\psi}{dx} = 0 \qquad \text{at} \qquad x = 0, L \ . \tag{B.10}$$

Multiplying (B.4) by ψ and (B.9) by p', subtracting the two resulting equations, and integrating over the chamber, we obtain

$$\int_0^L \left[\psi \frac{d^2 p'}{dx^2} - p' \frac{d^2 \psi}{dx^2} \right] dx - \int_0^L \psi h \, dx + (k^2 - k_o^2) \int_0^L p' \psi \, dx = 0 \ .$$

The first integral can be integrated by parts, and after using (B. 7) and (B. 10), we find

$$k^2 = k_o^2 + \frac{1}{E^2} \left\{ \int_0^L h \psi \, dx + [f \psi]_0^L \right\} \ , \qquad \text{(B. 11)}$$

where

$$E^2 \equiv \int_0^L p' \psi \, dx \ .$$

To obtain k^2 to first order, it is valid to replace p' and u' by their unperturbed values on the right hand side of (B. 11). Thus,

$$p' \cong \psi = \cos k_o x \qquad \text{(B. 12a)}$$

$$u' \cong \frac{i}{\bar{\rho} \bar{a} k_o} \frac{d\psi}{dx} \qquad \text{(B. 12b)}$$

where $k_o = n\pi/L$ for the n^{th} mode. With these substitutions, we find

$$E^2 \cong \int_0^L \cos^2 k_o x \, dx = \frac{L}{2} \ . \qquad \text{(B. 13)}$$

Also, the integral in (B. 11) can be written

$$\int_0^L h \psi \, dx \cong - \frac{i}{\bar{a} k_o} \int_0^L \psi \frac{d^2}{dx^2} \left(\bar{u} \frac{d\psi}{dx} \right) dx + \frac{ik_o}{\bar{a}} \left\{ \int_0^L \bar{u} \psi \frac{d\psi}{dx} \, dx + \gamma \int_0^L \psi^2 \frac{d\bar{u}}{dx} \, dx \right\} .$$

The first integral can be integrated by parts twice, and, after (B. 9) and (B. 10) are used, becomes

$$\int_0^L \psi \frac{d^2}{dx^2} \left(\bar{u} \frac{d\psi}{dx} \right) = \left[\psi \frac{d}{dx} \left(\bar{u} \frac{d\psi}{dx} \right) \right]_0^L - k_o^2 \int_0^L \bar{u} \psi \frac{d\psi}{dx} \, dx \ .$$

Thus,

$$\int_0^L h\psi dx = \frac{2ik_o}{\bar{a}} \int_0^L \bar{u}\psi \frac{d\psi}{dx} + \frac{i\gamma k_o}{\bar{a}} \int_0^L \psi^2 \frac{d\bar{u}}{dx} dx - \frac{i}{\bar{a}k_o} \left[\psi \frac{d}{dx}(\bar{u}\frac{d\psi}{dx})\right]_0^L .$$

But,

$$\int_0^L \bar{u}\psi \frac{d\psi}{dx} dx = \tfrac{1}{2}\int_0^L \bar{u}\frac{d\psi^2}{dx} dx = \tfrac{1}{2}[\bar{u}\psi^2]_0^L - \tfrac{1}{2}\int_0^L \psi^2 \frac{d\bar{u}}{dx} dx .$$

Therefore,

$$\int_0^L h\psi dx = \frac{ik_o}{\bar{a}}[\bar{u}\psi]_0^L - \frac{i}{\bar{a}k_o}\left[\psi \frac{d}{dx}(\bar{u}\frac{d\psi}{dx})\right]_0^L + \frac{ik_o}{\bar{a}}(\gamma-1)\int_0^L \psi^2 \frac{d\bar{u}}{dx} dx .$$

Now

$$\bar{u}(x) = \begin{cases} u_b & 0 < x < L/2 \\ -u_b & L/2 < x < L \end{cases}$$

where u_b is the speed of the gases leaving the burning propellant.

Thus,

$$\int_0^L \psi^2 \frac{d\bar{u}}{dx} = 0 ,$$

since $d\bar{u}/dx$ is zero except where ψ vanishes. Hence,

$$\int_0^L h\psi dx = -2ik_o \frac{u_b}{\bar{a}} \frac{S_b}{S_c} - \frac{i}{\bar{a}k_o}\left[\psi \frac{d}{dx}(\bar{u}\frac{d\psi}{dx})\right]_0^L , \qquad (B.14)$$

where the factor S_b/S_c is included to take into account the fact that the propellant covers only a partion of the chamber ends. Now

$$[f\psi]_0^L = ik_o\bar{\rho}\bar{a}[u'\psi]_0^L + \bar{\rho}[\psi \frac{d}{dx}(\bar{u}u')]_0^L \cong ik_o\bar{\rho}\bar{a}[u'\psi]_0^L + \frac{i}{\bar{a}k_o}[\psi \frac{d}{dx}(\bar{u}\frac{d\psi}{dx})]_0^L .$$

But u' is related to p' at the burning surface by the admittance:

$$u' = \pm \frac{a_b}{\gamma P} A_b p' \begin{cases} - & x = L \\ + & x = 0 \end{cases}$$

Since $p' \sim \psi$ we have

$$[u'\psi]_0^L \cong \frac{a_b}{\gamma P} A_b [-\psi^2(L) - \psi^2(0)] \frac{S_b}{S_c} = -2 \frac{a_b}{\gamma P} \frac{S_b}{S_c} A_b ,$$

where, again, the factor S_b/S_c reflects the fact that the propellant covers only a portion of the chamber ends. Thus,

$$[f\psi]_0^L = -2ik_o \frac{a_b}{\bar{a}} A_b \frac{S_b}{S_c} + \frac{i}{\bar{a} k_o} \left[\psi \frac{d}{dx} \left(\bar{u} \frac{d\psi}{dx} \right) \right]_0^L . \qquad \text{(B. 15)}$$

Combining (B. 14) and (B. 15), we find

$$\int_0^L h\psi dx + [f\psi]_0^L = -2ik_o \frac{a_b}{\bar{a}} \frac{S_b}{S_c} (A_b + M_b) \qquad \text{(B. 16)}$$

where $M_b \equiv u_b/a_b$. Thus, by (B. 11) and (B. 13) we see that

$$k^2 = k_o^2 - \frac{4ik_o}{L} \frac{a_b}{\bar{a}} \frac{S_b}{S_c} (A_b + M_b) . \qquad \text{(B. 17)}$$

From (B. 3) and (B. 5) we find that if the growth constant is small compared to the frequency, then

$$k^2 \cong \frac{\omega^2}{\bar{a}^2} - \frac{2i\alpha\omega}{\bar{a}^2} .$$

Taking real and imaginary part of (B. 17) we find

$$\frac{\omega^2}{\bar{a}^2} = k_o^2 + \frac{4ik_o}{L} \frac{a_b}{\bar{a}} \frac{S_b}{S_c} A_b^i \qquad \text{(B. 18a)}$$

$$\alpha = \frac{2a_b}{L} \frac{S_b}{S_c} (A_b^r + M_b) . \qquad \text{(B. 18b)}$$

APPENDIX C. Transport Properties of the Combustion Gases

According to Hirschfelder, Curtiss, and Bird[30], the viscosity of an N-component mixture is approximately

$$\mu = \sum_{i=1}^{N} \frac{X_i^2}{\frac{x_i^2}{\mu_i} + 2.308 \sum_{\substack{k=1 \\ k\neq i}}^{N} \frac{X_i X_k}{A_{ik}\mu_{ik}} \frac{M_k}{M_i+M_k}} \quad , \qquad (C.1)$$

where X_i, μ_i, and M_i are the mole fraction, viscosity, and molecular weight, respectively, of the i^{th} component. A_{ik} is a tabulated function related to the molecular collision processes. The individual viscosity coefficients, expressed in gm/cm-s, are given as a function of the temperature in degrees Kelvin by

$$\mu_i = 2.67 \times 10^{-5} \frac{(M_i T)^{\frac{1}{2}}}{\sigma_i^2 \Omega(T/T_i^*)} \quad , \qquad (C.2)$$

where σ_i is the "collision diameter" for the i^{th} component and T_i^* is a reference temperature related to the intermolecular potential. Also, Ω is another tabulated function associated with the collision processes. The μ_{ik} in equation (C.1) is the viscosity obtained from equation (C.2) for a hypothetical gas whose properties are:

$$M_{ik} \equiv \frac{2M_i M_k}{M_i+M_k}$$

$$\sigma_{ik} \equiv \tfrac{1}{2}(\sigma_i+\sigma_k)$$

$$T_{ik}^* \equiv \tfrac{1}{2}(T_i^*+T_k^*)$$

where i and k refer to two components in the mixture.

Below are values given in reference 30 for the σ_i and T_i^* of the main components present in the combustion gases of the propellants used. Also included are the approximate mole fractions for the various species present in the exhaust gases of A-13 and 540-A. The latter were obtained from the normal computer programs used to predict the theoretical performance of the propellants.

Species	σ_i (Å)	T_i^* (°K)	X_i (A-13)	X_i (540-A)
CO	3.7	88	.30	.16
H_2	2.9	38	.27	.09
H_2O	2.8	230	.19	.37
$HC\ell$	3.3	360	.14	.15
N_2	3.8	80	.07	.08
CO_2	3.9	213	.04	.09

Using these values along with those given in reference 30 for A_{ik} and Ω, the viscosity was calculated as a function of temperature for the combustion gas mixtures of A-13 and 540-A propellants:

T (^{o}K)	μ_{A-13} (10^{-4} gm/cm-s)	μ_{540-A} (10^{-4} gm/cm-s)
500	2.55	2.59
1000	4.23	4.41
1500	5.53	5.79
2000	6.65	6.97
2500	7.66	8.00

Clearly, the values for the two mixtures are very nearly equal. This is mainly because the viscosity coefficients for the individual components do not differ greatly. By plotting the above values against temperature, it was found that the viscosity is given very well by

$$\mu = 3.2 \times 10^{-6} \; T^{0.7} \; , \qquad \text{(C.3)}$$

where μ is expressed in gm/cm-s and T in degrees Kelvin.

To calculate the thermal conductivity, the Eucken relation[30] was used. This relation, which applies rather well to a single polyatomic species is

$$k = \frac{15}{4} R \left(\frac{4}{15} \frac{C_v}{R} + \frac{3}{5} \right) \mu \; ,$$

where R is the gas constant and C_v the specific heat at constant volume. For a perfect gas, $R = (\gamma - 1) C_v$. Thus,

$$k = \frac{9\gamma - 5}{4(\gamma - 1)} R \mu \; . \qquad \text{(C.4)}$$

It was assumed that this relation applies reasonably well to the gas mixtures. Assuming a γ of 1.25 and an average molecular

weight of 25 in the mixture, equations (C. 3) and (C. 4) indicate that the thermal conductivity is given approximately by:

$$k = 1.6 \times 10^{-6} T^{0.7} \qquad (C.5)$$

where k is expressed in cal/cm-s-^{o}K.

It is interesting to note that reasonably accurate values of the viscosity can be obtained simply by averaging the viscosities of the various components with respect to the mole fractions. Thus,

$$\mu \cong \Sigma X_i \mu_i \ , \qquad (C.6)$$

where the μ_i are given by (C. 2). Below are values obtained in this way for A-13 at several temperatures:

T (^{o}K)	μ (10^{-4} gm/cm-s)
500	2.32
1000	3.60
1500	4.98
2000	6.02

Comparing these with the values found earlier, we see that (C. 6) agrees with (C. 1) to an accuracy of 10 - 15 percent.